A first approach on how to solve contact problems using the Inequality Level-Set

Matthieu Graveleau

Institut de Recherche en Génie Civil et Mécanique

Centrale Nantes

THESIS at École Centrale Nantes
for the degree of
DOCTEUR DE L'ÉCOLE CENTRALE DE NANTES
Specialty : GÉNIE MÉCANIQUE

Proposed by
Matthieu Graveleau
DOCTORAL SCHOOL : SPIGA
DEPARTMENT : Gem – UMR CNRS 6183

A first approach on how to solve contact problems using the Inequality Level-Set

Proposal on the Friday 20th November 2015
before a jury composed of :

Bruno Cochelin
Professor at Laboratoire de Mécanique et d'Accoustique, Marseille / *Reporter*

Yves Renard
Professor at Institut Camille Jordan, Institut National des Sciences Appliquées de Lyon / *Reporter*

Stanisław Stupkiewicz
Professor at Institute of Fundamental Technological Research, Warsaw / *Examiner*

Benoit Magnain
Associate professor at Institut National des Sciences Appliquées Centre Val de Loire, Blois / *Examiner*

Nicolas Moës
Professor at École Centrale Nantes / *Thesis supervisor*

Nicolas Chevaugeon
Associate professor at École Centrale Nantes / *Thesis co-supervisor*

erc

cnrs

I hope that this manuscript will help the reader understand what was done during this work as much as it did for me.

How do I know what I think until I see what I say?
Edward Morgan Forster

This thesis was exiting as it was full of interesting surprises.

The most exciting phrase to hear in science, the one that heralds new discoveries, is not "Eureka!" but "That's funny..."
Isaac Asimov

With this thesis conducted in Nantes, one could not help quoting a local writter who underlined so well what research is about:

Science, my lad, is made up of mistakes, but they are mistakes which it is useful to make, because they lead little by little to the truth.
Jules Verne

High five à tous les doctorants et surtout les réguliers de la pause café: Bérenger, Jorge, Kévin, Loïc, Mathieu, Olivier, Qian, Romain. Un grand merci à Claude Stolz et Anthony Nouy qui m'ont donné un coup de main pour résoudre tous les problèmes mathématiques qui ce sont manifestés tout au long de cette thèse.

Pour avoir gardé à flot ma santé mentale, un grand merci à Terry Pratchett et tous ses personages du Disque-Monde ainsi qu'a Alexandre Astier et sa série Kaamelott.

Merci à tous ceux qui m'ont donné un coup de pouce durant ces trois années: Éric et Pierre-Emmanuel à l'informatique; Karine, Caroline et Mélissa au secrétariat; Kévin et Alexis les baygons du bug informatique et enfin Grégory pour l'apport design à ce manuscrit.

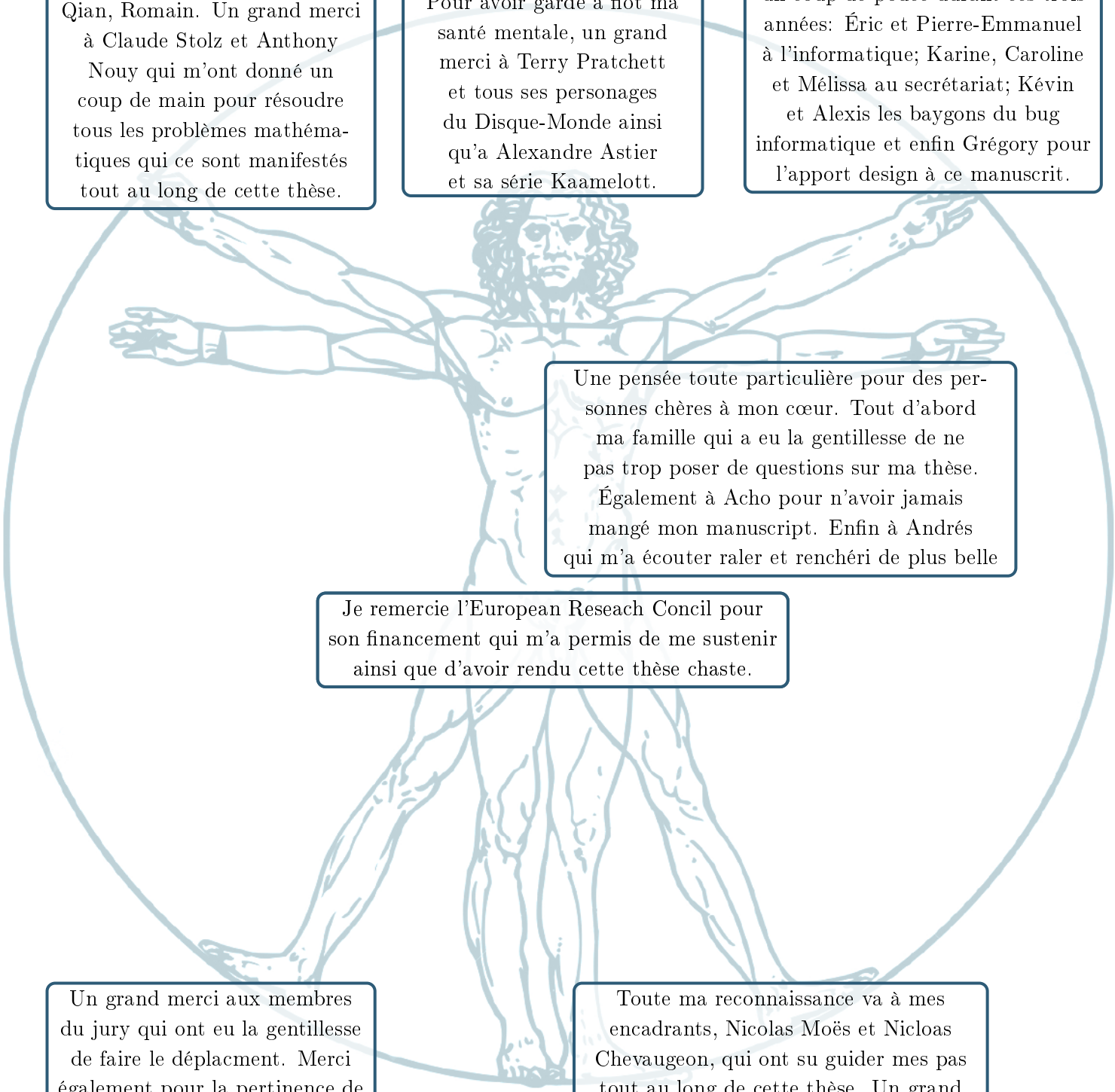

Une pensée toute particulière pour des personnes chères à mon cœur. Tout d'abord ma famille qui a eu la gentillesse de ne pas trop poser de questions sur ma thèse. Également à Acho pour n'avoir jamais mangé mon manuscript. Enfin à Andrés qui m'a écouter raler et renchéri de plus belle

Je remercie l'European Reseach Concil pour son financement qui m'a permis de me sustenir ainsi que d'avoir rendu cette thèse chaste.

Un grand merci aux membres du jury qui ont eu la gentillesse de faire le déplacment. Merci également pour la pertinence de leurs remarques sur ce travail.

Toute ma reconnaissance va à mes encadrants, Nicolas Moës et Nicloas Chevaugeon, qui ont su guider mes pas tout au long de cette thèse. Un grand merci également pour m'avoir mis le pied à l'étrier de ma carrière future.

Résumé

La suite de ce rapport étant en Anglais, un résumé de ce qui a été accomplis durant cette thèse est fait ici en français. Commençons dans un premier temps par situer le sujet d'étude. Le lecteur ne sera pas surpris d'apprendre que les simulations numériques du comportement mécanique des structures prennent rapidement une place de plus en plus importante dans le monde industriel. Un tel engouement est justifié entre autre par le gain financier entraîné par une diminution des essais expérimentaux. Cependant, cet attrait pour les méthodes numérique implique une forte demande dans ce domaine pour être capable de représenter précisément et efficacement divers phénomènes mécaniques.

Parmi ces phénomènes, nous allons nous intéresser aux phénomènes de contact. Présent dans nos vies quotidiennes, le contact joue un rôle majeur dans de nombreux cas. Il est donc crucial de disposer d'outils nous permettant de traiter ces problèmes.

De manière plus générales, il n'est pas injuste de dire que la méthode des éléments finis est largement la plus usitée pour traiter numériquement des problèmes de mécanique du solide. C'est donc en se fondant sur cet outil que des méthodes de résolutions adaptées au contact ont été développées. Plusieurs difficultés émergent directement de l'utilisation de la méthode des éléments finis pour traiter les problèmes de contact.

Avant de définir ces obstacles, définissons certaines spécificités des problèmes de contact. Sans prendre en compte des phénomènes spécifiques liés au contact, tels que la friction ou l'adhésion, le problème de contact semble être équivalent à un problème de mécanique du solide classique avec des conditions aux limites adaptées. Cependant, il faut connaître la zone sur laquelle les solides rentrent en contact afin de pouvoir appliquer ces conditions aux limites. Or, cette zone de contact est *a priori* inconnue. Nonobstant cette difficulté, des méthodes itératives ont été développées pour trouver l'état d'équilibre du système ainsi que la zone de contact.

L'évolution de cette zone pause un problème concret pour la méthode des éléments finis. Cette méthode s'appuie sur une discrétisassion du domaine en un ensemble fini d'"éléments". Les frontières, internes comme externes, sont contraintes par celles des éléments. Ne connaissant pas les positions que va occuper la frontière de la zone de contact il n'est pas possible de positionner les éléments (durant l'opération que l'on nomme maillage) pour représenter au mieux cette frontière. Sans adaptation, il faut alors se contenter de sa meilleur approximation pour le maillage donné. Une autre option consiste à remailler (changer la position des éléments) avec le déplacement de la zone de contact. Cependant, cette opération reste coûteuse.

L'importance de la précision de la zone de contact n'est plus à prouver. Outre l'influence

directe qui peut être imaginée lorsqu'une erreur est faite sur la zone où une condition aux limites est appliquées, d'autres considérations sont à prendre en compte. À la limite de la zone de contact, de nombreux phénomènes complexes peuvent apparaîtrent aboutissant à la création de singularités. Pour bien approximer la solution du problème, il faut être capable de capter ces singularités. Cela n'est pas aisé avec les approximations classiques aux éléments finis.

Dans cette thèse, vous l'aurez compris, nous allons proposer une méthode qui permettra de s'affranchir des problèmes de maillage. Cette méthode que nous mettons ici en avant est l'Inequality Level-Set ou en bref l'ILS. Elle est, comme nous le verrons, une méthode crée pour permettre de résoudre des problèmes comportant des inégalités émergentes de la méconnaissance d'une zone. Si cette zone est connue, il est alors possible de transformer les inégalités en égalités. Le problème du contact rentre évidemment dans cette catégorie.

Essayons de donner ici l'essence de cette méthode. Pour cela nous allons fournir une explication sur les caractéristiques qui font cette méthode de manière graduelle. Avant de s'y atteler, il est bon de rappeler ses origines. Elle utilise les outils développés pour modéliser l'évolution de fissures (tels que les fonctions de niveaux et la mécanique configurationnelle), pour laquelle un parallèle avec le contact peut être dressé. La première étape consiste à s'affranchir de la forte dépendance au maillage en utilisant des fonctions de niveaux pour représenté la frontière de la zone de contact. En plus de définir la frontière de contact, cette fonction de niveaux permet d'avoir accès facilement, entre autres, à la distance d'un point à cette frontière et à sa normale. Couplée à cela, l'eXtended Finite Element Method (X-FEM) permet de prendre en compte les singularités déjà mentionnées ainsi que d'intégrer une connaissance de modélisation du problème. En effet, cette méthode permet d'enrichir les approximations classiques éléments finis localement par une fonction censée être proche de la solution exacte. Ce tandem permet d'avoir une bonne représentation d'une zone de contact ainsi que des phénomènes singuliers y ayant lieux. Nous pourrions nous arrêter là et utiliser une méthode classique (active-set notamment) pour faire évoluer cette zone de contact. Cependant, une autre méthode est proposée. Un algorithme très prisé est la méthode de Newton de part son efficacité et sa relative simplicité. Cette méthode est utilisée pour trouver le zéro ou le minimum d'une fonctionnelle. Elle a déjà était utilisée dans le cadre du contact notamment avec la méthode du Lagrangien augmenté. Ici, le problème est transformé en optimisation de forme associé à la zone de contact. Pour ce faire il faut définir un critère caractérisant sa bonne position. Ce choix peut être effectué via des considérations de mécanique configurationnelle ou phénoménologique comme nous le verrons. La bonne position de la zone de contact implique l'annulation de ce critère. De ce fait, s'il est possible de calculer la variation de ce critère avec le déplacement de la zone de contact, une méthode de Newton peut être appliquée. Cette variation est obtenue en calculant la dérivée directionnelle du critère. Un avantage de cette méthode est la facilité à prendre en compte les phénomènes d'adhésions.

La suite de ce rapport est composé comme suit. Le chapitre I permet de dresser un cadre général pour le problème qui nous concerne. De plus, un inventaire des méthodes les plus utilisées est fait. Le chapitre II se concentre sur la présentation de l'ILS dans un cadre général. En effet, il a été noté que l'ILS était faite pour résoudre une classe générale de problème et cette définition, de part la nouveauté de la méthode, n'a pas encore été faite. Les deux derniers chapitres III et IV donnent des exemples d'applications de cette méthode aux problèmes de membranes puis de solides pleins. De nombreux tests ont été menés afin de qualifier et quantifier les avantages et inconvénients de cette méthode.

Ce travail met en exergue le potentiel de l'ILS pour traiter les problèmes de contact. L'ILS ce montre à la fois efficace et précise sans sacrifier pour cela son adaptabilité. Elle a l'avantage de permettre directement de prendre en compte l'adhésion. De plus, un bon comportement de la méthode pour les interpolations de haut ordre la rend attractive. Tout au long de ce rapport, une attention particulière est prêtée au choix de la formulation variationnelle qui conditionne la stabilité du problème.

Glossary

BB (condition): *Babuška-Brezzi*;
DMT : *Derjaguin-Muller-Toporov*;
FEM : *Finite Element Method*;
JKR : *Johnson-Kendall-Roberts*;
KKT (conditions): *Karush Kuhn Tucker*;
ILS : *Inequality Level Set*;
X-FEM :*eXtended Finite Element Method*;
dofs :*degrees of freedom*;

Notation

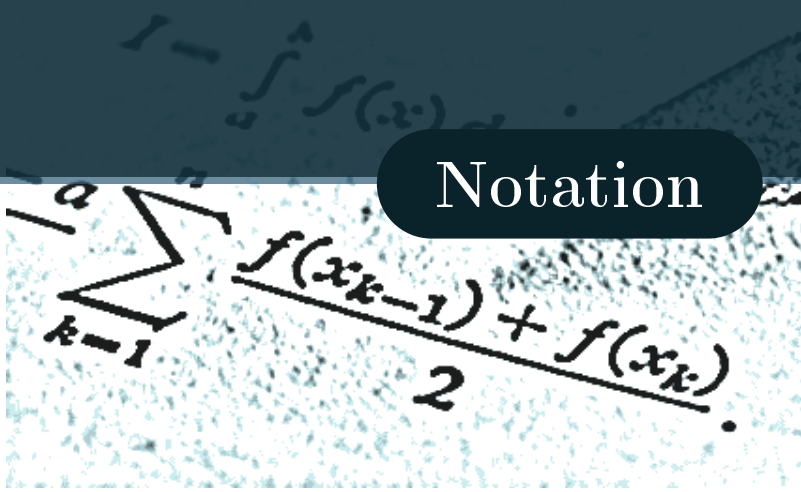

Elements notation

- $L^2(\Omega)$: ensemble of square integrable function over Ω;
- $H^1(\Omega)$: ensemble of function in $L^2(\Omega)$ for which their first derivative is in $L^2(\Omega)$ too;
- $\underline{t}$: first order tensor;
- $\underline{\underline{T}}$: second order tensor;
- $\underline{\underline{\mathrm{I}}}$: second order identity tensor;
- $\underline{\underline{\underline{\underline{\mathrm{T}}}}}$: fourth order tensor;
- $\mathbf{v}$ or $\{\mathbf{v}\}$: a vector;
- $\mathbf{M}$ or $[\mathbf{M}]$: a matrix.

Operators

- $(\blacklozenge) \cdot (\blacklozenge)$ scalar product;
- $(\blacklozenge) \wedge (\blacklozenge)$ cross product;
- $\det(\blacklozenge)$ determinant;
- $\nabla_X(\blacklozenge)$ gradient in the initial configuration;
- $\nabla_x(\blacklozenge)$ gradient in the current configuration;
- $\mathrm{div}(\blacklozenge)$ divergence (the same distinction can be made for the configuration).

Classical mechanics

- Ω a domain;
- Ω^γ the domain γ;
- $\partial\Omega$ the boundary of the domain;
- $\partial\Omega_t$ part of $\partial\Omega$ where external forces $\underline{t_d}$ are imposed;
- $\partial\Omega_u$ part of $\partial\Omega$ where displacements $\underline{u_d}$ are imposed;
- $\underline{f_d}$ body forces;
- $\underline{u}$ displacement;
- $\underline{\underline{\epsilon}}$ strain;
- $\underline{\underline{\sigma}}$ stress;
- $\underline{\underline{\underline{\underline{\mathrm{K}}}}}$ Hooke's tensor;
- $\underline{n}$ outward normal to Ω;
- $\underline{\underline{F}}$ deformation gradient;
- Ψ energy density;
- Π total elastic potential;
- T membrane tension.

Contact

- Ω^- part Ω possibly in contact (also called $\partial\Omega_c$ before the settlement of the level-set);
- Γ boundary of Ω^-;
- g_n gap function;
- d initial distance to the rigid solid;
- p_n contact pressure;
- $\underline{\mathfrak{n}}$ normal to Γ included in Ω^-;
- γ surface tension.

Configurational mechanics

- ϕ level-set ;
- ϱ shape optimization criterion ;
- $\underline{w}$ shape optimization displacement;
- w_n nth mode;
- $D_{[\underline{w}]}(f(\underline{x}))$ directional derivative of a function f for a displacement $\underline{w}$;
- D^m mechanical dissipation;
- $\underline{\underline{C}}$ Eshelby tensor;
- g configurational force;
- $\mathcal{B}$ computing band;

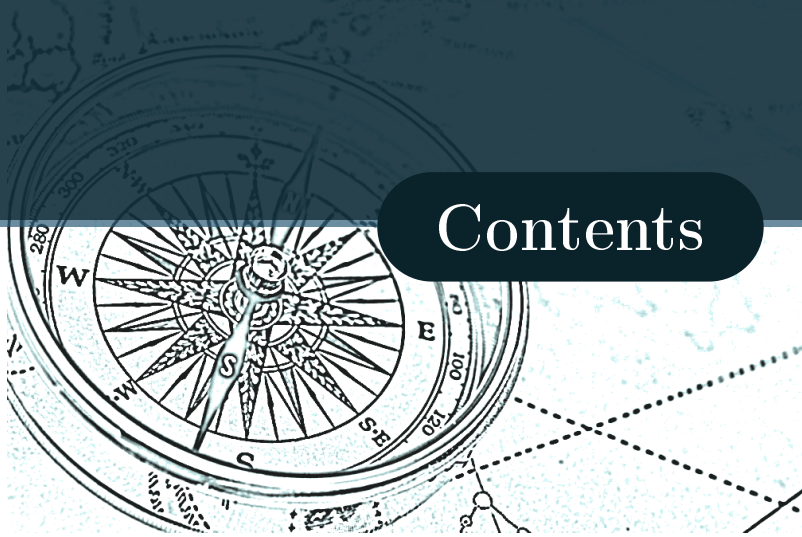

Contents

Why the ILS for contact?

BEFORE reading a little bit over one hundred pages, the reader is entitled to know what was the motivation for filling these pages and what is hoped to be achieved by it. Basically, what he is getting into. The suspense was mostly removed by the title "*solve contact problems using the Inequality Level-Set*". Let us first focus on the most common topic: contact problems.

Contact is present everywhere in our everyday life. Objects have widely interacted with one each others way before the creation of the "connected objects". One of the oldest one we can imagine is what is referred as contact. That is to say when two bodies come close enough and "touch" themselves. This naive description allows nonetheless to grasp the extend of the variety of problems for which contact play a part if not the main part. Therefore we have tried to understand and master this phenomenon, going through the scientific process of observation, modelization and computation. Tremendous progress has been made in the later century on the subject. Several phenomena have been observed and modeled such as friction, adhesion, wear... What seems at first a trivial problem is in fact subtle and difficult. But where does this work fit into? We mentioned also the desire to be able to carry out computations in order to predict the solution of contact problems. Of course a desirable method to solve such problem shall be efficient and accurate, allowing the user to represent accurately all the phenomena involved. It is admitted that one of the challenge of contact problems is to find and represent precisely the contact zone. It raises majors difficulties with the classical framework used for solid mechanics. We wish to propose a method designed to ease these difficulties. Furthermore we wish it to be able to include, as much as possible, the knowledge gotten from the observation and the modelization.

Let us have a foretaste of the Inequality Level-Set method. Its basis is the classical Finite Element Method which is widely use. To that, an extra layer is added. Level-sets are used in order to represent accurately and freely the contact zone. The eXtended Finite Element Method is also used to capture efficiently the singularities of the problem. Coupled to this framework, a shape optimization problem is set up. Its goal is to drive the contact zone to its correct position and shape. This shape configuration problem is based on configurational mechanics.

This report aims at detailing the Inequality Level-Set method and at giving examples of its use. The first chapter settles the framework around contact problems and give a brief overview of the methods and formulations available to tackle these problems. The second chapter gives a general overview of the Inequality Level-Set method. Indeed contact mechanics is not the only

field where it can be applied. A general presentation of this method was never done before and therefore we want to settle that. The two last chapters provide examples of the application of the method to contact problems. First membrane problems are dealt with. Then plain solids are the subject of interest. In any case, a comparison of the method with a more classical one is done. Several tests are conducted in order to underline both its assets and its drawbacks.

A journey toward contact problems

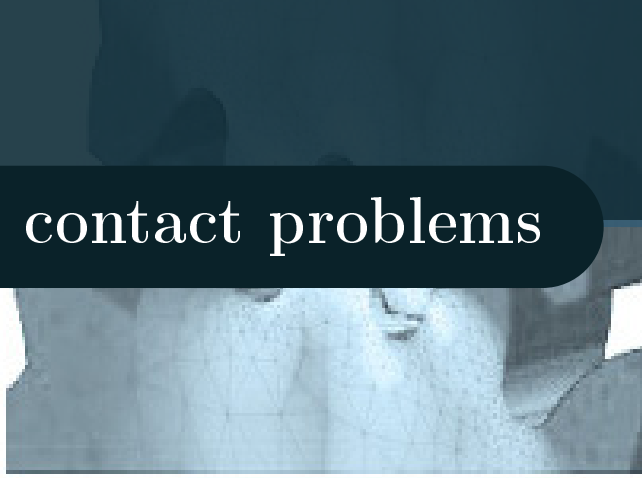

Contents

Summary

This chapter is dedicated to introduce the main framework of contact mechanics. Even if a broad overview is given, some aspects are left aside or only refered to. Nevertheless, a special focus is made on the aspect related to the aimed improvement that are tried to be made by the original work of this thesis. As the method proposed here is a rather new approach, the problems considered will be restricted by some hypothesis defined below. First the modelization and the mathematical framework is presented. Then, some numerical methods are listed. Difficulties in the resolution process are underlined as the ILS will try to answer to them.

Résumé

Dans ce premier chapitre, une présentation de la théorie de la mécanique du solide et du contact est faite. Elle n'a pas pour prétention d'être exhaustive, des livres entiers ont été nécessaires pour traiter chacun de ces sujets, mais d'assurer l'établissement des fondations requises à la compréhension du problème. Dans un premier temps, la théorie des milieux continus est exposée. Cela nous permet de modéliser le comportement d'un solide soumis à des sollicitations extérieures. Certaines hypothèses simplificatrices sont ensuite proposées car elles seront utilisées dans les chapitres suivants. Ensuite, les bases de la théorie du contact sont présentées afin de nous permettre de prendre en compte les interactions entre solides. Plusieurs choix de formulations sont offerts et représentent un panel des plus usités. Enfin les méthodes numériques à dispositions sont étudiées ainsi que les difficultés émergeant du passage au numérique.

I.1 Continuum mechanics, the common ground

As knowledge and technology improve, matter is known to be built of smaller and smaller elements. Atoms were guessed to be elementary constituents since the antiquity but the 19^{th} century taught us about smaller elements such as proton. The last step (for now) was made in 1964 with the quark theory. Let us just stop at the atomic level. Dealing with matter at this scale is clearly an impossible task when looking at macro-scale problems. Furthermore, the interest would be limited as quantities of interest are also macro-scaled. Therefore, a more global model, suited for macro-scaled problems, is required. As, at this scale, matter appears to be continuous, a continuous model seams the logical choice. This observation leads to continuum mechanics which will be the basis of this work. An overview of this theory can be found in [Marsden and Hughes, 1994], only a brief sum up is given here.

I.1.1 A first approach without contact

Let us begin by describing briefly the general groundwork of continuum mechanics. Most of the notations are illustrated in Figure I.1. First, let us focus on the kinematic of the problem. The focus of this study is on quasi-static problems, meaning that dynamical effects are neglected. A body in an initial configuration Ω_0 goes through a transformation into Ω. This means that every material point in a position $\underline{X}$ changes to a new one $\underline{x}$. The relation between these positions is given by the function Φ such that:

$$\Phi : \left| \begin{array}{ccc} \Omega_0 & \rightarrow & \Omega \\ \underline{X} & \rightarrow & \underline{x} \end{array} \right. \tag{I.1}$$

With this definition we can define an interesting quantity: the displacement $u(\underline{X})$. The displacement of a point $\underline{X}$ is naturally:

$$\underline{u}(\underline{X}) = \underline{x} - \underline{X} = \Phi(\underline{X}) - \underline{X} \tag{I.2}$$

When the movement is not a rigid body motion some deformations occur. Deformations arises from the change of distance between points of the body as the transformation occurs. In order to measure this change, it is convenient to define an operator which links an elementary distance in the initial configuration to its transformation. This operator is called the deformation gradient $\underline{\underline{F}}$.

$$\mathrm{d}\underline{x} = \underline{\underline{F}}\mathrm{d}\underline{X} \tag{I.3}$$

Remark

In the following, the notion of derivation is going to be a key point. Several types of derivative are going to be used and it is crucial to not confuse them. The first one encountered here is the partial derivative. Let f be a function such that f: $\mathbb{R}^n \to \mathbb{R}$ and $\underline{x} = (x_1, \dots, x_n) \mapsto f(\underline{x})$ then, the first order derivative regards to the i^{th} component of $\underline{x}$ is defined as:

$$\frac{\partial f(\underline{x})}{\partial x_i} = \lim_{h \to 0} \frac{f(x_1, \dots, x_i + h, \dots, x_n) - f(x_1, \dots, x_i, \dots, x_n)}{h} \quad . \tag{I.4}$$

With this definition, the gradient of f can be defined:

$$\nabla_x f = \frac{\partial f(\underline{x})}{\partial \underline{x}} = \left(\frac{\partial f(\underline{x})}{\partial x_1}, \dots, \frac{\partial f(\underline{x})}{\partial x_n} \right) \quad . \tag{I.5}$$

When no confusion can be made, the subscript of the gradient (here x) can be dropped. In our case, the subscript allows us for instance to differentiate the gradient on the initial configuration $\nabla_X(\bullet)$ and the current configuration $\nabla_x(\bullet)$.

Therefore, $\underline{\underline{F}}$ can be defined using the gradient:

$$\underline{\underline{F}} = \frac{\partial \underline{x}}{\partial \underline{X}} = \nabla_X \underline{x} = \nabla_X \Phi(\underline{X}) = \underline{\underline{I}} + \nabla_X \underline{u} \tag{I.6}$$

A transformation, to be kinetically admissible, must be invertible. Using the determinant of $\underline{\underline{F}}$, called the Jacobian $J = \det(\underline{\underline{F}})$, the condition translates as $J > 0$. On top of allowing the verification of the transformation's invertibility , the Jacobian quantifies the volumic change from $\mathrm{d}v$ into $\mathrm{d}V$ such that $\mathrm{d}v = J\mathrm{d}V$. Finally, the last kinematic quantity we are going to define is the Green-Lagrange tensor $\underline{\underline{E}}$. This is the most common choice of tensor to characterize a strain measure. Is definition is:

$$\underline{\underline{E}} = \frac{1}{2} \left(\underline{\underline{F}}^\top \underline{\underline{F}} - \underline{\underline{I}} \right) = \frac{1}{2} \left(\nabla_X \underline{u}^\top + \nabla_X \underline{u} + \nabla_X \underline{u}^\top \nabla_X \underline{u} \right) \tag{I.7}$$

Dual quantities to the kinematic one are defined by means of a strain-energy density function. Such class of material models are the hyper-elastic material. One example is the Saint Venant–Kirchhoff model which, providing the material Lamé constants (λ, μ), gives the following strain-energy density function:

$$\Psi(\underline{\underline{E}}) = \frac{\lambda}{2} \mathrm{Tr}(\underline{\underline{E}})^2 + \mu \mathrm{Tr}(\underline{\underline{E}}^2) \tag{I.8}$$

Several stress tensors can be derived from this energy function. Two are going to be defined. The first one first express the stress relative to the reference configuration. It is called the first Piola–Kirchhoff stress tensor $\underline{\underline{P}}$. It is related to the strain-energy density function with the relation:

$$\underline{\underline{P}} = \frac{\partial \Psi}{\partial \underline{\underline{F}}} \tag{I.9}$$

The second one, is the Cauchy stress tensor $\underline{\underline{\sigma}}$ and gives the stress relative to the current configuration:

$$\underline{\underline{\sigma}} = \frac{1}{J}\frac{\partial \Psi}{\partial \underline{\underline{F}}} \cdot \underline{\underline{F}}^{\top} \tag{I.10}$$

Then the local equilibrium can be written in the reference configuration, neglecting the dynamical effects:

$$\underset{X}{\mathrm{div}}(\underline{\underline{P}}) + \underline{F}_d = \underline{0} \quad \text{in } \Omega_0 \tag{I.11}$$

or in the current configuration:

$$\underset{x}{\mathrm{div}}(\underline{\underline{\sigma}}) + \underline{f}_d = \underline{0} \quad \text{in } \Omega \tag{I.12}$$

where $\underline{F}_d$ (resp. $\underline{f}_d = J\underline{F}_d$) are the body forces in the reference (resp. current) configuration and $\underset{X}{\mathrm{div}}(\bullet)$ (resp. $\underset{x}{\mathrm{div}}(\bullet)$) the divergence in the reference (resp. current) configuration.

Now that the internal behavior has been defined, let us talk about the interaction of the body with its environment. On top of the already defined body force, the influence of the environment can also appears on the boundary of the body. That could translate into imposed displacement $\underline{u}_d$ or forces $\underline{t}_d$ on the boundary as defined in Figure I.1.

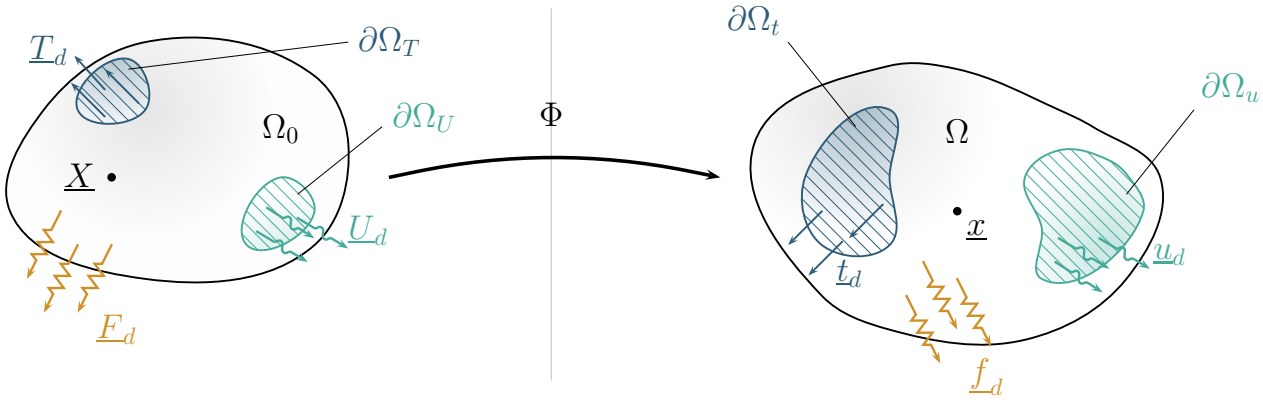

Figure I.1: Illustration of the notations used

In this section, the classical formulation for continuum mechanics was stated. A sum up of the principal notations is given below.

Check point

- Ω_0 initial configuration of the solid;
- $\underline{X}$ a point of Ω_0;
- $\partial\Omega_0$ the boundary of Ω_0;
- $\partial\Omega_T$ where forces $\underline{T}_d$ are imposed on the initial configuration;
- $\partial\Omega_U$ where displacements $\underline{U}_d$ are imposed on the initial configuration;
- Ω deformed configuration;
- $\underline{x}$ a point of Ω;
- $\partial\Omega$ its boundary;
- $\partial\Omega_t$ where forces $\underline{t}_d$ are imposed on the deformed configuration;
- $\partial\Omega_u$ where displacements $\underline{u}_d$ are imposed on the deformed configuration;
- $\underline{F}_d$, $\underline{f}_d$ body forces;

I.1.1.1 Small deformation hypothesis

A common simplification of the general theory is the small deformation hypothesis. This simplification is legitimate if displacements and deformations are small compared to body dimensions. This is usually the case for stiff elastic materials. In small deformation theory, the geometry and the constitutive properties are supposed unchanged with the deformation. In this context, a linearization of the strain tensor $\underline{\underline{E}}$ is made. The linearized strain tensor is:

$$\underline{\underline{\epsilon}} = \frac{1}{2}\left(\nabla\underline{u}^\top + \nabla\underline{u}\right) \tag{I.13}$$

The reader will notice the disappearance of the subscript of the gradient operator. Indeed as the reference and the current configurations are identical therefore $\nabla(\bullet) = \nabla_X(\bullet) = \nabla_x(\bullet)$.

The stress tensor $\underline{\underline{\sigma}}$ is related to this strain tensor through the equivalence of the Saint Venant–Kirchhoff law called the generalized Hooke's law:

$$\underline{\underline{\sigma}} = \lambda \mathrm{Tr}(\underline{\underline{\epsilon}})\underline{\underline{I}} + 2\mu\underline{\underline{\epsilon}} = \underline{\underline{\mathrm{K}}}\,\underline{\underline{\epsilon}} \tag{I.14}$$

and therefore the energy density then is written:

$$\Psi(\underline{\underline{\epsilon}}) = \frac{1}{2}\underline{\underline{\epsilon}} : \underline{\underline{\mathrm{K}}} : \underline{\underline{\epsilon}} \tag{I.15}$$

I.1.1.2 Membrane formulation

Another model simplification used in this thesis is the membrane formulation. This modelization takes into account geometrical specificities. Indeed, when one or several dimensions of a body are negligible compare to the other ones, simplifications can be made. That is also what is done with beam theory or shell theory. For the membrane case, one dimension is negligible allowing the solid to be assimilated to a 2D body. For the small deformation case we are only interested in the normal displacement u of the membrane. The tension in it is considered to be constant and denoted T. In this case, f_d represent the surface force applied to the membrane. The equilibrium equation stated in (I.12) is replaced by:

$$T\Delta u + f_d = 0 \quad \text{in } \Omega \tag{I.16}$$

Then the energy density is given by:

$$\Psi(u) = \frac{1}{2} T \nabla u \cdot \nabla u \tag{I.17}$$

I.1.1.3 Weak formulation for small deformation hypothesis

The equation (I.12), called strong formulation of the problem is not well suited computationally. Another formulation, called weak formulation, is usually preferred. This formulation is designed to allow the use of linear algebra tools to solve partial differential problems. These tools allow to characterize the existence and uniqueness of the solution. There is several ways to derive the weak formulation from the strong equations. Here the energetic approach will be followed. The unknowns are chosen to be displacement based. Let us define the space in which the displacement lives. This space has to guarantee enough regularity (without too much restrictions) and the fulfillment of the imposed displacement u_d. Jumping ahead, the right displacement field space is given:

$$\mathcal{U} = \left\{ \underline{u} \in H^1(\Omega) \quad | \quad \underline{u} = \underline{u}_d \text{ on } \partial\Omega_u \right\} \tag{I.18}$$

with $H^1(\Omega)$ the Sobolev space which guarantees the integrability of a function and its first derivative respect to the L^2-norm on Ω. Staying with the small deformation hypothesis the total elastic potential is:

$$\Pi(\underline{u}) = \int_\Omega \left(\Psi(\underline{u}) + \underline{f}_d \cdot \underline{u} \right) \mathrm{d}V - \int_{\partial\Omega_t} (\underline{t}_d \cdot \underline{u}) \, \mathrm{d}S \tag{I.19}$$

Finding the minimum of this function gives a solution that fulfills the equilibrium equation (I.12).

Remark

In order to find the minimum, the total derivative of the total elastic potential is computed. Let us take time to define the total derivative. Taking a functional $f(a)$, then its total derivative in the direction a^* is:

$$D_{[a^*]}(f(a)) = \lim_{\varepsilon \to 0} \frac{f(a + \varepsilon a^*) - f(a)}{\varepsilon} \tag{I.20}$$

Therefore if $\underline{u}^\star$(often called test field) represents a variation of $\underline{u}$ and thus lives in $\mathcal{U}_0 = \{\underline{u} \in H^1(\Omega) \,|\, \underline{u} = 0 \text{ on } \partial\Omega_u\}$ the total derivative of $\Pi(\underline{u})$ is:

$$D_{[\underline{u}^\star]}(\Pi(\underline{u})) = \int_\Omega \left(\underline{\underline{\epsilon}}(\underline{u}^\star) : \underline{\underline{\mathrm{K}}} : \underline{\underline{\epsilon}}(\underline{u}) - \underline{u}^\star \cdot \underline{f}_d \right) \mathrm{d}V - \int_{\partial\Omega_t} (\underline{u}^\star \cdot \underline{t}_d) \, \mathrm{d}S \tag{I.21}$$

Then, to be a minimum for Π, $\underline{u}$ must verifies:

$$D_{[\underline{u}^\star]}(\Pi(\underline{u})) = 0 \quad \forall \underline{u}^\star \in \mathcal{U}_0 \tag{I.22}$$

which is equivalent to say that the sum of virtual works arising from a virtual displacement $\underline{u}^\star$ at the equilibrium solution u is equal to zero.

The same reasoning can be followed for the membrane case with:

$$D_{[u^\star]}(\Pi(u)) = \int_\Omega (T\nabla u^\star \cdot \nabla u - u^\star f_d)\ \mathrm{d}S - \int_{\partial\Omega_t} (u^\star t_d)\ \mathrm{d}\ell \tag{I.23}$$

I.1.2 Addition of contact contributions

Previously, we only considered one body and we defined its mechanical behavior. In the following we will stay with the small deformation hypothesis. Nevertheless, it is uncommon to find isolated bodies. Generally, solids are part of a system of several bodies interacting with each other. Without being the only possible interaction, contact is the most obvious one. Nevertheless, the addition of contact in the mathematical formulation requires work for modelization, formulation and simulation (cf. Figure I.2). In this thesis, we are working mainly on the simulation part. However, a first step is to understand and model phenomena arising from contact. Then, their contributions must be added into the formulation. After that, there are two options. The first one is that an analytical solution can be found. The Hertz problems class introduced in [Hertz, 1882] is one of the few for which an analytic solution can be exhibited. An explanation of the Hertz theory, but also of more recent work on analytical solutions, can be found in the book [Johnson, 1987]. Furthermore, additional contributions to analytical contact have been made lately in order to widen its scope (for instance see [Goryacheva, 2001, Vorovich and Aleksandrov, 2001]). However, the list of problems with an analytical solution is succinct. Therefore, problems often fall into the other category where only an approximate solution can be found. This is commonly a job for numericians. Therefore, special mathematical formulations are needed and were developed. The first step was made by Signorini ([Signorini, 1933, Signorini, 1960]) who gave his name to the general formulation for linear elastic frictionless contact. Work as been done to assert the existence and uniqueness of the solution for instance by [Fichera, 1973]. Others have highlighted examples of non-uniqueness or non-existence as it is the case in [Klarbring, 1990, Martins et al., 1994]. A wide mathematical analysis was performed in [Kikuchi and Oden, 1988]. For the numerical implementation [Wriggers, 2006] or [Laursen, 2002] are reliable references. Trying to summarize every aspect of the work already done in the above-named references would be out of the scope of this thesis and only a pale imitation of them. Therefore, in this review we will only give a brief state of the art of what will be important to understand and compare the method designed in this thesis.

An important but difficult point for contact formulations is the definition of geometrical quantities. To echo Figure I.1, Figure I.3 schematizes two solids Ω^1 and Ω^2 coming into contact with each other without the small deformation hypothesis. However, as it was said this work is confined to small deforation and thus only the right configuration in Figure I.3 is studied. The contact zone is called $\partial\Omega_c$ and its boundary is Γ. The external normal to a body Ω^γ is denoted as $\underline{N}^\gamma$ in the reference configuration and $\underline{n}^\gamma$ in the current configuration. The main quantity of interest is the gap function g_n in the current configuration. Indeed, g_n characterizes the gap between the two solids. Let us be more precise, in order to avoid penetration for every material

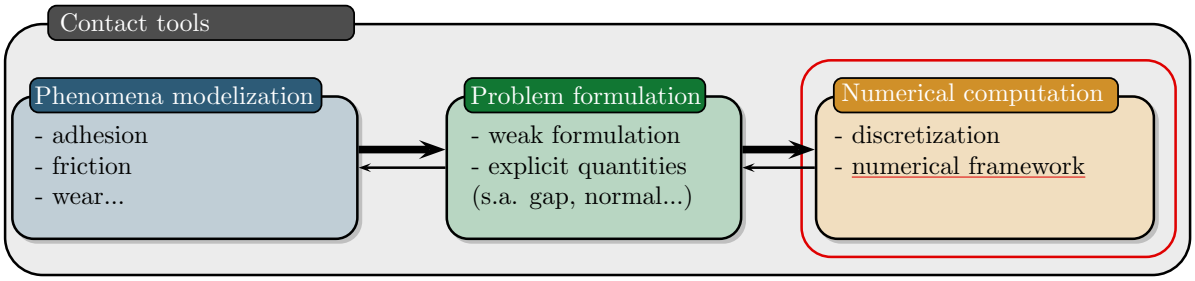

Figure I.2: Additional contact contribution to continuum mechanics

points $\underline{x}^1 \in \partial\Omega^1$ and $\underline{x}^2 \in \partial\Omega^2$ the following inequality must be verified:

$$(\underline{x}^2 - \underline{x}^1) \cdot \underline{n}^1 \geq 0 \tag{I.24}$$

This formulation is not numerically convenient. It is usually preferred to pick one of the surface as a "master surface". In the following $\partial\Omega^1$ is arbitrarily chosen. Then, for each point $\underline{x}^2$ its closest point $\hat{\underline{x}}^1 \in \partial\Omega^1$ and its associated normal $\hat{\underline{n}}^1$ are defined. Allowing therefore to define the non-penetration condition using the gap function as follows:

$$g_n = (\underline{x}^2 - \hat{\underline{x}}^1) \cdot \hat{\underline{n}}^1 = (\underline{u}^2 - \hat{\underline{u}}^1) \cdot \hat{\underline{n}}^1 + d \geq 0 \tag{I.25}$$

with the initial gap d being the initial distance between $\underline{x}^2$ and $\hat{\underline{x}}^1$.

Another important quantity is the normal reaction on the contact zone $\partial\Omega_c$.

$$p_n = \underline{n}^1 \cdot \underline{\underline{\sigma}}^1 \cdot \underline{n}^1 = \underline{n}^2 \cdot \underline{\underline{\sigma}}^2 \cdot \underline{n}^2 \tag{I.26}$$

As long as there is no adhesion, the normal reaction p_n cannot be positive. Indeed, having $p_n > 0$ means that there is an attraction between the two bodies.

Consequently, two quantities are defined and must verify some conditions. On one hand, where the two bodies are in contact, meaning that $g_n = 0$, there must be no attraction thus $p_n \leq 0$. On the other hand, if there is no contact (and no imposed effort) the boundary is stress free with $p_n = 0$ and there must be no penetration $g_n \geq 0$. These set of conditions can be translated into three equations known as the Kuhn Tucker Karush (KKT) conditions in the general framework of optimization theory or as the other triptych Hertz Signorini Moreau conditions for contact:

$$\begin{cases} g_n & \geq & 0 & \text{no penetration} \\ p_n & \leq & 0 & \text{no attraction} \\ p_n g_n & = & 0 & \text{normal condition} \end{cases} \tag{I.27}$$

These conditions are focused on the normal quantities on the boundary. If we keep to frictionless problems, as it will be the case, it is sufficient. For the frictional case the reader is referred to [Persson, 2000].

Nevertheless, it was said that a weak formulation was better suited. The equations (I.27) must then be introduced into the weak formulation. First, let us define a new admissible displacement space $\mathcal{U}_d = \left\{u \in \mathcal{U} | (\underline{u}^2 - \hat{\underline{u}}^1) \cdot \hat{\underline{n}}^1 + d \geq 0\right\}$. The virtual work for one body Ω^γ

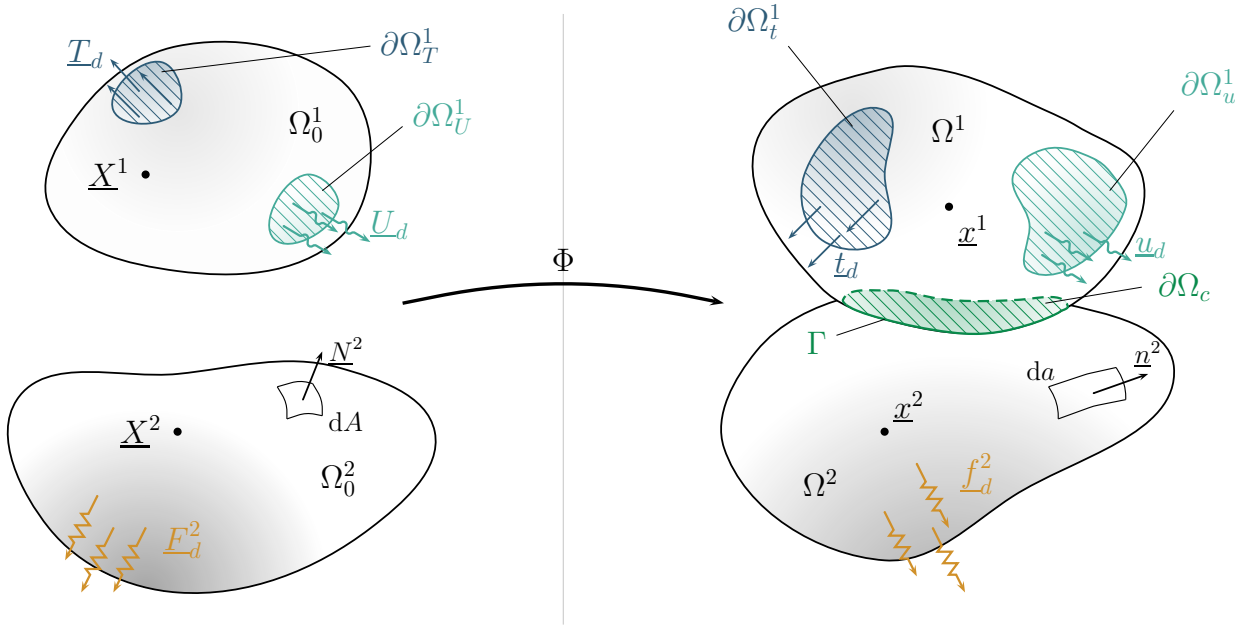

Figure I.3: Notation for two solids coming in contact without small deformation hypothesis

at the equilibrium solution, defined in the case without contact by (I.21), can be formulated taking into account the contact interaction for a virtual displacement $(\underline{v}-\underline{u})$ with $\underline{u}$ and $\underline{v}$ in $\mathcal{U}_d$ as:

$$\int_{\Omega^\gamma}\left(\underline{\underline{\epsilon}}(\underline{v}-\underline{u}):\underline{\underline{\underline{\underline{K}}}}:\underline{\underline{\epsilon}}(\underline{u})-(\underline{v}-\underline{u})\cdot\underline{f}_d\right)\mathrm{d}V-\int_{\partial\Omega_t^\gamma}((\underline{v}-\underline{u})\cdot\underline{t}_d)\,\mathrm{d}S-\int_{\partial\Omega_c}((\underline{v}-\underline{u})\cdot\underline{n}\,p_n)\,\mathrm{d}S \tag{I.28}$$

since $(\underline{v}-\underline{u})\cdot\underline{n}\,p_n=(\underline{v}\cdot\underline{n}-g)p_n\geq 0$ because of (I.27) and $v\in\mathcal{U}_d$, the following variational inequality characterizes the solution of the contact problem:

Problem 1

Find $u\in\mathcal{U}_d$ such that for all $v\in\mathcal{U}_d$

$$a(\underline{u},\underline{v}-\underline{u})\geq f(\underline{v}-\underline{u}) \tag{I.29}$$

with:

$$\left|\begin{array}{rcl} a(\underline{u},\underline{v}-\underline{u}) & = & \displaystyle\int_{\Omega^1\cup\Omega^2}\left(\underline{\underline{\epsilon}}(\underline{v}-\underline{u}):\underline{\underline{\underline{\underline{K}}}}:\underline{\underline{\epsilon}}(\underline{u})\right)\mathrm{d}V \\ f(\underline{v}-\underline{u}) & = & \displaystyle\int_{\Omega^1\cup\Omega^2}(\underline{v}-\underline{u})\cdot\underline{f}_d\,\mathrm{d}V+\int_{\partial\Omega_t^1\cup\partial\Omega_t^2}(\underline{v}-\underline{u})\cdot\underline{t}_d\,\mathrm{d}S \end{array}\right. \tag{I.30}$$

In this brief review, several difficult points have been left aside. For instance, how does the closest point and the normal are computed? Is there existence and uniqueness of them?

The answer to this last question is no. If surfaces are not smooth enough, the normal cannot be well defined. A regularization is needed in this case by smoothing for instance the master surface as it was done in [Wriggers et al., 2001] and [Krstulović-Opara et al., 2002]. Even if the surface is smooth, there might be problem of uniqueness and it was discussed in [Heegaard and Curnier, 1996]. Not to mentioned the assymetry in the choice of the master surface. Indeed if the former definition of the closest point give both pairs $(x^2,\hat{x}^1)$ and $(x^1,\hat{x}^2)$ (taking $\partial\Omega^1$ or $\partial\Omega^2$ as the master surface) then taking $x^2{=}\hat{x}^2$ does not implies $x^1{=}\hat{x}^1$.

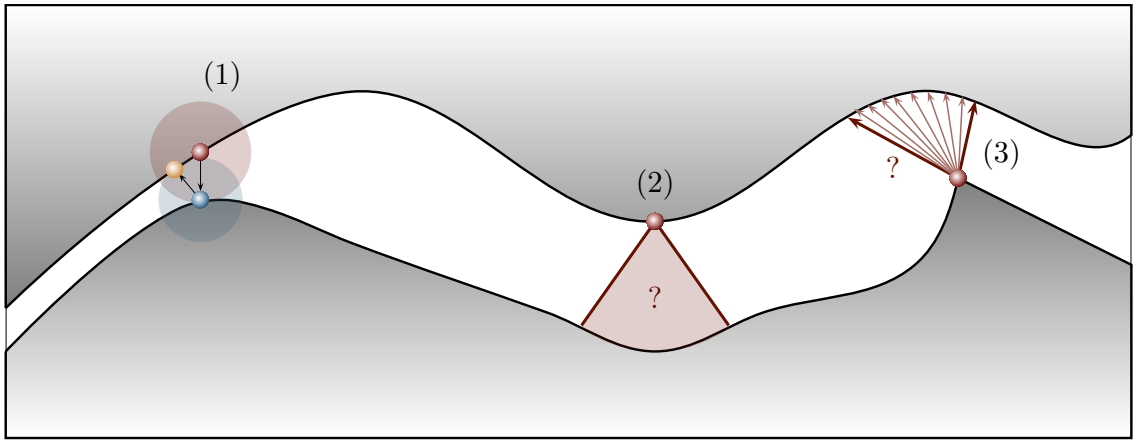

Figure I.4: Geometrical problems represented by red spheres. (1) shows the assymetry depending on the choice of the master surface; (2) hilights the non uniqueness of the closest point; (3) stages the non-excistance of the normal vector

In order to, if not delete, limit any extra-burden not relevant to the contribution of this thesis we will focus on simple problems. On top of the small deformation hypothesis,the boundary of the solids are considered smooth enough (at least C^2). Furthermore, only unilateral contact with one deformable solid coming into contact with a rigid one is considered. With this last hypothesis the functional of Problem 1 are simplified by carrying the computation only on the deformable solid (called Ω here).

$$\left|\begin{array}{rcl} a(\underline{u},\underline{v}-\underline{u}) & = & \displaystyle\int_\Omega \left(\underline{\underline{\epsilon}}(\underline{v}-\underline{u}) : \underline{\underline{\underline{\underline{K}}}} : \underline{\underline{\epsilon}}(\underline{u})\right) \mathrm{d}V \\ f(\underline{v}-\underline{u}) & = & \displaystyle\int_\Omega (\underline{v}-\underline{u})\cdot\underline{f}_d \,\mathrm{d}V + \int_{\partial\Omega_t} (\underline{v}-\underline{u})\cdot\underline{t}_d \,\mathrm{d}S \end{array}\right. \tag{I.31}$$

Furthermore, the gap function g_n can be simplified. With d the initial distance between the deformable and the rigid solids, then:

$$g_n = d - \underline{u}\cdot\underline{n} \tag{I.32}$$

The non-linearity of contact problems appears clearly as the formulation involves a variational inequality. Special frameworks are designed to solve these problems, including special formulations (see Section I.1.3) and associated algorithm (see Section I.2.2).

I.1.3 Several possible formulations

In the last section, a variational inequality formulation was derived for contact problems. It was said to be numerically challenging. An option to simplify it is to design a formulation for a given contact zone. Indeed, knowing the contact zone removes the inequality as the contact contributions can be directly taken into account. This leads, with our hypothesis, to a linear problem. Several formulations for the contact contributions can be devised and an overview of the most widely used will be given. A special focus will be put on the penalty, the Lagrange multiplier and the augmented Lagrange formulation. All these methods are well known in optimization under constraints theory, which is often applied in mechanics (see [Duvaut and Lions, 1976]). Obviously, the complexity of the formulation did not vanished. Indeed the contact zone is not *a priori* known. Therefore, the choice of a contact zone can be erroneous at first and a correction need to be made. Algorithms, depending on the chosen formulation, are designed to do so and will be discussed in Section I.2.2.

Taking into account the contact contributions is achieved by adding to the total energy (defined in Equation (I.19)) the energy coming from the contact Π_c. It was said earlier that, as a choice, the unknown was to be the displacement. Then, as the strain was derived from the displacement using a constitutive law, the contact reaction as to be modeled. Let us look into several modelizations.

I.1.3.1 Penalty

The penalty formulation is widely use. Its main advantages are that only displacement quantities are involved and it is easy to implement. The general idea of the method is that the rigid body is not impenetrable anymore but resists to the penetration. This resistance is modeled by a penalty function. Even if it is not compulsory, the classical function is a linear function of the gap as long as there is no penetration. The classical image given to illustrate it is Figure I.4 where one can see springs which represent the reaction of contact. These springs have a chosen stiffness ϵ_n and thus the normal contact reaction is $p_n \leftarrow \min(0, \epsilon_n g_n)$ such that no traction is applied where there is no penetration. The additional energy coming from contact is, in this

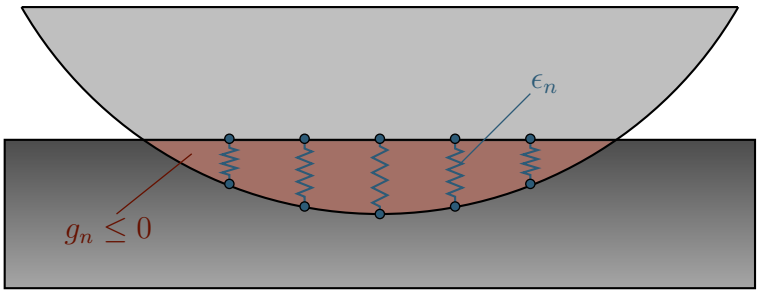

Figure I.5: Interpretation of the penalty method with springs

case:

$$\Pi_c^p = \frac{1}{2} \int_{\partial\Omega_c} \epsilon_n (\min(0, g_n))^2 \, \mathrm{d}S = \frac{1}{2} \int_{\partial\Omega_c} \epsilon_n (\min(0, d - \underline{u} \cdot \underline{n}))^2 \, \mathrm{d}S \tag{I.33}$$

and consequently the problem can be stated as:

Problem 2

Find $\underline{u} \in \mathcal{U}$ such that for all $\underline{u}^\star \in \mathcal{U}_0$

$$a(\underline{u}, \underline{u}^\star) + c^p(\underline{u}, \underline{u}^\star) = f(\underline{u}^\star) \tag{I.34}$$

with:

$$\left| \quad c^p(\underline{u}, \underline{u}^\star) \quad = \quad -\epsilon_n \int_{\partial\Omega_c} (\underline{u}^\star \cdot \underline{n}) \min(0, g_n) \, \mathrm{d}S \right. \tag{I.35}$$

A major drawback of this formulation is the choice of ϵ_n. If taken too small the solution might allow strong penetration of the rigid body. On the other hand, if ϵ_n is taken too big, the problem becomes ill-conditioned. Hence, its choice was fairly discussed in the literature, let us cite [Nour-Omid and Wriggers, 1987] which propose an estimate of the best choice for ϵ_n.

I.1.3.2 Lagrange multiplier

Another classical method is the well known Lagrange multiplier method. From a mechanical point of view, the contact pressure p_n is added to the unknown of the problem through Lagrange multiplier p living in a space $\mathcal{P}^- = \{p \text{ regular enough s.t. } p \leq 0\}$. The addition of more unknowns is the main drawback of such formulation. The total energy is then a functional of the two fields $\underline{u}$ and $\underline{p}$. The p-dependence arises only from the contact contribution:

$$\Pi_c^l = \int_{\partial\Omega_c} p g_n \, \mathrm{d}S = \int_{\partial\Omega_c} p(d - \underline{u} \cdot \underline{n}) \, \mathrm{d}S \tag{I.36}$$

It is well-known that such a constrained minimization problem is equivalent to a saddle point problem. Indeed, if both energy, Π and Π_c^l are summed, the notorious Lagrangian functional is obtained $\mathcal{L}(\underline{u}, p) = \Pi(\underline{u}) + \Pi_c^l(\underline{u}, p)$. The solution of the problem is given by:

$$\min_{\underline{u} \in \mathcal{U}} \max_{p \in \mathcal{P}^-} (\mathcal{L}(\underline{u}, p)) \tag{I.37}$$

This last equation is equivalent to find (u, p) which satisfy for all $\underline{u}^\star \in \mathcal{U}_0$ and $p^\star \in \mathcal{P}^-$ the two equations:

$$\begin{cases} D_{[\underline{u}^\star]}(\mathcal{L}(\underline{u}, p)) = 0 \\ D_{[p^\star]}(\mathcal{L}(\underline{u}, p)) \geq 0 \end{cases} \tag{I.38}$$

Finally, the problem is explicitly given by:

Problem 3

Find $\underline{u} \in \mathcal{U}$ and $p \in \mathcal{P}^-$ such that for all $\underline{u}^\star \in \mathcal{U}_0$ and $p^\star \in \mathcal{P}^-$

$$\left\{ \begin{array}{lcll} a(\underline{u},\underline{u}^\star) & + & c^l(p,\underline{u}^\star) & = & f(\underline{u}^\star) \\ c^l(p^\star,\underline{u}) & & & \geq & l^l(p^\star) \end{array} \right. \tag{I.39}$$

with:

$$\left| \begin{array}{lcl} c^l(p,\underline{u}) & = & \displaystyle\int_{\partial\Omega_c} p(\underline{u}\cdot\underline{n})\,\mathrm{d}S \\ l^l(p^\star) & = & \displaystyle\int_{\partial\Omega_c} dp^\star\,\mathrm{d}S \end{array} \right. \tag{I.40}$$

The variational formulation still holds an inequality. However the constrain on u is passed to p. This can be of great help if the constrained on u is complex as the constrain on p is only to be negative. To remove the inequality in the equation a given contact zone must be picked.

I.1.3.3 Augmented Lagrange

In order to overcome the drawbacks of these last two methods, a combination of them has been developed for general minimization under constraints in [Powell, 1969, Hestenes, 1969]. Applied to contact (see [Wriggers et al., 1985]), the equivalent contact reaction is a combination of the Lagrange multiplier and the penalty reaction. We define thus this reaction with the above notations as $p_n \leftarrow p + \min(0, \epsilon_n g_n)$. The main difference with a classical Lagrange formulation (i.e. $p_n \leftarrow p$) is that the formulation is valid for $p_n \leq 0$ but also for $p_n > 0$, meaning that the gap is open. Therefore, the non-positiveness of the Lagrange multiplier does not have to be imposed. The contact energy contribution is defined by the functional:

$$\Pi_c^a(\underline{u},p) = \int_{\partial\Omega_c \cap \{\underline{x}/p+\min(0,\epsilon_n g_n)\leq 0\}} p g_n + \frac{\epsilon_n}{2} g_n^2 \,\mathrm{d}S + \int_{\partial\Omega_c \cap \{\underline{x}/p+\min(0,\epsilon_n g_n)>0\}} -\frac{p^2}{2\epsilon_n}\,\mathrm{d}S \tag{I.41}$$

The augmented Lagrangian functional is defined as previously, $\mathcal{L}^a(\underline{u},p) = \Pi(\underline{u}) + \Pi_c^a(\underline{u},p)$. It was proven that a solution of $\min_{\underline{u}\in\mathcal{U}} \max_{p\in\mathcal{P}^-} (\mathcal{L}(\underline{u},p))$ is also one of $\min_{\underline{u}\in\mathcal{U}} \max_{p\in\mathcal{P}} (\mathcal{L}^a(\underline{u},p))$.

Taking again the total derivative of the Lagrangian allows to write the problem as:

Problem 4

Find $\underline{u} \in \mathcal{U}$ and $p \in \mathcal{P}$ such that for all $\underline{u}^\star \in \mathcal{U}_0$ and $p^\star \in \mathcal{P}$

$$\left\{ \begin{array}{rcrcl} a(\underline{u},\underline{u}^\star) + c^{ap}(\underline{u},\underline{u}^\star) & + & c^{al}(p,\underline{u}^\star) & = & f(\underline{u}^\star) \\ c^{al}(p^\star,\underline{u}) & + & c^{aa}(p,p^\star) & = & l^a(p^\star) \end{array} \right. \tag{I.42}$$

with:

$$\left| \begin{array}{lcllcl} c^{ap}(\underline{u},\underline{u}^\star) & = & -\epsilon_n \displaystyle\int_{\partial\Omega_c \cap \{\underline{x}/p_n \leq 0\}} (\underline{u}^\star \cdot \underline{n}) g_n \, \mathrm{d}S & c^{al}(p,\underline{u}) & = & \displaystyle\int_{\partial\Omega_c \cap \{\underline{x}/p_n \leq 0\}} p(\underline{u} \cdot \underline{n}) \, \mathrm{d}S \\ c^{aa}(p,p^\star) & = & -\dfrac{1}{2\epsilon_n} \displaystyle\int_{\partial\Omega_c \cap \{\underline{x}/p_n > 0\}} p p^\star \, \mathrm{d}S & l^a(p^\star) & = & \displaystyle\int_{\partial\Omega_c \cap \{\underline{x}/p_n \leq 0\}} dp^\star \, \mathrm{d}S \end{array} \right. \tag{I.43}$$

In exchange for more complexity, the variational formulation is unconstrained and a Newton method can be used. Nevertheless, because of a lack of smoothness in the functional $\mathcal{L}^a(\underline{u},p)$ special methods (such as a generalized Newton method) are used (cf. [Alart and Curnier, 1991]) and confer a good convergence rate.

A simpler formulation can be obtained if $(\underline{u},p)$ are not searched simultaneously. This lead to a formulation adapted to the Usawa algorithm discussed later on. At one iteration of this algorithm, Lagrange multiplier are supposed to be constant, $p = p^c$. The associated formulation is:

Problem 5

Find $\underline{u} \in \mathcal{U}$ given p^c such that for all $\underline{u}^\star \in \mathcal{U}_0$

$$a(\underline{u},\underline{u}^\star) + c^u(\underline{u},\underline{u}^\star) = f(\underline{u}^\star) \tag{I.44}$$

with:

$$\left| \; c^u(\underline{u}^\star) = \int_{\partial\Omega_c} ((p^c + \epsilon_n g_n)\underline{u}^\star \cdot \underline{n}) \, \mathrm{d}S \right. \tag{I.45}$$

Then, a method to update p_c after each iteration needs to be designed. This will be discussed in the algorithm section.

I.1.3.4 Other formulations

In the last section, the most used formulations for contact problems have been established. In this sections, less common ones are going to be exposed. As they are not going to be used later on, only a brief summary is given. For more details the reader is referred to [Wriggers, 2006].

Direct elimination It was said that we supposed the contact zone. Therefore, the displacement on this part is known. An obvious option is to consider it as a classical Dirichlet boundary condition. On top of being easy to implement, this method reduce the number of unknowns by removing all the contact zone unknowns on one side of the boundary. Nevertheless, as it will be discussed later, to work numerically without extra efforts special discretization is needed. This in not always feasible and special constrained elimination technique have to be used such as Mortar Methods which is equivalent to a Lagrange multiplier formulation.

Nitsche formulation The Nitsche formulation [Chouly et al., 2015, Annavarapu et al., 2014] might be compared to a Lagrange multiplier formulation but with a more straightforward way to take into account the contact contributions. Indeed, rather than using Lagrange multiplier to represent the normal reaction, the constitutive law is used: $p_n \leftarrow p^{nf}(\underline{u}) = \underline{n} \cdot \underline{\underline{\mathrm{K}}}\,\underline{\underline{\epsilon}}(\underline{u}) \cdot \underline{n}$. Therefore no extra unknowns are added. Like with the augmented Lagrange method, a penalty term is generally appended in order to avoid ill-conditioning. This leads to the formulation:

Problem 6

Find $\underline{u} \in \mathcal{U}$ such that for all $\underline{u}^\star \in \mathcal{U}_0$

$$a(\underline{u}, \underline{u}^\star) + c^{nf}(\underline{u}, \underline{u}^\star) = f(\underline{u}^\star) \tag{I.46}$$

with:

$$c^{nf}(\underline{u}, \underline{u}^\star) = \int_{\partial\Omega_c} p^{nf}(\underline{u})\,(\underline{u}^\star \cdot \underline{n})\,\mathrm{d}S - \int_{\partial\Omega_c} p^{nf}(\underline{u}^\star) g_n\,\mathrm{d}S - \epsilon_n \int_{\partial\Omega_c} (\underline{u}^\star \cdot \underline{n})\, g_n\,\mathrm{d}S \tag{I.47}$$

Nevertheless, this formulation is less flexible than the Lagrange formulation. As soon as the constitutive law is complicated the computation becomes difficult.

Perturbed Lagrange Perturbed Lagrange is another way to combine the penalty and the Lagrange multiplier rather than the augmented Lagrange method. Instead of using the gap as a penalizing function the Lagrange multiplier are chosen. This leads to:

Problem 7

Find $\underline{u} \in \mathcal{U}$ and $p \in \mathcal{P}$ such that for all $\underline{u}^\star \in \mathcal{U}_0$ and $p^\star \in \mathcal{P}$

$$\left\{ \begin{array}{rcrcl} a(\underline{u}, \underline{u}^\star) & + & c^l(p, \underline{u}^\star) & = & f(\underline{u}^\star) \\ c^l(p^\star, \underline{u}) & + & c^{pl}(p^\star, p) & = & l^l(p^\star) \end{array} \right. \tag{I.48}$$

with:

$$\left| \begin{array}{rcl} c^{pl}(p^\star, p) & = & -\dfrac{1}{\epsilon_n} \displaystyle\int_{\partial\Omega_c} p p^\star \, \mathrm{d}S \end{array} \right. \tag{I.49}$$

Sadly, this formulation is only valid for the friction-less and stick case

Barrier formulation This last formulation discussed here is a well known to solve inequality constrained problems. A barrier function is added to the total energy. A classical choice for such addition is:

$$\Pi_c^b = -\epsilon_n \int_{\partial\Omega_c} \frac{1}{g_n} \, \mathrm{d}S \tag{I.50}$$

The formulation linked to this energy is:

Problem 8

Find $\underline{u} \in \mathcal{U}$ such that for all $\underline{u}^\star \in \mathcal{U}_0$

$$a(\underline{u}, \underline{u}^\star) + c^b(\underline{u}, \underline{u}^\star) = f(\underline{u}^\star) \tag{I.51}$$

with:

$$\left| \begin{array}{rcl} c^b(\underline{u}, \underline{u}^\star) & = & -\epsilon_n \displaystyle\int_{\partial\Omega_c} \frac{\underline{u}^\star \cdot \underline{n}}{g_n^2} \, \mathrm{d}S \end{array} \right. \tag{I.52}$$

With this formulation the penetration needs to never be violated (g_n must be greater or equal to zero) and therefore a numerical difficulty is to find a starting point which does not violate this condition. Moreover, during the iterations, an algorithm is necessary to ensure that it is not violated. As for the penetration formulation ϵ_n has to be well chosen to avoid ill-conditioning. Nonetheless, the advantage is that all the constraints are active. Lately this method was also coupled with augmented Lagrangian.

I.1.4 A special phenomenon: adhesion

In the set of KKT equations (I.27) the condition $p_n \leq 0$ has been highlighted. This reflects an impossibility to have attraction between two solids. However, several physical examples show that positive normal contact stresses can appear. For instance the reader can think about a

tape on a solid surface or when two flat surfaces are pressed together with a layer of water in between. Such phenomena exhibit what is called adhesion.

A key point to adhesion modeling is the energy interactions and more particularly the energy per unit contact area γ called the surface energy. Early on, some parallel have been drawn with damage theory and the work of [Griffith, 1921, Irwin, 1957, Rice, 1968]. The first model was introduced in [Johnson et al., 1971] and became the Johnson-Kendall-Roberts (JKR) formulation. However, this model gives an infinite stress at the boundary of the contact zone. Later, [Maugis and Barquins, 1983] confirm the parallel with the Griffith theory. In the same line of thought, [Fremond, 1982, Raous et al., 1999] derived a constitutive equation allowing a transition from adhesion to adhesion-free contact. This modelization is similar to damage models. A function β is then introduced such that:

$$\begin{cases} \beta = 0 & \text{no adhesion} \\ 0 < \beta < 1 & \text{partial adhesion} \\ \beta = 1 & \text{total adhesion} \end{cases} \tag{I.53}$$

An adhesion force is added to p_n proportional to the gap with a constitutive parameter C_n with the expression $C_n g_n \beta^2$. Then, an evolution law of β needs to be given (see for instance [Raous et al., 1999]).

Another point of view is to take into account the micro-structural interaction and molecular forces. Such standpoint was taken in [Derjaguin et al., 1975] giving the well known Derjaguin-Muller-Toporov (DMT) formulation. Even if the molecular forces act outside of the contact zone, the profile outside of the contact zone is unchanged which is not physically consistent.

A bridge between the two classical JKR and DMT formulations was given in [Maugis, 1992].

Lately, lot of effort was made for micro/nano-scale contact computation using both above mentioned theories. This interest is explained by a growth of micro-electro-mechanical systems [Zhao et al., 2003], nano-indentation [Fischer-Cripps, 2011] or biological [Chu et al., 2005, Autumn et al., 2002] needs. Numerical improvements of classical methods have been proposed for example by R. Sauer [Sauer, 2011].

I.2 From the formulation to the solution: numerical frameworks

In this chapter, several partial differential equations were established. They need to be solved on possibly complex domains. Anyone who has studied partial differential equations knows that analytic solutions are seldom. Therefore approximations are made. In mechanical engineering different methods are used. To name but a few, let us mentioned the Finite Volume Method [LeVeque, 2002], the Boundary Element Method [Banerjee et al., 1981] and the Isogeometric Analysis [Cottrell et al., 2009, Temizer et al., 2011]. However, in the solid community, the most widely used is the Finite Element Method (FEM). Its success is mostly due to its robustness, adaptability and simplicity. Since its beginnings in the seventies, the FEM has expanded quickly. Several books devoted to this method have been written such as [Hughes, 2012, Zienkiewicz and Taylor, 2005]. The great interest shown by the mechanical community is underlined in the last mentioned book as shown by this quote:

> *"The size of each of these editions expanded geometrically (from 272 pages in 1967 to the fifth edition of 1482 pages). This was necessary to do justice to a rapidly*

expanding field of professional application and research. Even so, much filtering of the contents was necessary to keep these editions within reasonable bounds."

The main idea is to approximate the domain by the union of sub-domains Ω_e called elements:

$$\Omega \approx \cup \Omega_e \tag{I.54}$$

Then, the fields are approximated by a linear combination of shape functions N_i which are only locally non-zero, on supports that fit with the elements.

$$u(x) \approx \sum_I u_i N_i(x) \tag{I.55}$$

The coefficients u_i of this combination become the unknowns of the problem and are called the degrees of freedom (dofs). This approximation is injected in the variational formulation and leads to a linear system to be solved for a given contact zone. This system is usually put in a matricial form:

$$[\mathbf{K}]\{\mathbf{u}_i\} = \{\mathbf{f}\} \tag{I.56}$$

I.2.1 Difficulties arising from the discretization

The contact boundary An obvious problem with a discretization of the fields and the geometry is the representation of the contact zone. As the contact zone is *a priori* unknown the generated mesh cannot be adapted to fit it. Therefore, as there cannot be any discontinuity in an element with the classical FEM, a problem appears if an element is cut by the contact boundary as shown in Figure I.6.

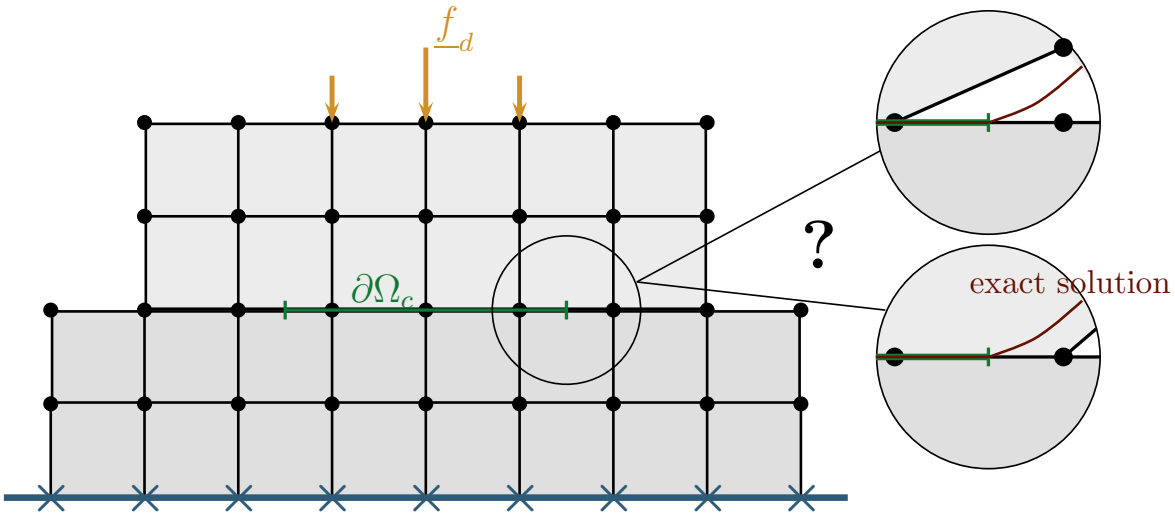

Figure I.6: Problem with the boundary of the contact zone for a linear approximation

A straightforward answer would be to change the mesh at every step in order to match the supposed contact zone. Nevertheless re-meshing is a costly operation and one might want to avoid it if possible. Rather than doing a full re-meshing of the domain only part of the node are moved. This method is often used for high-order FEM and leads to the *rp*-FEM. The *r* stand for the relocation of the nodes and *p* represents the order of the approximation. A study

of this method can be found in [Nübel et al., 2006] and an application to contact problems is done in [Franke et al., 2010].

Another possibility to overcome this problem without modifying to the mesh is to use the eXtended Finite Element Method (X-FEM) and will be presented later on.

Compatibility of meshes Contact is a matter involving several bodies and interaction between them. Therefore discretizations of the solids have to allow the synergy of each contributions. In order to do so, the discretization of the elements involved in contact interfaces have to be carefully designed. The simplest discretization is to have the nodes of the mesh, which are part of the contact zone, match their counterparts on both solids involved (the meshes are then referred as matching). Therefore this method is referred as Node to Node method. Even if this method passes the patch test (good transfer of a uniform pressure through the contact interface), it restrains the domain of application. Indeed the degree of approximation of the field is limited and no sliding nor large deformations can be taken into account.

Another option is to use a Node to Segment approach which allows non-matching meshes [Hughes et al., 1977]. This method is not as restrictive as the Node to Node and also easy to implement but does not pass the patch test as it is [Crisfield, 2000]. Some adaptation of it was designed in order to overcome this drawback and recover some symmetry in the problem [Zavarise and De Lorenzis, 2009, Oliver et al., 2009]. However it increases the cost and the complexity of the method.

Last, let us mentioned a Segment to Segment discretization and the associated framework: the Mortar Method. It is closely related to the Domain Decomposition method [Wohlmuth, 2001]. For an application to contact problem, the reader is referred to [Belgacem et al., 1998] and [McDevitt and Laursen, 2000]. The main idea is to use a "mortar surface" (which can be one of the solid contact surface) to define the pressure. This method has good stability properties but can be quite challenging to implement. A great care has also to be taken in the choice of discretization space as it will be mentioned in the next paragraph.

Stable approximation fields It is common in mechanical engineering to use, in a same formulation, fields of a different nature. Such formulation is called a "mixed problem". A typical example is the formulation often used for incompressible Navier-Stokes equations where the two fields of interest are the velocity and the pressure. Previously, we mentioned several possible formulations for contact problems. Several of them fit in the mixed problem category, particularly the formulation involving Lagrange multiplier.

With such problems, a special care has to be taken both with the formulation and the discretization of the fields in order to be numerically stable. Such considerations were raised in [Babuška, 1973, Brezzi, 1974]. In these papers, a mathematical study has been done. It leads to the so called Babuška-Brezzi (BB) condition or more generally to the inf-sup condition. Let us take again the previous notations and name $c(p, \underline{u})$ the bilinear forms coupling the two fields p and $\underline{u}$. The inf-sup condition associated to this form is satisfied when:

$$\inf_{p \in \mathcal{P}} \sup_{\underline{u} \in \mathcal{U}} \frac{|c(p, \underline{u})|}{\|p\|_{\mathcal{P}} \|\underline{u}\|_{\mathcal{U}}} = \beta > 0 \tag{I.57}$$

Coupled with continuity property, the inf-sup condition controlled the conditioning of this operator. As it was mentioned, a discretize version of the fields are used. Let us approximate

$p \in \mathcal{P}$ by $p^h \in \mathcal{P}^h$ and $\underline{u} \in \mathcal{U}$ by $\underline{u}^h \in \mathcal{U}^{h'}$. The parameters h and h' handle the discretization coarseness. Then, the discretize inf-sup condition is:

$$\inf_{p^h \in \mathcal{P}^h} \sup_{\underline{u}^h \in \mathcal{U}^{h'}} \frac{|c(p^h, \underline{u}^{h'})|}{\|p^h\|_{\mathcal{P}^h} \|\underline{u}^{h'}\|_{\mathcal{U}^{h'}}} = \beta_{hh'} > 0 \tag{I.58}$$

In order to guarantee the stability of the formulation a constant β_0 needs to be found such that $\beta_{hh'} \geq \beta_0 > 0$ for all h and h'. Not achieving the inf-sup condition can lead for instance to spurious oscillations of the solution. Such condition can be fulfilled by picking a compatible pairing for the approximation fields $(\mathcal{P}^h, \mathcal{U}^{h'})$. Also, if different options are available, the choice of the operator $c(\bullet, \bullet)$ is of a tremendous influence on β_0. Several studies have been carried to find the right pairing for different operators as for instance in [Kikuchi and Oden, 1988, Hughes, 2012]. A particular effort on this matter was made by the Domain Decomposition community for the Mortar Method. Special Lagrange multiplier spaces have been designed to fulfill the inf-sup condition for non-matching meshes. The conception of these particular spaces are based on the trace operator on the mortar zone [Bernardi et al., 1993] and more recently on dual space properties [Wohlmuth, 2001]. Examples of these special space for 1D discretization is given Figure I.7.

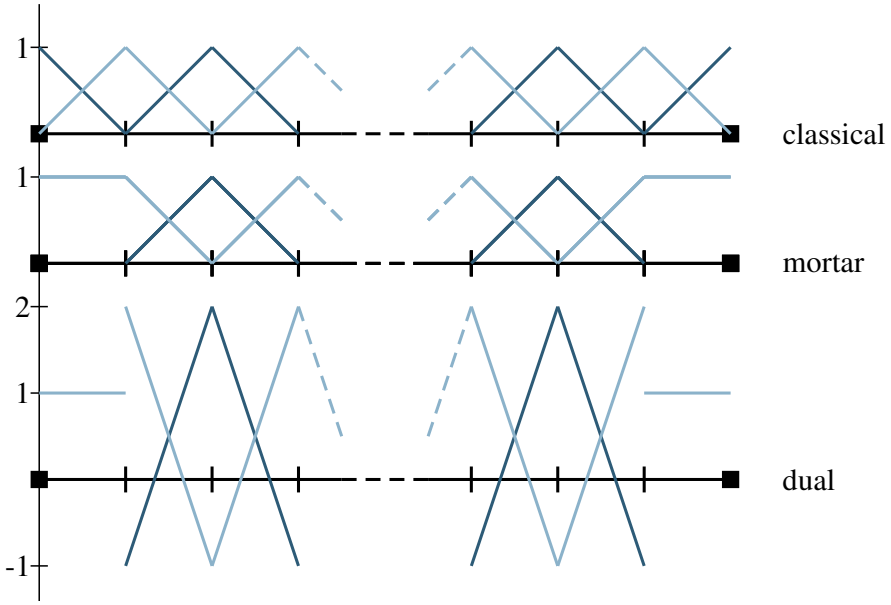

Figure I.7: Different approximation fields for the Lagrange multiplier. From top to bottom there are the classical approximation then the original mortar approximation and finally the one using dual properties as a construction basis.

I.2.2 Different methods of resolution

In section I.1.3 several possibilities were offered to build a mathematical framework for contact problems. In this section, we will now present some methods in order to compute numerically the solution of these problems. It was explained previously that a discretized version of the formulation given in section I.1.3 leads to a linear problem to be solved if the contact zone is known. Obviously, the contact zone is *a priori* unknown and iterative algorithms are used to

solve this problem. The contact problems fit into the minimization under constraints class of problems. This quite active field of study led to numerous iterative algorithms. The focus will be maintained on the two most used algorithms in contact mechanics, namely the active-set and Uzawa algorithms.

The simplest and widely use algorithm is the active-set. It can be used both with the penalization and the Lagrange multiplier formulation. To begin with, potential contact nodes are classified into two "sets": the active set and the non-active set. Being part of the active set means that the constraint is supposed to be active on this node (i.e. the node is part of the contact zone). The other nodes are obviously members of the second set. For a given set and thus a given contact zone the equilibrium equations are solved. Then, the KKT conditions are checked. Every nodes part of the active set for which $p_n > 0$ is removed from this set. On the contrary, every node in the non-active set for which $g_n < 0$ is added to the active set. This process is repeated up to convergence. A drawback of this algorithm is that flip-flop phenomena can appear. The convergence of this algorithm has only been proven if a single state (active/none-active) is changed at a time. Also, the convergence criteria (crit) is not easy to define. A minimal tolerance can be set or detection of a loop (the algorithm is coming back to an active set already obtained) in the iterations can be used. Nevertheless it is really easy to implement. When used with penalty parameter, it can be updated if the algorithm does not match the required tolerance on the contact constraints at the end of a set of iterations.

Algorithm 1: Active-set algorithm

```
Initialize active set (AS): usually AS=∅;
(Initialize penalty term ϵ_n ← ϵ_0);
while !crit do
    Solve equilibrium problem (Equation (I.34) or (I.39));
    Check penetration:
    for every nodes in non-active set (NAS) do
        if g_n < 0 then AS← node;
    Check reaction:
    for every nodes in AS do
        if p_n > 0 then NAS← node;
    (Update ϵ_n if necessary);
```

The other widely used method in contact mechanics is the Augmented Lagrange formulation. Even if this formulation was designed to allow the use of a Newton's method, an Uzawa algorithm is often used instead as mentioned in section I.1.3. With an Augmented Lagrange formulation, two fields have to be found: the displacement field and the Lagrange multiplier field. In the Uzawa method, both fields are searched separately. Indeed at one iteration step, the Lagrange multiplier p are maintain constant (thus the notation $p = p^c$). Then the equilibrium equation (I.42) is solved for this given p^c. Using the result of this equation the Lagrange multiplier are updated with a defined law. A classical example of such law can be found in

Algorithm 2 but the reader will find different options in [Wriggers, 2006] or [Bertsekas, 1982].

Algorithm 2: Uzawa algorithm

Initialize fields and penalty: $u \leftarrow u_0$, $p^c \leftarrow p_0^c$ and $\epsilon_n \leftarrow \epsilon_0$;
while *!crit* **do**
  Solve equilibrium problem (Equation (I.42));
  Update Lagrange multiplier:
  for *every possible contact nodes* **do**

$$p^c \leftarrow \begin{cases} p^c + \epsilon_n g_n, & p^c + \epsilon_n g_n \leq 0 \\ 0, & p^c + \epsilon_n g_n > 0 \end{cases}$$

  (Update ϵ_n if necessary);

Up to now, only two major resolution algorithms have been presented. We will now only mentione two other possibilities coming from the optimization community (see [Luenberger, 1984])and give the reader the references in which a detailed explanation can be found:

- Successive Quadratic Programming (SQP) [Spellucci, 1998, Björkman et al., 1995]
- Linear Complementary Programming (LCP) [Klarbring, 1999]

Conclusion

In this chapter a brief state of the art was made. We remind the reader that a more complete work was done in [Wriggers, 2006] for contact mechanics. After setting the mathematical framework, several methods of resolution were proposed. The reader is urged to pay special attention to the Lagrangian formulation as it is going to be used later on. A special focus was put on the difficulties arising from the discretization. In the next chapter, a method is proposed to overcome some of these difficulties combined with an efficient iterative algorithm.

II

Generalities about the ILS

Contents

Summary

The inequality level-set has been first developed for kinematic constraints in [Bonfils, 2011]. However, a general description of this method was never done. Therefore, the goal of this chapter is to present a broad framework for a class of problems that can be handled by the ILS. The ILS is based on two main features to solve constrained problems. The first one is a good representation of the constraint zone. The second one is an efficient framework to find this zone. In this chapter we aim to explain the method and the numerical tools needed to apply the ILS.

Résumé

Ce chapitre est consacré à la mise en place de l' ILS dans un cadre général. En effet, cet méthode n'est pas restreinte aux seuls problèmes de contact. De ce fait, une première étape consiste à définir les classes de problèmes pouvant être traités par cette méthode. Pour résumer, cette méthode s'adresse aux problèmes pour lesquels, en plus d'une équation d'équilibre, des contraintes d'inégalités apparaissent du fait d'une méconnaissance d'une zone. Par exemple, une contrainte d'inégalité portant sur tout le domaine peut être transformer en égalité en fixant la quantité contrainte à sa valeur seuil sur une zone précise. Cependant, cette zone n'est pas connue *a priori*. Il est évident que le contact rentre dans cette catégorie avec comme contrainte d'inégalité la non-pénétration et la zone inconnue étant la zone de contact.
Le principe de l'ILS est de découpler le problème d'équilibre et la recherche de la zone inconnue. Dans un premier temps, les équations d'équilibre sont résolues pour une zone donnée. Grâce à la solution obtenue, une optimisation de forme est faite afin de se rapprocher de la zone exacte donnant ainsi lieu à un algorithme itératif. Afin de pouvoir appliquer cette optimisation de forme, il faut dans un premier temps être capable de définir précisément la zone inconnue. Pour ce faire, les fonctions de niveau (ou *level-set*) sont utilisées. Elles autorisent une représentation de la zone sans être fortement contraint par le maillage. De plus l'implémentation de ces fonctions ouvre la porte à l'utilisation d'enrichissements (via X-FEM) afin de représenter au mieux les phénomènes frontaliers. Ensuite, il faut avoir un critère pour pouvoir estimer la bonne position de la zone à trouver. Ce critère peut se fonder sur une connaissance du problème ou sur l'utilisation de la mécanique configurationnelle. De ce critère, il faut être capable de connaître sa variation pour une modification de la zone inconnue. Cette information est obtenue grâce à la dérivée directionnelle appliquée aux équations d'équilibre. Avec toutes ces cartes en main, une méthode de Newton peut être mise en place afin d'annuler le critère en modifiant la forme de la zone jusqu'à s'approcher suffisamment de la position exacte.
Finalement, la procédure numérique associée à cette méthode est mise en place. La prise en compte de nombreux paramètres garantissant une bonne convergence de la méthode donne lieu à la proposition d'un algorithme général (Algorithm 3).

II.1 Type of problems handled by the ILS

As its name suggests, the ILS method was designed to solve problems involving inequalities. More particularly, inequalities arising from the ignorance of a zone where criterion have to be met. This means that, if we do know the mentioned zone then, the problem is only a set of equalities. Let us take, in this chapter, a general problem to explain the method. The unknown of our problem is a finite set of fields $\{u_i(x)\} \in \mathcal{U}_i$ defined on a physical domain $\mathcal{D}$ or a part of it $\mathcal{D}_i$. The problem is composed of a set of equalities ($\mathcal{E}$) and of a set of inequalities ($\mathcal{I}$) which need to be fulfilled in all the domain of definition. This can be written as:

Problem 9

Find $u_i \in \mathcal{U}_i$ such that:

$$\left\{ \begin{array}{rcll} a(u_i) & = & f & \text{on } \mathcal{D}_i \quad (\mathcal{E}) \\ c(u_i) & \geq & 0 & \text{on } \mathcal{D}_i \quad (\mathcal{I}) \end{array} \right. \tag{II.1}$$

This last formulation is, for several reasons, not well suited for computational purpose. Therefore, some steps have to be taken before solving these equations. The first one is to rewrite the set of equalities ($\mathcal{E}$) into their weak form. The motivation for such a change was already highlighted in Section I.1.1.3. Therefore, given that $\{u_i(x)\}$ satisfies the needed regularity properties, we introduce the test functions $u_i^\star \in \mathcal{U}_i^\star$ with $\mathcal{U}_i^\star$ a space regular enough associated to $\mathcal{U}_i$. Then, the former problem can be written as:

Problem 10

Find $u_i \in \mathcal{U}_i$ such that $\forall u_j^\star \in \mathcal{U}_j^\star$:

$$\left\{ \begin{array}{rcll} a_{\mathcal{D}}(u_i, u_j^\star) & = & f_{\mathcal{D}}(u_j^\star) & \quad (\mathcal{E}_v) \\ c(u_i) & \geq & 0 \quad \text{on } \mathcal{D}_i & \quad (\mathcal{I}) \end{array} \right. \tag{II.2}$$

For the following, it is important to notice the dependence of the applications to their domain of definition. Hence, the supscript notation is used which might appear heavy to read but shall help the comprehension of the method. For instance $a_{\mathcal{D}}(\bullet, \bullet)$ and $f_{\mathcal{D}}(\bullet)$ depend on $\mathcal{D}$ as hinted by the subscript. Nevertheless, the inequalities are still present. As underlined earlier, the particularity of our problem is that there is a set of zones $\{\mathcal{D}_i^c\}_{\text{ex}} \subset \{\mathcal{D}_i\}$ such that the inequalities can be converted to equalities with this extra information. These particular zones represent the domains where the constraints are active inside and not violated outside. Consequently, Problem 10 is equivalent to:

Problem 11

Find $u_i \in \mathcal{U}_i$, knowing $\{\mathcal{D}_i^c\}_{\text{ex}}$ such that $\forall u_j^\star \in \mathcal{U}_j^\star$:

$$\left\{ \begin{array}{rcll} a_{\mathcal{D}}(u_i, u_j^\star) & = & f_{\mathcal{D}}(u_j^\star) & (\mathcal{E}_v) \\ c(u_i) & = & 0 \quad \text{on } \mathcal{D}_i^c & (\mathcal{E}^{\mathcal{D}_i^c}) \end{array} \right. \tag{II.3}$$

or in its full weak form with coupled equations:

$$\left\{ \begin{array}{rcrcll} a_{\mathcal{D}}(u_i, u_j^\star) & + & c^a_{\mathcal{D}_i^c}(u_i, u_j^\star) & = & f_{\mathcal{D}}(u_j^\star) & (\mathcal{E}_v) \\ c^c_{\mathcal{D}_i^c}(u_i, u_j^\star) & & & = & l_{\mathcal{D}_i^c}(u_j^\star) & (\mathcal{E}_v^{\mathcal{D}_i^c}) \end{array} \right. \tag{II.4}$$

As advertised, there is only equalities in this last formulation. Depending on the method used, the passage from the strong constraint formulation in (II.3) to the weak one (II.4) might require the addition of unknowns (this is the case for Lagrange multiplier based method for instance). Practically, it means that we tried to find not only $\{u_i(x)\} \in \mathcal{U}_i$ but also $(\{u_i(x)\}, \{u_{i'}(x)\}) \in \mathcal{U}_i \times \mathcal{U}_{i'}$. For the sake of simplicity the additional unknowns are included without any change of indices and without more precision $\{u_i(x)\}$ refers to the set of all unknowns.

That last formulation is obviously of no practical use as $\{\mathcal{D}_i^c\}^{\text{ex}}$ is unknown. A pragmatic version would therefore be:

Problem 12

Find $\{\mathcal{D}_i^c\}$ such that all constraints are fulfilled ($\{\mathcal{D}_i^c\} = \{\mathcal{D}_i^c\}_{\text{ex}}$):

$$c(u_i) \geq 0 \quad \text{on } \mathcal{D}_i \text{ (the all domain)}$$

and find $u_i \in \mathcal{U}_i$ such that $\forall u_j^\star \in \mathcal{U}_j^\star$:

$$\left\{ \begin{array}{rcrcll} a_{\mathcal{D}}(u_i, u_j^\star) & + & c^a_{\mathcal{D}_i^c}(u_i, u_j^\star) & = & f_{\mathcal{D}}(u_j^\star) & (\mathcal{E}_v) \\ c^c_{\mathcal{D}_i^c}(u_i, u_j^\star) & & & = & l_{\mathcal{D}_i^c}(u_j^\star) & (\mathcal{E}_v^{\mathcal{D}_i^c}) \end{array} \right. \tag{II.5}$$

As it was already mentioned in Section I.2.2, an iterative algorithm is used in these circumstances. A classical method is to start with a supposed set $\{\mathcal{D}_i^c\}_0$. Then Problem 12 is solved with $\{\mathcal{D}_i^c\}_0$. Using the solution of the later problem, a correction is made which makes $\{\mathcal{D}_i^c\}_0$ evolve leading to a new constraint zone $\{\mathcal{D}_i^c\}_1$. Then this process is started again, leading after k iterations to a constraint zone $\{\mathcal{D}_i^c\}_k$. It is stopped when $\{\mathcal{D}_i^c\}_k$ is considered close enough to $\{\mathcal{D}_i^c\}_{\text{ex}}$ (of course this notion as to be defined carefully as $\{\mathcal{D}_i^c\}_{\text{ex}}$ is unknown).

The question is how to drive the correction on $\{\mathcal{D}_i^c\}_k$ in order to converge to $\{\mathcal{D}_i^c\}_{\text{ex}}$. The

main goal of the ILS is to offer a method to define and compute $\{\mathcal{D}_i^c\}_k$ efficiently in a discrete setting.

The attentive reader would have noticed the parallel of this general problem with the contact problems. Indeed, taking the notations of Section I.1.2 the Problem 9 is equivalent to the contact problem. The equation set $(\mathcal{E})$ being the equilibrium equations and the inequality set $(\mathcal{I})$ the contact constrains. Then, any weak formulation of Section I.1.3 fits into the general formulation of Problem 12. More detailed explanations will be given in the next chapter.

Let us give another concrete examples of this class of problem. The first ever treated by the ILS method was involving inequality kinematic constraints. It was studied in a former thesis [Bonfils, 2011] and lead to an article [Bonfils et al., 2012]. It was applied to a linear, two dimensional, elastic problem on a domain Ω. The kinematic constrain was a limitation of the trace of $\underline{\underline{\epsilon}}$ by a constant α_ϵ. As it was mentioned Section I.1.3.2, Lagrange multipliers can be used and must fulfill $p \geq 0$. We define $\mathcal{D}^c$ as the zone where $\mathrm{Tr}(\underline{\underline{\epsilon}})$ should be equal to α_ϵ. Thus the problem to solve, written in Problem 12's fashion is:

Problem 13

Find $\mathcal{D}^c$ such that:

$$p \geq 0 \quad \text{and} \quad \alpha_\epsilon - \mathrm{Tr}(\underline{\underline{\epsilon}}) \geq 0$$

and find $u \in H^1(\Omega)$ and $p \in L^2(\mathcal{D}^c)$ such that $\forall u^\star \in H^1(\Omega)$ and $p^\star \in L^2(\mathcal{D}^c)$:

$$\begin{cases} \underbrace{\int_\Omega \underline{\underline{\epsilon}}(\underline{u}) : \underline{\underline{\underline{\underline{K}}}} : \underline{\underline{\epsilon}}(\underline{u^\star}) \, \mathrm{d}\Omega}_{a_{\mathcal{D}}(\underline{u},\underline{u^\star})} + \underbrace{\int_{\mathcal{D}^c} p \mathrm{Tr}(\underline{\underline{\epsilon}}(\underline{u^\star})) \, \mathrm{d}\Omega}_{c^a_{\mathcal{D}_i^c}(p,\underline{u^\star})} = \underbrace{\int_\Omega \underline{f_d} \underline{u^\star} \, \mathrm{d}\Omega + \int_{\partial\Omega_t} \underline{t_d} \underline{u^\star} \, \mathrm{d}\Gamma}_{f_{\mathcal{D}}(\underline{u^\star})} \\ \underbrace{\int_{\mathcal{D}^c} p^\star \mathrm{Tr}(\underline{\underline{\epsilon}}(\underline{u})) \, \mathrm{d}\Omega}_{c^c_{\mathcal{D}_i^c}(\underline{u},p^\star)} = \underbrace{\int_{\mathcal{D}^c} p^\star \alpha_\epsilon \, \mathrm{d}\Omega}_{l_{\mathcal{D}_i^c}(p^\star)} \end{cases} \tag{II.6}$$

To sum up, Problem 12 gives a formulation which, coupled with an iterative algorithm, gives the solution of Problem 9 (see Figure II.1). Some iterative algorithms have already been presented in Section I.2.2. In the following, the motivation for several aspects of the ILS method are going to be presented leading naturally to the ILS formulation.

II.2 Use of level-sets and the X-FEM

The last section highlights the importance of $\{\mathcal{D}_i^c\}$. It is therefore crucial to be able to represent efficiently these zones. Furthermore, at the boundary of them, discontinuities might appear. For instance, in the contact case, if there is adhesion on the contact zone or simply if the contact zone is erroneous , a weak discontinuity of the displacement occurs. Thus it is also essential to be able to represent these discontinuities. We propose here an answer based on two key

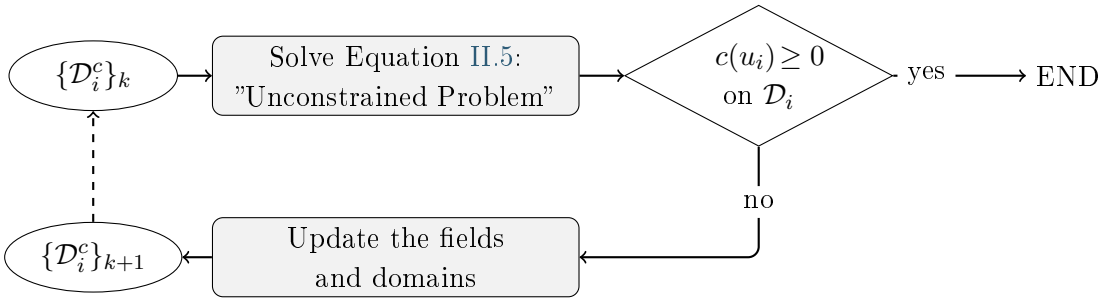

Figure II.1: General principle of resolution for Problem 12's type.

points: level-sets and X-FEM. For the sake of simplicity (and as it will be the case for contact problems) we are going to assume that only one type of constraint is to be enforced, that is to say $\{\mathcal{D}_i^c\} = \mathcal{D}^c$.

II.2.1 An answer to define the boundary of a domain

Following a moving interface is of a great interest in several domains. To name but a few, there is image processing, optimal design, material interfaces, domain interfaces such as burning flame or waves. In this thesis, the boundary that is followed is the frontier of the constraint domain $\mathcal{D}^c$ and will be noted Γ. Different techniques have been developed to track and move interfaces. Among them let us cite the Marker and Cell method [Harlow et al., 1965], the Immersed Boundary method [Peskin, 2002] or the Volume Of Fluid method [Hirt and Nichols, 1981]. A state of the art review was given in [Tryggvason et al., 2001].

Here we will focus on a family of method introduced in [Osher and Sethian, 1988] which are based on a mathematical object called level-set. A summary of the fundamental work on this subject was published in the two books [Sethian, 1999, Osher and Fedkiw, 2003]. The use of level-sets is particularly well coupled with the FEM. Furthermore, a lot of level-sets mathematical properties will be useful for the ILS. Let us first define what is a level-set:

Check point

A level-set L is a set associated to a function ϕ (called the level-set function) and a constant c such that

$$L_{[\phi]}(c) = \{\{x_1, \cdots, x_n\} | \phi(x_1, \cdots, x_n) = c\} \tag{II.7}$$

If the value of c is fixed, the corresponding set is called an iso-level. A particular case is the iso-zero, being the place where ϕ is equal to zero:

$$L_{[\phi]}(0) = \{\{x_1, \cdots, x_n\} | \phi(x_1, \cdots, x_n) = 0\} \tag{II.8}$$

Therefore one can use a level-set to define a boundary on a domain. Indeed, if the function ϕ is defined on the domain such that $\phi = c$ on the boundary, then $L_{[\phi]}(c)$ is the set of all points

on this boundary. Classically, the iso-zero level set is used:

$$\Gamma = L_{[\phi]}(0) = \{\{x_1, \cdots, x_n\} | \phi(x_1, \cdots, x_n) = 0\} \tag{II.9}$$

A particularly interesting type of level-set function is the signed distance function. Starting from the iso-zero level-set, the function ϕ is equal to the distance to it with an arbitrary sign depending on the side to the boundary.

A first asset of level-sets is that it is straightforward to know if a point on one side or the other. For the sake of simplicity assume that the boundary is set to be the iso-zero. Then, depending if $\phi(x) > 0$ or $\phi(x) < 0$ the point x is on one side or the other of the boundary. As a choice, the concept of "inside" is defined as the set of points where $\phi(x) \leq 0$. On the contrary if $\phi(x) \geq 0$ then it is considered as "outside". It is easy to also define the notion of strictly inside (resp. outside) by changing the inequality to $\phi(x) < 0$ (resp. $\phi(x) > 0$). Therefore, all domains or quantities inside the boundary will be denoted with a exponent "$-$" whereas the ones outside with a "$+$".

Example of level-set in 1D In one dimension, the level-set function is a one-variable function. The boundary is a point and the signed distance function associated is therefore the function giving the signed distance to this point.

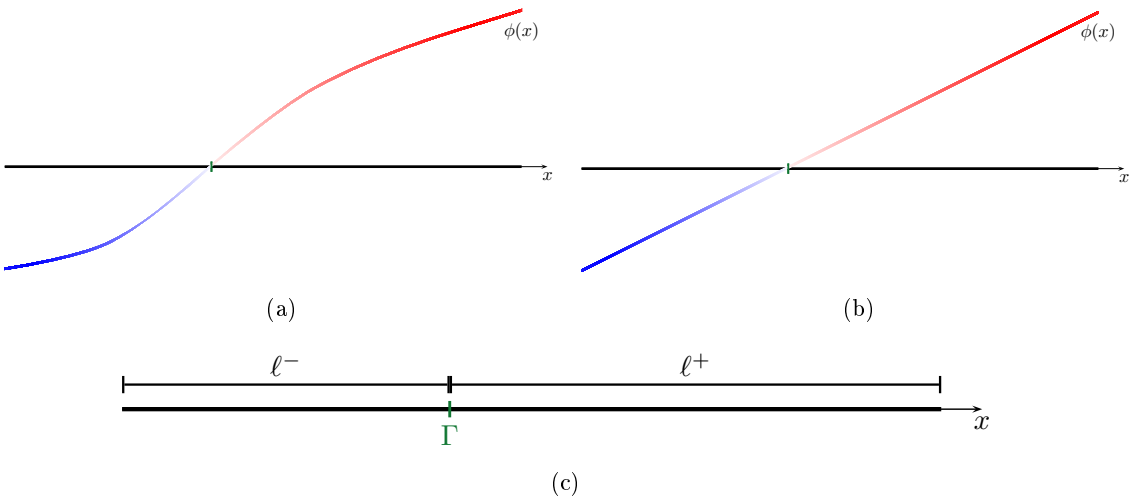

Figure II.2: The level-set has to fulfill the properties illustrated in (c), (b) shows one of the possible choice and (a) the particular case of a signed distance function.

Example of level-set in 2D Taking the case of a surface, the associated boundary is a curve. It is not to be confused with a simplification of the 3D case under hypothesis such as axy-symmetry. This situation is the most interesting one for contact problems since the contact zone is a surface.

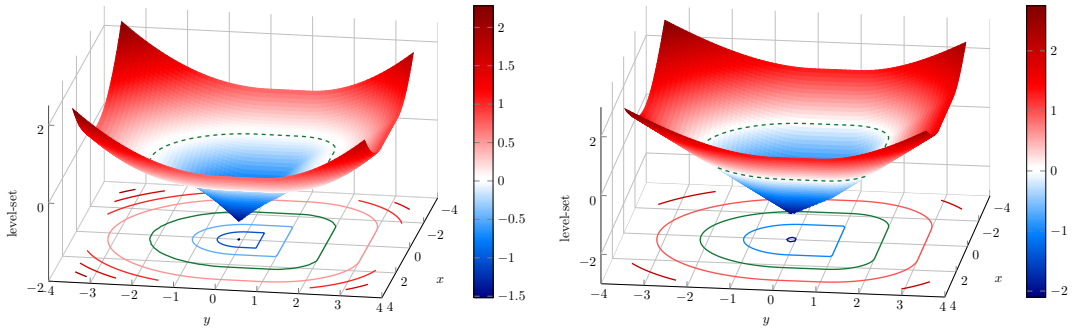

(a) (b)

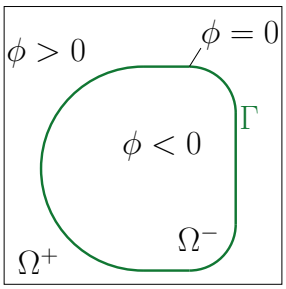

(c)

Figure II.3: As before (a) represents a possible level-set whereas (b) illustrates the signed distance function associated.

Example of level-set in 3D Last, the 3D case has a 2D boundary.

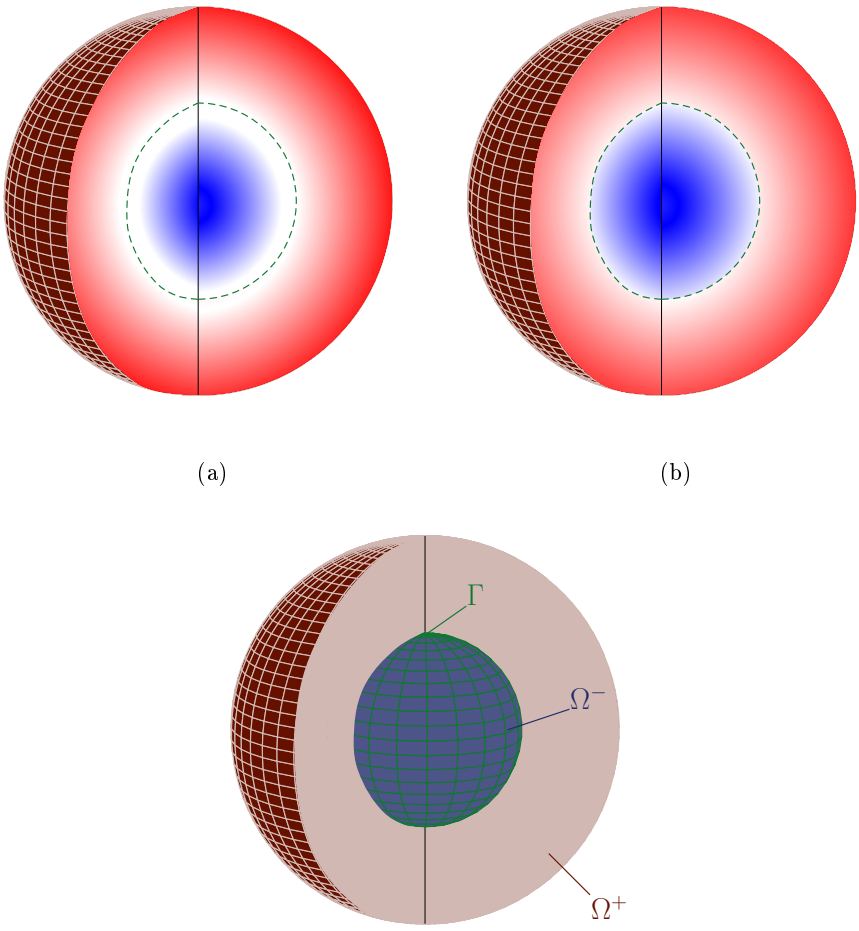

(a) (b)

(c)

Figure II.4: Again, (a) is a level-set and (b) the special signed distance level-set.

II.2.1.1 Useful properties

On top of being able to differentiate easily on which side of the boundary a point is, level-sets have a great adaptability. For instance, Boolean operations can easily be done. Taking two level-set functions ϕ_1 and ϕ_2 the associated level-set function ϕ for:

- the intersection is $\phi = \max(\phi_1, \phi_2)$,
- the union is $\phi = \min(\phi_1, \phi_2)$,
- the complement of ϕ_1 is $\phi = -\phi_1$.

Several information can be deduced from the level-set function ϕ. Its gradient is normal to all the iso-levels. Therefore it can be used to define the unit outward normal vector $\underline{n}$ to these iso-levels:

$$\underline{n} = \frac{\nabla\phi}{|\nabla\phi|} \tag{II.10}$$

This is obviously of great interest for the particular case of the iso-zero as it gives access to the normal to the boundary. Another information one can get about an iso-level is its mean curvature κ. The mean curvature is defined as the divergence of the normal. Thus it can be computed using the level-set function:

$$\kappa = \text{div}(\underline{\mathfrak{n}}) = \text{div}\left(\frac{\nabla\phi}{|\nabla\phi|}\right) \tag{II.11}$$

In the special case of signed distance function $|\nabla\phi| = 1$ and can thus be removed from the precedent formulae. Moreover, taking a point $\underline{x}$, it is easy to find its closest point $\underline{x}_c$ of the iso-zero using the formula:

$$\underline{x}_c = \underline{x} - \phi(\underline{x})\underline{\mathfrak{n}} = \underline{x} - \phi(\underline{x})\nabla\phi(\underline{x}) \tag{II.12}$$

II.2.1.2 Compulsory use of level-sets for ILS

Level-sets were introduced in this thesis in order to track the constraint zone. In order to match the level-sets notations, the constrained zone previously noted $\mathcal{D}^c$ will from now on be called $\mathcal{D}^-$. A big advantage of using implicit functions to represent this boundary is that, with a FEM strategy, the position of the boundary is not strongly dependent of the mesh. It is indeed still dependent of the mesh as any such approximation methods. An error is made if the exact position of the boundary does not live in the approximation space and the error is linked to the characteristic size of the mesh h. Nevertheless it is not directly linked to the position of the nodes itself. That means that if the characteristic size of mesh used is the same, the shape position is not strongly influenced. This property will be highlighted in the numerical example sections.

Let us focus a moment on the particular case of contact problems. The constrained zone $\mathcal{D}^-$ is the zone in contact (formally called $\partial\Omega_c$ in Figure I.3 and denoted Ω^- from now on) and Γ the boundary of the contact zone. Therefore in most cases, the possible contact domain is of a one lower dimension as the full body (this is not the case if working with degenerated model such as membrane, shell or beam as it will be seen in Chapter III). For instance, the contact zone of a 3D body is at most a surface which can be defined in a 2D space. Therefore, a lot of the computation specific of the ILS method will be carried only on this lower dimensional entity or a small part of the whole domain, saving a lot of computational cost.

II.2.1.3 Another interesting use

Another independent use of level-sets is to represent the boundary of the body. Indeed, for complicated domains, mesh generation can be of great difficulties. The idea is therefore to create a simple mesh and represent the boundary of the body on it. Several methods can be used but we will focus on the level-set approach. This work was started in [Belytschko et al., 2003] and improvement were brought by many contributions such as [Dréau et al., 2010, Legrain et al., 2012] for higher order representation. With this approach, it is easy to compute the penetration function between two solids (as it is the value of the level-set associated to one solid on the boundary of the other), the closest point or the normal vector. Furthermore, having an easy access to the curvature allows the detection of possible problems and the smoothing of the geometry if necessary. An example of this use can be found in [Khoei and Nikbakht, 2006].

II.2.1.4 Useful algorithms

Most of the algorithms for level-sets are based on a type of equation called Hamilton-Jacobi equation. Indeed, most equations driving the motion of the level-set can be written in the form:

$$\frac{\mathrm{d}\phi}{\mathrm{d}t} + H(\nabla\phi) = 0 \tag{II.13}$$

with H the functional called the Hamiltonian and t a fictitious time. For instance, the displacement of the level-set in its normal direction with a speed w is governed by the equation:

$$\frac{\mathrm{d}\phi}{\mathrm{d}t} + w|\nabla\phi| = 0 \tag{II.14}$$

Likewise, the propagation of a function f defined on the iso-zero level-set to the whole domain can be computed using the equation:

$$\frac{\mathrm{d}f}{\mathrm{d}t} \pm \frac{\nabla\phi}{|\nabla\phi|}\nabla f = 0 \tag{II.15}$$

The sign "$\pm$" changes with the side on which the function is extended. The sign "$+$" is used for a propagation on Ω^+ and "$-$" for Ω^-.

Finally, the construction of a signed distance function can also use an Hamilton-Jacobi equation with an initialization on the iso-zero level-set:

$$\frac{\mathrm{d}\phi}{\mathrm{d}t} \pm |\nabla\phi| = \pm 1 \tag{II.16}$$

Hamilton-Jacobi equations are really common in mechanics and especially in computational fluid dynamic. A review of most of the algorithms used for level-set are given in [Sethian, 1999, Osher and Fedkiw, 2003].

Usually, these equations are solved using finite differences for both space and time. It was shown in [Shu and Osher, 1988] that in order to improve the resolution only high order accurate approximation for the space discretization was really needed. Indeed, forward Euler time discretization is often enough for this purpose. Nonetheless, in order to ensure stability of the method, condition linking the space (Δx) and time (Δt) discretization have to be met. For instance, the Courant Friedreichs Lewy (CFL) condition is often used:

$$\Delta t < \frac{\Delta x}{\max(|w|)} \tag{II.17}$$

On the other hand, an accurate spacial discretization makes a tremendous difference on the quality of the solution. Based on physical properties of these equations, "upwind" discretizations are used. Some advance discretization were also developed with for instance the Hamilton-Jacobi essentially non-oscillatory (ENO) [Harten et al., 1987] and weighted essentially non-oscillatory (WENO) [Liu et al., 1994] methods.

A special algorithm was also designed to solve the particular problem of the propagation of a function in the normal direction or the creation of a signed distance function from the iso-zero. This specific algorithm is called the Fast Marching Method. Starting from the iso-zero, a small band of nodes around it (the size depending on the spacial discretization) is initialized using a classical method and make the set of fixed value nodes. Then, for a trial set composed of all the adjacent nodes to the fixed value nodes, a tentative value of the problem is computed using

only the fixed value nodes. The trial node with the smaller tentative value is then added to the fixed value nodes and its computed value is set. The trial test is updated and the tentative values are:

- computed on the new nodes,
- updated on the former trial nodes adjacent to the newly added fixed node.

This update process is carried on up to the point where all the nodes are fixed. This algorithm is particularly efficient, especially if a proficient sorting algorithm is used to find the smallest tentative value. For example, a sorting algorithm was designed in [Tsitsiklis, 1995] for binary tree.

It is worthwhile to mentioned that adaptive algorithms are often used to focus the computational cost close to the iso-zero. Indeed, in most situation only the iso-zero is really worth computing accurately.

II.2.2 The strategy to use it with the FEM: X-FEM

Being able to represent boundary by implicit functions is not enough to carry a full computation. Indeed, in the classical FEM the computation is done on the full element. Therefore, as the boundary can cut through the element, strategies have to be designed. Furthermore, the possible singularities at the boundary have to be handled with care in order to keep a good convergence of the method. The X-FEM is going to be introduced here. It first appears in [Moës et al., 1999] in order to handle crack growth. It has been since a dynamic field of research with applications in different domains and several improvements. Let us see, point by point, what makes the X-FEM.

II.2.2.1 A specific integration scheme

To illustrate our point, let us take the example given in Figure II.5(a). The computation needs to be carried only on Ω^-. In order to deal with the computation a classical discretization of the domain is taken. It is chosen here to work with triangular elements and a linear interpolation. The equivalent numerical strategy can be find in [Moës et al., 1999] for other type of elements, [Dréau et al., 2010, Legrain et al., 2012] for higher order interpolations or in [Belytschko et al., 2003] for 3D problems. On the discretized version Figure II.5(b) the boundary cut through the elements. As it was explained in Section I.2, a key point of the FEM is the integration over each elements. Thus it is important to design an integration scheme that allows to take into account only the desirable contributions without modifications of the degrees of freedom or re-meshing. For every cut elements, integration sub-elements are created following the cut (see Figure II.5(c) for different cases). This sub-elements do not have to fulfill the geometrical properties needed by the classical elements for a good behavior of the FEM. Therefore the complexity of mesh-generation is avoided and they can be created in a straightforward fashion. It is to notice that the degrees of freedom are unchanged. The integration is then carried usually on the original mesh except that when the integration are made on a cut element the sub-elements are used. The sign of the level-set is used as a filter in order to know if the integration should be done or not on a sub-element.

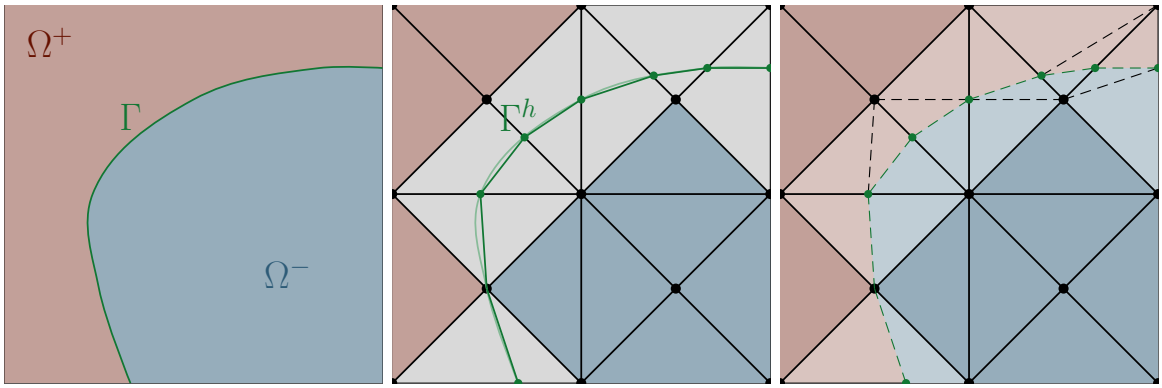

(a) (b) (c)

Figure II.5: Example of the special integration technique to integrate only on a part of a domain defined by a level-set. (a) represents the problem to handle, (b) its discretization and (c) shows the integration mesh.

II.2.2.2 Enrichment of the fields

To enrich a field means adding to the classical interpolating functions new ones. There can be different motivations to do so. First let us take back the problem of the above section and assume that the domain Ω^+ is also a domain of interest but is independent of Ω^-. Even with the special integration, the degrees of freedom in Ω^+ which belong to a cut element come into the integration over Ω^-. We will see that an Heaviside enrichment deals with the problem. Another interesting use of enrichment is to increase the rate of convergence of the problem. If the numerician as some knowledge of a special behavior of the solution, such as some discontinuities or a local analytic solution then, it is interesting to add it into the formulation.

Let us see how it is done in practice. In order to incorporate these functions into the finite element approximation, the property of the partition of unity (introduced in [Melenk and Babuška, 1996]) is used. For example, let us say that a classical scalar field needs to be enriched by a function $F(\underline{x})$. It is recalled that the classical field discretization given in Section I.2 is $u(\underline{x}) \approx \sum_I u_i N_i(\underline{x})$. First, imagine we want to enrich the whole domain. Then, to the basic discretization is added the enrichement function times a partition of unity (classically the shape functions) such that the new approximation is:

$$u(\underline{x}) \approx \sum_I u_i N_i(\underline{x}) + \sum_I u_i^e N_i(\underline{x}) F(\underline{x}) \tag{II.18}$$

This is obviously really costly as the number of unknown is doubled. A practical approach is to limit the enrichment to a local zone. Indeed, where the solution is smooth enough no enrichment is needed. Let us call J a subset of I which contains the chosen enrichment nodes (i.e. the nodes where the classical approximation is not enough). Thence, the new approximation can be obtained:

$$u(\underline{x}) \approx \sum_I u_i N_i(\underline{x}) + \sum_J u_j^e N_j(\underline{x}) F(\underline{x}) \tag{II.19}$$

Even if it is often convenient, having the same interpolation functions for the classical field and the enriched one (i.e. for a same node $N_i = N_j$) is not compulsory. The use of a partition of unity allows a good representation of the enrichment but keeps a local influence. Indeed,

outside the elements containing an enriched node n_j the associated function $N_j(\underline{x})F(\underline{x})$ is equal to zero. Hence the matrices associated to the formulation have nice properties such as sparsity and are bloc diagonal. Moreover, the use of the partition of unity gives a good transition from the enriched zone to the classical one. An example of a simple approximation with enrichment is given Figure II.6.

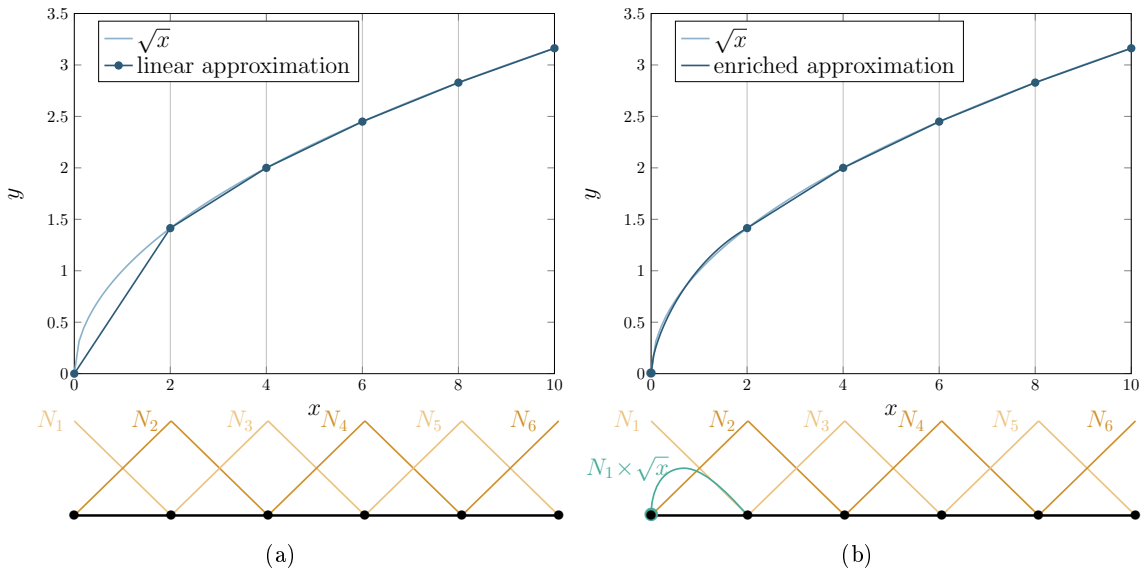

(a) (b)

Figure II.6: The function $\sqrt{x}$ is first represented by only the classical linear finite element (a) and then with the first node enriched (b). In (b) only the first node is enriched as the classical linear approximation does an handy job on the rest of the domain.

Of course these definitions are easily extended to non-scalar fields.
In the following, several useful enrichments are presented.

Heaviside enrichment (Figure II.7) The Heaviside enrichment was the first one to be used in [Moës et al., 1999]. This allows typically to uncouple the two domains separated by the iso-zero. Indeed, the Heaviside function $H(x)$ has a strong discontinuity for $x = 0$. There is several definitions of an Heaviside function. It is chosen here to use the function $H(x)$ defined as:

$$H(x) = \begin{cases} 0 & x > 0 \\ 1 & x \leq 0 \end{cases} \tag{II.20}$$

This functions has been shown to be easy to implement even with high order interpolations and will be extensively used in this thesis.

Ridge enrichment (Figure II.8) This enrichment is designed to allow a weak discontinuity (i.e. a discontinuity of the first derivative of the field). Again, several definitions were proposed. Here the definition given in [Moës et al., 2003] is used:

$$R_{\mathrm{i}}(\underline{x}) = \sum_I |\phi(\underline{x})| N_i(\underline{x}) - \left| \sum_I \phi(\underline{x}) N_i(\underline{x}) \right| \tag{II.21}$$

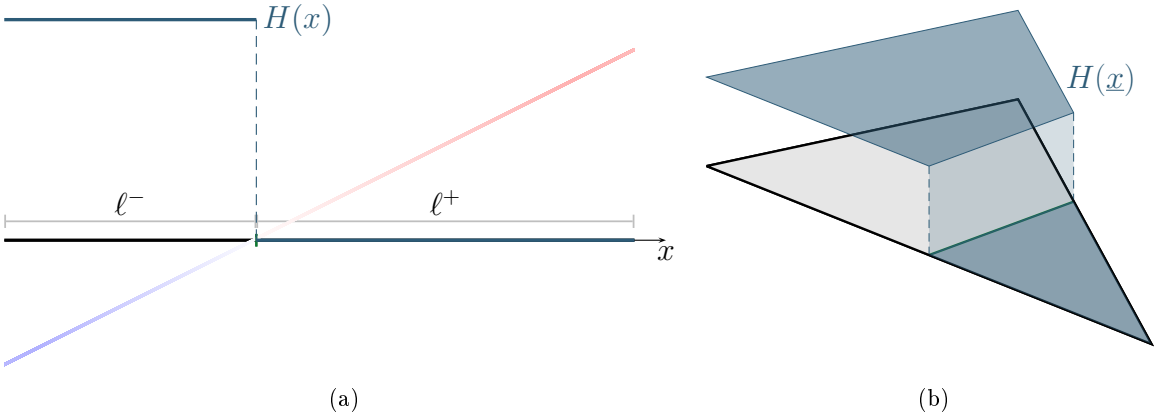

(a) (b)

Figure II.7: Representation of the Heaviside function for 1D elements (a) and 2D elements (b)

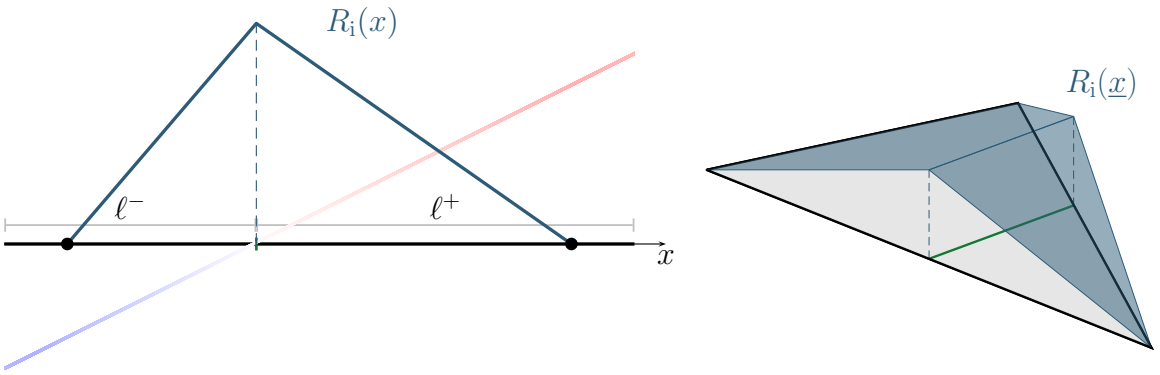

(a) (b)

Figure II.8: Representation of the ridge function for 1D elements (a) and 2D elements (b)

Crack-like enrichment (Figure II.9) As it was pointed out, the first use of X-FEM in [Moës et al., 1999] was to model 2D crack growth. The displacement field at a crack tip can be approximated by the knowledge of the analytic solution with infinite boundary. It is interesting to add this knowledge in the formulation. Furthermore, the gradient of the displacement and therefore the strain is singular at the crack tip. Using X-FEM to model this allows a better convergence of the method. Analytic solutions were developed in [Griffith, 1921, Irwin, 1957]. This leads to a possible family of functions used to enriched a crack tip (see Figure II.9):

$$F_c(r,\theta) = \left\{ \sqrt{r}\sin\left(\frac{\theta}{2}\right); \sqrt{r}\cos\left(\frac{\theta}{2}\right); \sqrt{r}\sin\left(\frac{\theta}{2}\right)\sin(\theta); \sqrt{r}\cos\left(\frac{\theta}{2}\right)\sin(\theta) \right\} \tag{II.22}$$

where (r,θ) are the polar coordinate associated with the crack tip. In this work we will focus only on the first function $F_{c1} = \sqrt{r}\sin\left(\frac{\theta}{2}\right)$. Its gradient is also going to be needed:

$$\nabla F_{c1}(r,\theta) = \left\{ \frac{\partial F_{c1}}{\partial r}, \frac{1}{r}\frac{\partial F_{c1}}{\partial \theta} \right\}_{\underline{e}_r,\underline{e}_\theta} = \left\{ \frac{1}{2\sqrt{r}}\sin\left(\frac{\theta}{2}\right), \frac{1}{2\sqrt{r}}\cos\left(\frac{\theta}{2}\right) \right\}_{\underline{e}_r,\underline{e}_\theta} \tag{II.23}$$

In order to compute the local polar coordinates level-sets are drawn upon again. A first level-set ϕ_n is the one giving the distance to the crack plane in the normal direction as described

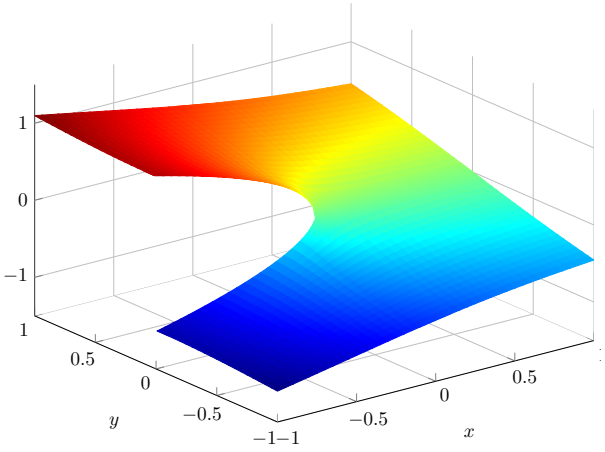

(a) $\sqrt{r}\sin\left(\frac{\theta}{2}\right)$

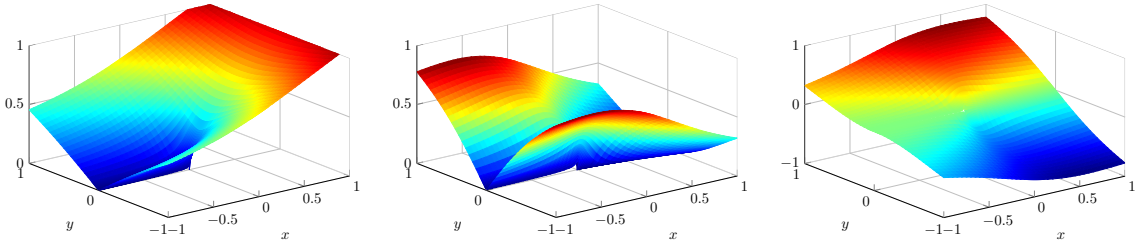

(b) $\sqrt{r}\cos\left(\frac{\theta}{2}\right)$ (c) $\sqrt{r}\sin\left(\frac{\theta}{2}\right)\sin(\theta)$ (d) $\sqrt{r}\cos\left(\frac{\theta}{2}\right)\sin(\theta)$

Figure II.9: Crack enrichment functions

Figure II.10(a). The other one ϕ_t is giving the distance to the crack tip in the tangential direction as in Figure II.10(b). With both level-sets the local coordinates at a point $\underline{x}$ can be

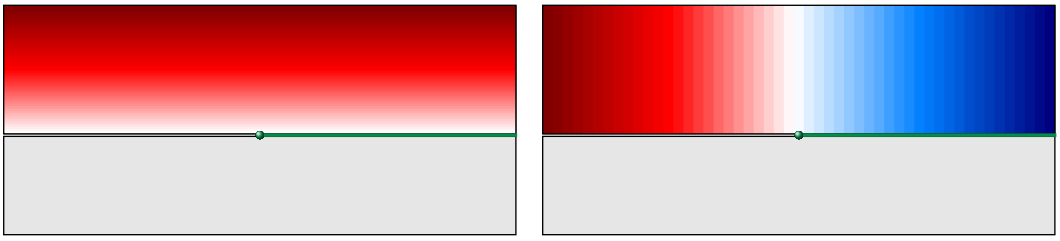

(a) ϕ_n (b) ϕ_t

Figure II.10: Level-set used as local coordinates for a contact zone represented in green and its boundary by a green dot

obtained as

$$\begin{cases} r &= \sqrt{\phi_n^2(\underline{x}) + \phi_t^2(\underline{x})} \\ \theta &= \arctan\left(\dfrac{\phi_n(\underline{x})}{\phi_t(\underline{x})}\right) \end{cases} \tag{II.24}$$

II.2.2.3 Dirichlet conditions on the boundary

A common boundary condition is to impose the value of the unknowns on a given region. This type of condition is refereed as Dirichlet boundary condition. However, with an implicit boundary as with level-set method, it is not an easy task. As mentioned, a classical way to impose such conditions in FEM is to use Lagrange multiplier [Babuška, 1973]. In order to do so with level-set, a mesh of the boundary needs to be created. Furthermore, a careful construction of the Lagrange multiplier has to be done to avoid the previously mentioned violation of the BB condition. A framework was settled in [Béchet et al., 2009] and a summary is given here. The first task is to create the boundary mesh. It is effortless to find the cutting point of element's edges by the iso-zero. Therefore this points can be used as a first set of nodes for the boundary mesh. The straightforward idea would be to use all these nodes to create it. However such a method was shown in [Ji and Dolbow, 2004] to not fulfill the BB condition. Another strategy needs to be set. First only part of the cutting vertices are kept as nodes and called vital vertices. As stated in [Béchet et al., 2009], the rules to chose these nodes are:

(i) an isolated vertex is always vital,

(ii) a vital vertex is not allowed to be connected to any other vital vertex,

(iii) a non-vital vertex must be connected to at least one vital vertex.

It is to be noticed that the set of vital vertex is note unique and an algorithm to obtain such set can be found in the above mentioned article. The shape functions associated to these vital vertices are the trace of the associated elements shape functions. Then, if I_Γ is the set of the classical shape functions such that their restriction to Γ is not zero, the shape function $\gamma_k(\underline{x})$ of a vital vertex v_k can be expressed as:

$$\gamma_k(\underline{x}) = \sum_{I_\Gamma} u_k^\gamma N_i(\underline{x})|_\Gamma \tag{II.25}$$

with $u_k^\gamma \in \mathbb{R}$ defined in [Béchet et al., 2009].

Check point

Let us take a moment to summarize the tools at our disposal so far and what we are missing. The coupling of level-set and X-FEM allows an accurate representation of a boundary in a domain without having to design specific meshes. Furthermore, particularities such as singularities or discontinuities can be handled efficiently. Thus, Problem 12 can be efficiently solved for a given contact zone. Methods have also be given to make the boundary evolve for a given displacement. Therefore, the only missing point for a complete method is to find the necessary displacements of a boundary Γ to make it converge to the boundary Γ_{ex} of the exact constraint domain $\mathcal{D}^c_{\text{ex}}$. That will be the subject of the next chapter.

II.3 How to find the right constraint zone

The goal of this section is to develop a method to find the right constraint zone. Several methods were described in Section I.2.2 for the contact case. These methods are classically

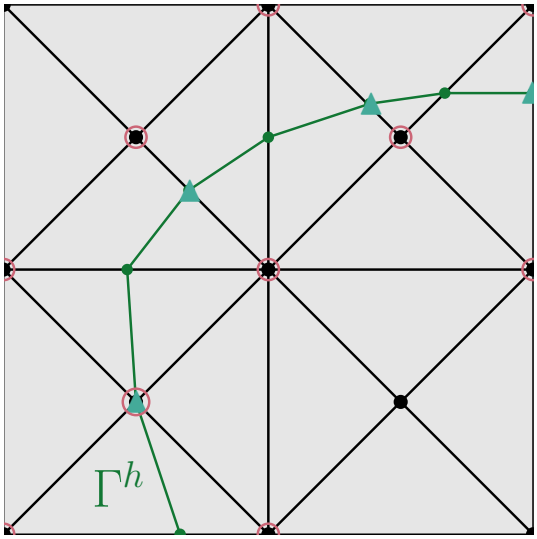

Figure II.11: Example of the creation of the boundary space field based on the domain decomposition of Figure II.5. The vital vertices are represented by ▲ and the nodes for which the shape function are part of I_Γ are selected by ○

used for general constraint problems. Without extra work, such classical strategy could be used. Let us say for instance that a classical active set strategy is chosen coupled with an enforcement of the constraints by Lagrange multipliers. The application of this strategy to a constraint zone defined by a level-set is developed below with the graphical support of Figure II.12.

The starting point is an initial level-set (see Figure II.12(a)). Then, after solving equation II.5 of Problem 12, constraints verifications are made. We recall that the main constraint is $c \geq 0$ on all the domain. Furthermore, a constraint is added on the Lagrange multipliers and reads $p \geq 0$. Using an active set update means:

- checking if the constraint $c \geq 0$ is violated on $\mathcal{D}^+$ (as it is already imposed on $\mathcal{D}^-$),
- adding to the constraint zone the domains where violation was detected,
- checking if the constraint $p \geq 0$ is violated on $\mathcal{D}^-$,
- removing from the constraint zone the domains where violation was detected.

This update of $\mathcal{D}^-$ is easily handled with level-set. Indeed, we can use the value of c to create a level-set function ϕ_c (Figure II.12(b)) and the value of $-p$ for ϕ_p (Figure II.12(c)). With these functions it is easy to do topological operations. A level-set function, with the zones where $c < 0$ are added to $\mathcal{D}^-$, is given by $\min(\phi, \phi_c)$. Likely, a level-set function, with the zones where $p < 0$ are removed to $\mathcal{D}^-$, is obtained with $\max(\phi, \phi_p)$. Combining both expressions (the order does not matter) $\max(\min(\phi, \phi_c), \phi_p)$ creates a level-set representing the new domain $\mathcal{D}^-$ (Figure II.12(d)). In order to have an efficient level-set some post-treatment is required. First, the desired iso-zero is perturbed by zero values arising from the boundary of the domain of definition of ϕ_c and ϕ_p (see the dashed line in Figure II.12(d)). Numerically, it is noticed only if the boundary cut a node of the mesh. An easy fix is to shift ϕ_c (resp. ϕ_p) down (resp. up). These shifts changed obviously the shape of the new domain. However, only a small shift is

needed (not much greater than the machine epsilon) and the error is negligible. Then, using the iso-zero, a new level-set function is computed in order to be a signed distance function (using for instance the method described in II.2.1.4). The final result of the update is given Figure II.12(e). On top of the easy construction of the new constraint domain, the use of level-sets allows to have an update not linked to the nodes of the mesh. Indeed, the constraint are verified on all the domain and not only at each node. Even if simple, this method lacks

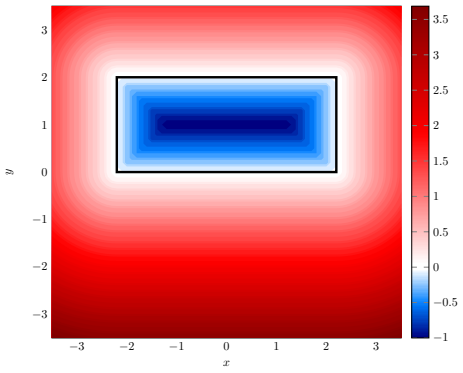

(a) ϕ

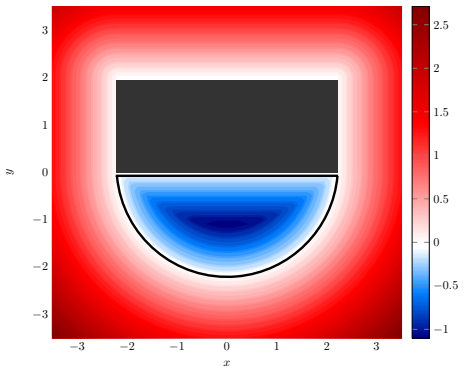

(b) ϕ_c

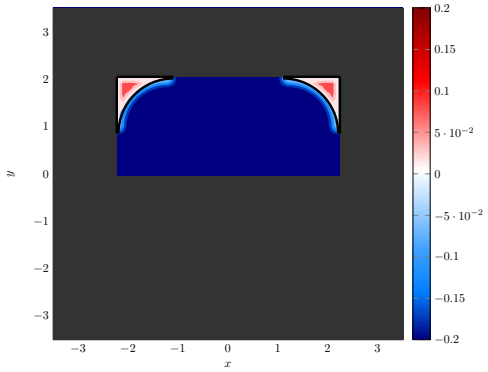

(c) ϕ_p

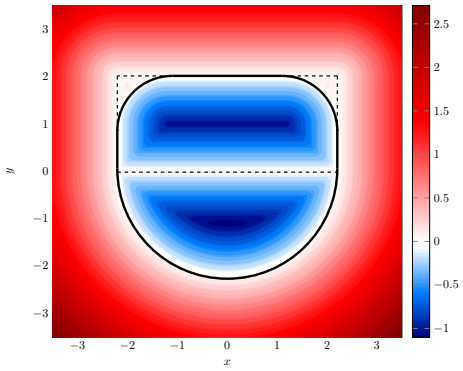

(d) new level-set

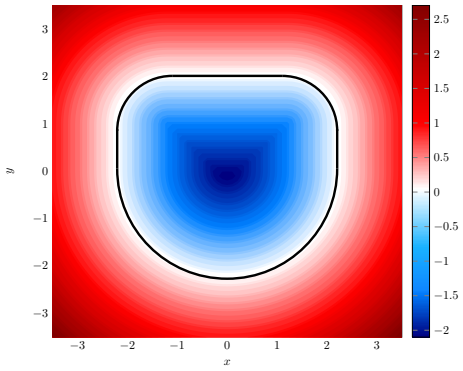

(e) associated signed distance function

Figure II.12: Example of an active-set strategy with level-sets. The starting level-set is (a) and the level-set ascociated with constraints are (b) and (c). The result of the level-sets operation is (d) and the final signed distance function (e). Solid lines represent the iso-zero of each one.

of robustness and rapidity. In order to improve that more information is used in the update algorithm. Indeed, with active set, there is only a "on or off" update of the region. More advance method like the augmented Lagrange method requires more information. For instance augmented Lagrange multiplier is designed to be used with Newton's methods and thus grant a faster convergence. These Newton's methods requires the derivative of the functional to cancel or the hessian if the functional is to be minimized. Here, another method is proposed, also linked to a Newton method, that use a special derivative.

II.3.1 The general framework

In this section, the general idea of how the evolution of the constraint zone is carried on using ILS is explained. A graphical representation of the problem is given Figure II.3.1. This figure only represent the case where a unique solution is possible. The extension in the other cases is similar but with no guaranty of convergence to one particular solution. As stated in Problem 9, the solution sought is the intersection of:

- the subspace of the admissible field $\mathcal{U}$, $S_{\mathcal{E}}$ satisfying the set of equalities $(\mathcal{E})$,
- the subspace $S_{\mathcal{I}}$ where the constraints $(\mathcal{I})$ are not violated.

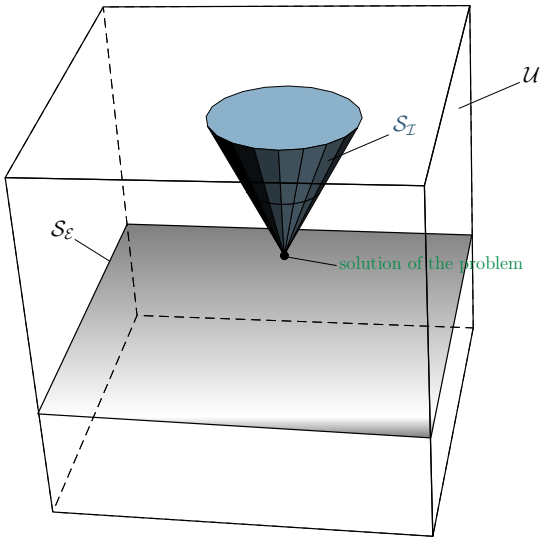

Figure II.13: Representation of the solutions space.$S_{\mathcal{E}}$ is the space where $(\mathcal{E})$ are satisfied and $S_{\mathcal{I}}$ is the space where $(\mathcal{I})$ are satisfied.

The ILS propose to find a criterion ϱ that must verified:

$$\Gamma = \Gamma_{\text{ex}} \Rightarrow \varrho = 0 \tag{II.26}$$

That means that when the right boundary is found then $\varrho = 0$. But it is possible to have $\varrho = 0$ and not be at the right solution, such a case is depicted in Figure II.15. Now, the key point is to know how this criterion is going to change when moving Γ. The derivative of ϱ with regards to the displacement $\underline{w}_\Gamma$ of Γ gives the linearized answer to this question. Let us for now suppose that we know how to compute this derivative that will be noted $\mathring{\varrho}(\underline{w}_\Gamma)$. Then a

Newton method can be used to find the displacement of Γ that cancel ϱ. This famous method iteratively solve the equation:

$$\varrho + \mathring{\varrho}(\underline{w}_\Gamma) = 0 \tag{II.27}$$

with $\underline{w}_\Gamma$ as unknown. An example of such scheme is given Figure II.3.1 for Γ being a point on a line.

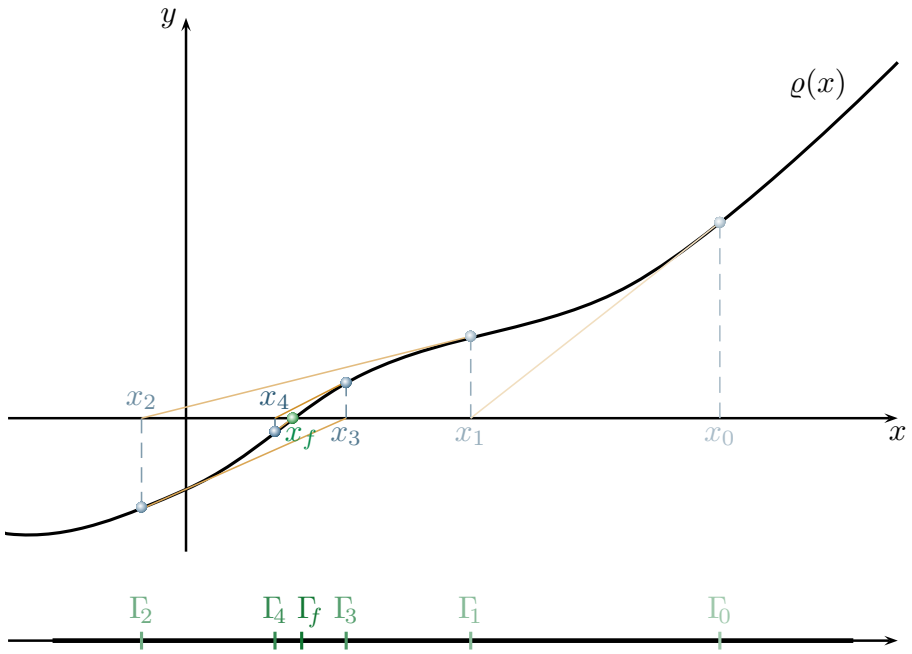

Figure II.14: Illustration of Newton's method iterations, the brown line are the tangents to the curve.

When the Newton method has converged one has to check if $(\mathcal{I})$ are satisfied. If it is the case then a solution has been reached. If not an active-set update is done and a new Newton algorithm is started with this new initial guess (see Figure II.15).

The general framework given in Figure II.1 is updated in Figure II.16 to give a general idea of how the ILS framework is designed.

II.3.2 Definition of the directional derivative

In the last section, a derivative was introduced (which physical meaning is to represent a variation of a quantity for a displacement of the boundary) without more details. The aim of this Section is to give a definition of such a derivative.

II.3.2.1 A generic definition

First, let us give the definition of a family of derivative that would meet the requirements. The directional derivative is a special case of the total derivative (see Equation I.20). Let us take a function $f(\Gamma)$ defined on Γ and which depends on its position. Then, given a displacement $\underline{w}_\Gamma$ of the boundary (see Figure II.17), the directional derivative of f in the direction $\underline{w}_\Gamma$ is defined

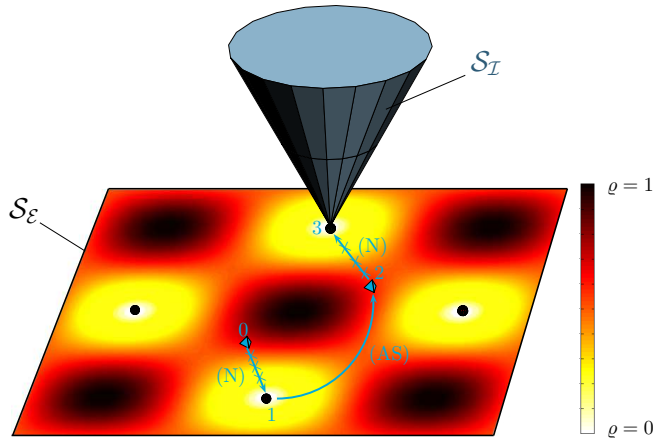

Figure II.15: The criterion ϱ is plotted for any point of the solution space $\mathcal{S}_\mathcal{E}$. Red dots represent the point where $\varrho = 0$ but the constraints are not fulfilled. A possible behavior of the ILS algorithm is shown in blue. Starting points are represented by a blue pyramid. The progress of the algorithm is: Newton update (0→1) leading to an unsatisfying solution (each iteration are blue cross); active set update (1→2); Newton update leading to the desire solution (2→3)

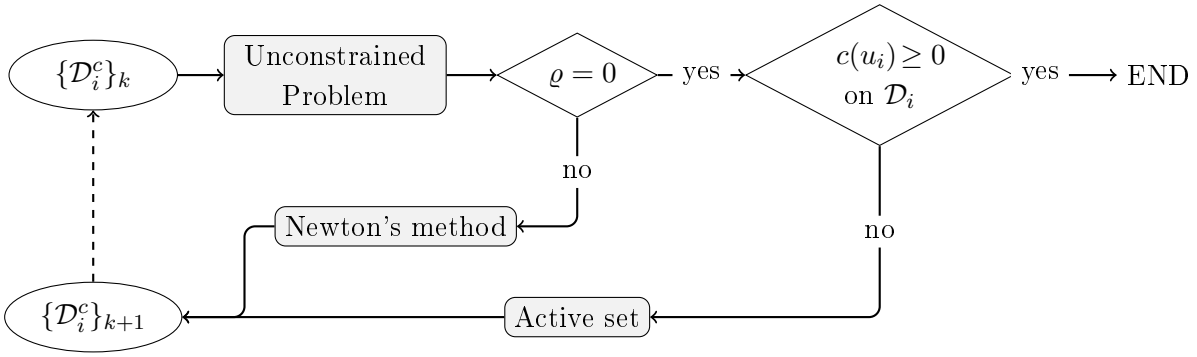

Figure II.16: The ILS global framework

as:

$$D_{[\underline{w}_\Gamma]}(f(\Gamma)) = \lim_{\tau \to 0} \frac{f(\Gamma + \tau \underline{w}_\Gamma) - f(\Gamma)}{\tau} \tag{II.28}$$

Another point of view, leading to the same definition, is to see $\underline{w}_\Gamma$ as the speed of the boundary and τ a time (fictitious in the case of static or quasi static problems).

The physical meaning of this derivative is difficult to grasp at first. Imagine a non-material point $\underline{s}$ on Γ. The value $f(\underline{s})$ could be for instance a physical property such as the temperature. Then, if the boundary moves with a displacement $\underline{w}_\Gamma$, $f(\underline{s})$ might change. This change can be decomposed in two parts:

- the point of measurement has changed as Γ moved,
- the displacement of Γ has changed the problem.

The combination of both contributions leads to the directional derivative.

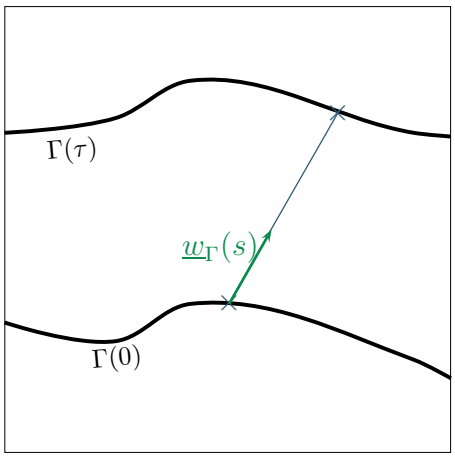

Figure II.17: Some unspecific displacement $\underline{w}_\Gamma$ of the boundary

II.3.2.2 The particular case of the normal directional derivative

The boundary Γ is represented by an implicit function and is not linked to physical points. That means that only its shape is of matter. Therefore, many displacement $\underline{w}_\Gamma$ can lead to the same change for Γ. As a choice, we will always use a displacement normal to the boundary. Indeed, the tangential displacements does not give a shape change. Hence, from now on, $\underline{w}_\Gamma = w_\Gamma \underline{n} = w_\Gamma \nabla\phi$. The directional derivative with this normal direction is called the normal directional derivative. The equivalent of Figure II.17 is presented Figure II.18.

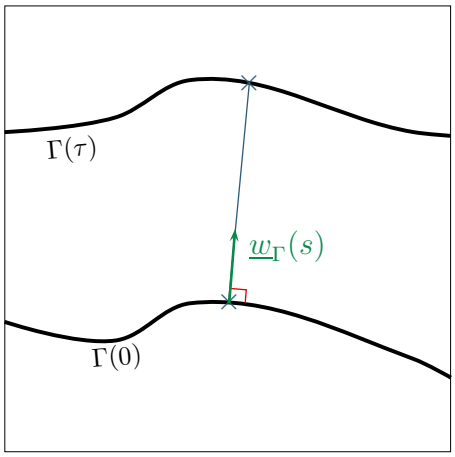

Figure II.18: Normal displacement $\underline{w}_\Gamma$ of the boundary

II.3.2.3 Extension of the definition to the whole domain

These last definition of the directional derivative is only valid for quantities defined on the boundary, as the displacement $\underline{w}_\Gamma$ is only defined there. However, it might be necessary to compute the derivative of quantities outside Γ. The previous definition is going to be extended to the whole domain. An handy way to do so is to create a mapping Φ_τ from the initial domain $\mathcal{D}$ with the constraint zone bounded by Γ to a new one $\mathcal{D}_\tau$. The displacement of a point $\underline{x}$ of

$\mathcal{D}$ to its new position is noted $\underline{w}(\underline{x})$. Let us define the transformation $\Phi_\tau(\underline{w})$ such that:

$$\left| \begin{array}{ccc} \mathcal{D} & \rightarrow & \mathcal{D}_\tau \\ \underline{x} & \rightarrow & \underline{x} + \tau \underline{w} \end{array} \right. \tag{II.29}$$

The first obvious requirement for $\underline{w}(\underline{x})$ is to be equal to $\underline{w}_\Gamma$ on Γ. Thus the new position of the boundary Γ_τ will match the previously defined update boundary. Moreover, in order to avoid boundary terms, $\underline{w}(\underline{x}) \cdot \underline{n} = 0$ is set on the outside boundary $\partial\mathcal{D}$ of the domain $\mathcal{D}$. This means that the mapping does not change the shape of the outside boundary. Furthermore it is taken smooth around Γ and continuous on the whole domain. For instance, $\underline{w}(\underline{x})$ may be set to zero outside a band $\mathcal{B}$ along Γ.

Then we can define for a function $f(\underline{x})$ its directional derivative as:

$$D_{[\underline{w}]}(f(\underline{x})) = \lim_{\tau \to 0} \frac{f(\underline{x} + \tau \underline{w}) - f(\underline{x})}{\tau} \tag{II.30}$$

and its normal directional derivative:

$$D_{[w \cdot \nabla \phi]}(f(\underline{x})) = \lim_{\tau \to 0} \frac{f(\underline{x} + \tau w \cdot \nabla \phi) - f(\underline{x})}{\tau} \tag{II.31}$$

This last derivative is chosen as the one mentioned Section II.3.2.1. As a short hand, we use the notation $\mathring{f} = D_{[w \cdot \nabla \phi]}(f(\underline{x}))$. The mapping Φ_τ can be viewed as a fictitious deformation and classical mechanics tools can be used. Such vision was applied by [Pradeilles-Duval and Stolz, 1995] and [Taroco, 2000]. Some useful formulae are given in Appendix A.

Check point

At this point, the main idea behind the ILS formulation has been given. What follows is technicality on how to apply it. Therefore let us sum-up the general concept. The first ILS key point is the representation of Γ by a level-set and the use of X-FEM to handle specific behaviors of the solution. The next step is to be able to update Γ. Here, rather than an active set method, configurational mechanics is used. Again, this relies on two key stones. Firstly, a criteria ϱ is designed such that when the right position of Γ is reached $\varrho = 0$. Then, to drive this quantity to zero, a Newton's method is used involving the normal directional derivative of ϱ.

II.3.3 Finding a criterion: the mechanical case

Now that the derivative is defined, let us explain how to find a criterion ϱ. First, a known property can be sufficient. It can be for instance a known regularity property of the solution. Several examples of *ad hoc* criteria are given in the numerical examples sections. Here, a more general framework for mechanical problem is presented if no obvious criterion is available. The method is based on configurational mechanics. The reader is referred to the reference books for an overview of it and some application examples [Gurtin, 2000, Maugin, 2010].

In order to show the generality of this method we will compute this criterion on a broader case without small deformation hypothesis. Since we did not consider friction or dissipative process in the bulk, dissipation should be zero as the contact zone evolves.

In the initial configuration, consider that the boundary of the contact zone Γ_0 evolves with some normal velocity $\underline{w}_0 = w_0 \underline{\mathfrak{I}}$ where $\underline{\mathfrak{I}}$ is the equivalent of $\underline{\mathfrak{y}}$ in the reference configuration. We consider a domain $\mathcal{B}_0$ inside Ω_0 surrounding the contact front Γ_0. We extend $\underline{w}_0$ from Γ_0 into $\mathcal{B}_0$, in the same fashion as explained in the previous section, with the following rules:

$$\begin{cases} \underline{w}_0 \text{ continuous over } \mathcal{B}_0 \\ \underline{w}_0 \text{ smooth around } \Gamma_0 \\ \underline{w}_0 = 0 \text{ on } \partial\mathcal{B}_0/\partial\Omega_0 \end{cases} \tag{II.32}$$

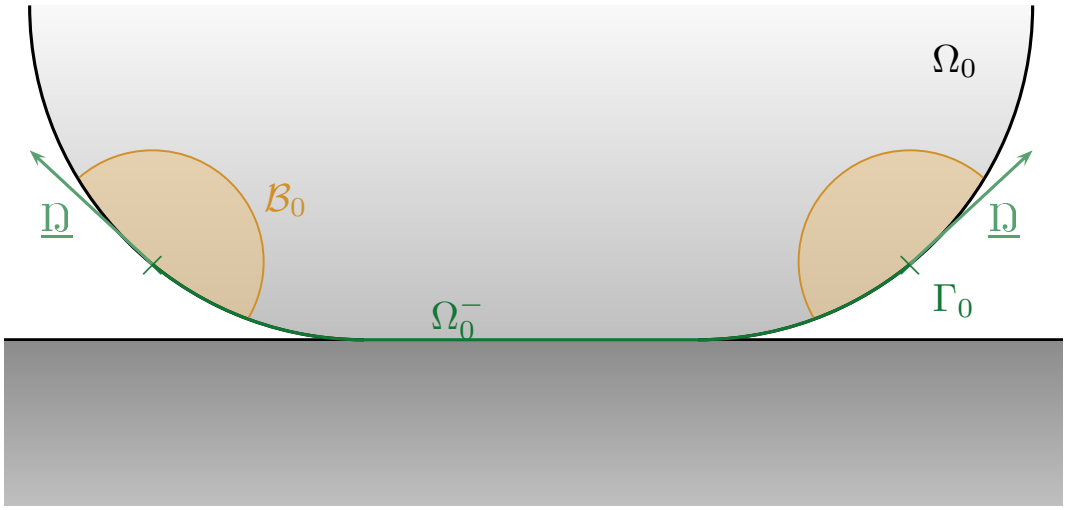

Figure II.19: Representation of the domains on the initial configuration

The mechanical dissipation is the external mechanical power minus the change in free energy of the system. We define $\underline{v} = \frac{\partial \underline{x}}{\partial t}$ as the material velocity.

$$D^m = P^m_{ext} - \frac{\mathrm{d}}{\mathrm{d}t} \int_{\Omega_0} \Psi \, \mathrm{d}V \tag{II.33}$$

We have

$$P^m_{ext} = \int_{\partial\Omega_0} \underline{\underline{P}}\,\underline{N} \cdot \underline{v} \, \mathrm{d}S = \int_{\Omega_0/\mathcal{B}_0} \underline{\underline{P}} : \underline{\underline{\dot{F}}} \, \mathrm{d}V + \int_{\partial\mathcal{B}_0} \underline{\underline{P}}\,\underline{N} \cdot \underline{v} \, \mathrm{d}S \tag{II.34}$$

$$\begin{aligned} \frac{\mathrm{d}}{\mathrm{d}t} \int_{\Omega_0} \Psi \, \mathrm{d}V &= \int_{\Omega_0/\mathcal{B}_0} \dot{\Psi} \, \mathrm{d}V + \int_{\mathcal{B}_0} D_{[\underline{w}_0]}(\Psi) + \Psi \operatorname*{div}_X(\underline{w}_0) \, \mathrm{d}V \\ &\quad - \int_{\partial\mathcal{B}_0} \Psi \underline{w}_0 \cdot \underline{N} \, \mathrm{d}S \end{aligned} \tag{II.35}$$

Regarding the directional derivative, we have

$$\begin{aligned} D_{[\underline{w}_0]}(\Psi) &= \frac{\partial \Psi}{\partial \underline{\underline{F}}} : D_{[\underline{w}_0]}(\underline{\underline{F}}) \\ &= \underline{\underline{P}} : \nabla_X \underline{w} - (\underline{\underline{F}}^\top \underline{\underline{P}}) : \nabla_X \underline{w}_0 \end{aligned} \tag{II.36}$$

where we have used

$$D_{[\underline{w}_0]}(\underline{\underline{F}}) = \nabla_X(D_{[\underline{w}_0]}(\underline{X})) - \underline{\underline{F}}\nabla_X \underline{w}_0 \tag{II.37}$$

and the short hand notation

$$\underline{w} = D_{[\underline{w}_0]}(\underline{x}) \tag{II.38}$$

where $\underline{w}$ has the meaning of the contact zone velocity in current configuration. Gathering terms, we get

$$\begin{aligned} D^m \;=\; & \int_{\Omega_0/\mathcal{B}_0} \underbrace{\underline{\underline{P}} : \dot{\underline{\underline{F}}} - \dot{\Psi}}_{0} \,\mathrm{d}V - \int_{\mathcal{B}_0} (\Psi \underline{\underline{I}} - \underline{\underline{F}}^\top \underline{\underline{P}}) : \nabla_X \underline{w} \,\mathrm{d}S \\ & - \int_{\mathcal{B}_0} \underline{\underline{P}} : \nabla_X \underline{w} \,\mathrm{d}V + \int_{\partial\mathcal{B}_0} \underline{\underline{P}}\,\underline{N} \cdot \underline{v} - \Psi\, \underline{w}_0 \cdot \underline{N} \,\mathrm{d}S \end{aligned} \tag{II.39}$$

The first term above is zero because we have no bulk dissipation whereas in the second one, the Eshelby tensor $\underline{\underline{C}}$ appears

$$\underline{\underline{C}} = \Psi \underline{\underline{I}} - \underline{\underline{F}}^\top \underline{\underline{P}} \tag{II.40}$$

Regarding the third one, we will use the equilibrium and the kinematics relation

$$\underline{w} = \underline{v} + \underline{\underline{F}}\,\underline{w}_0 \tag{II.41}$$

The final expression of the dissipation is

$$D^m = -\int_{\mathcal{B}_0} \underline{\underline{C}} : \nabla_X \underline{w}_0 \,\mathrm{d}V + \int_{\partial\mathcal{B}_0 \cap \partial\Omega_0} \underline{\underline{C}}\,\underline{N} \cdot \underline{w}_0 \,\mathrm{d}S \equiv g w_0 \tag{II.42}$$

In this last formula g is the configurational force associated to the displacement of the boundary. Assuming $\underline{w}_0$ is tangent to the boundary, the boundary term is zero and we get:

$$D^m = -\int_{\mathcal{B}_0} \underline{\underline{C}} : \nabla_X \underline{w}_0 \,\mathrm{d}V \tag{II.43}$$

With the small deformation hypothesis, the following formula for the Eshelby tensor is used:

$$\underline{\underline{C}} = \frac{1}{2}(\underline{\underline{\sigma}} : \underline{\underline{\epsilon}})\underline{\underline{I}} - \nabla \underline{u}^\top \underline{\underline{\sigma}} \tag{II.44}$$

and the dissipation is:

$$D^m = -\int_{\mathcal{B}_0} \underline{\underline{C}} : \nabla_x \underline{w} \,\mathrm{d}V \tag{II.45}$$

Therefore, for 2D problems, we have two possible criteria D^m and g. In this thesis, g is preferred for computational purpose. Indeed, it is easier to set up a Newton's method with g.

A straightforward interest in using one of these criteria is the direct link with adhesion phenomenon. Indeed, when adhesion is considered, the dissipation is no longer zero. We can correlate both D^m and the already mentioned surface energy γ

$$D^m = \gamma \tag{II.46}$$

Therefore a criterion for the case with adhesion could be $D^m - \gamma = 0$

II.3.4 Computing the derivative of the criterion

Theoretically, all the tools are in our hands to apply the method. Nonetheless, the reader might ask himself how does the derivative of the criteria is computed? This is not a straightforward task an it shall be enlightened in this section. First, the criteria is computed with the solution of the unconstrained problem (Equation II.5). This means that a functional can be found such that: $\varrho = f(u_i)$. Therefore, using the formulae given in Appendix A we can compute:

$$\mathring{\varrho} = \overline{\overset{\circ}{f(u_i)}} = \mathfrak{f}(\mathring{u}_i, u_i) \tag{II.47}$$

The special lettering of $\mathfrak{f}$ indicates that it is the derivative of a functional with no assumption made. We will see shortly that, under certain conditions, simplifications can be made. In Equation II.47, the operator $\mathfrak{f}$ is known and so is u_i thus only $\mathring{u}_i$ is to be found. The reader might complain on this point as we now have to compute the derivative of u_i on possibly the whole domain. However, we will see that it is actually easier. The unknowns u_i were obtained by solving Equation II.5. Then, taking the derivative of these equations gives a knew problem with $\mathring{u}_i$ as unknowns. It is chosen, in order to simplify the calculus, to imposed that $\mathring{u^\star_j} = 0$. That physically means that the test fields follow the transformation Φ_τ. The new problem obtained, called sensitivity problem, is:

Problem 14

Find $\mathring{u}_i \in \mathcal{U}$ such that $\forall u^\star_j \in \mathcal{U}^\star$ such that $\mathring{u^\star_j} = 0$:

$$\left\{ \begin{array}{rcl} \overline{\overset{\circ}{a_{\mathcal{D}}(u_i, u^\star_j)}} & = & \overline{\overset{\circ}{f_{\mathcal{D}}(u^\star_j)}} \\ \overline{\overset{\circ}{c_{\mathcal{D}^c}(u_i, u^\star_j)}} & = & \overline{\overset{\circ}{l_{\mathcal{D}^c}(u^\star_j)}} \end{array} \right. \tag{II.48}$$

$$\Leftrightarrow \left\{ \begin{array}{rcl} \mathfrak{a}(\mathring{u}_i, u_i, u^\star_j, w) & = & \mathfrak{f}(u_i, u^\star_j, w) \\ \mathfrak{c}(\mathring{u}_i, u_i, u^\star_j, w) & = & \mathfrak{l}(u_i, u^\star_j, w) \end{array} \right. \tag{II.49}$$

Let us consider a particular case: $a_{\mathcal{D}}(u_i, u^\star_j)$ and $c_{\mathcal{D}^c}(u_i, u^\star_j)$ are bilinear and $f_{\mathcal{D}}(u^\star_j)$ and $l_{\mathcal{D}^c}(u^\star_j)$ are linear. Then let us look at what happens for $\mathfrak{a}(\mathring{u}_i, u_i, u^\star_j, w)$. In order to apply Equation II.31 to $a_{\mathcal{D}}(u_i, u^\star_j)$ everything referring to the initial configuration will be labeled

with 0 and τ for the transformed configuration:

$$\mathfrak{a}(\mathring{u}_i, u_i, u_j^\star, w) = \lim_{\tau\to 0} \frac{a_{\mathcal{D}_\tau}(u_i^\tau(\underline{x}+\tau\underline{w}), \underline{u}_j^{\star\tau}(\underline{x}+\tau\underline{w})) - a_{\mathcal{D}_0}(u_i^0(\underline{x}), \underline{u}_j^{\star 0}(\underline{x}))}{\tau} \tag{II.50}$$

$$= \lim_{\tau\to 0} \frac{a_{\mathcal{D}_\tau}(u_i^\tau(\underline{x}+\tau\underline{w}), \underline{u}_j^{\star 0}(\underline{x})) - a_{\mathcal{D}_0}(u_i^0(\underline{x}), \underline{u}_j^{\star 0}(\underline{x}))}{\tau}$$

$$+ \lim_{\tau\to 0} a_{\mathcal{D}_\tau}\left(u_i^\tau(\underline{x}+\tau\underline{w}), \frac{\underline{u}_j^{\star\tau}(\underline{x}+\tau\underline{w}) - \underline{u}_j^{\star 0}(\underline{x})}{\tau}\right)^{=\mathring{u}_j^\star=0} \tag{II.51}$$

$$= \lim_{\tau\to 0} \frac{\left[a_{\mathcal{D}_\tau} - a_{\mathcal{D}_0}\right](u_i^\tau(\underline{x}+\tau\underline{w}), \underline{u}_j^{\star 0}(\underline{x})) + a_{\mathcal{D}_0}(u_i^\tau(\underline{x}+\tau\underline{w}) - u_i^0(\underline{x}), \underline{u}_j^{\star 0}(\underline{x}))}{\tau} \tag{II.52}$$

$$= \lim_{\tau\to 0} \frac{\left[a_{\mathcal{D}_\tau} - a_{\mathcal{D}_0}\right](u_i^\tau(\underline{x}+\tau\underline{w}), \underline{u}_j^{\star 0}(\underline{x}))}{\tau} + a_{\mathcal{D}}(\mathring{u}_i, u_j^\star) \tag{II.53}$$

The first term can be seen as the normal directional derivative of the operator $a_{\mathcal{D}}$ and will be written $\mathring{a}(u_i, u_j^\star, \underline{w})$. Doing the same with the other operators and assuming the derivative of all the operators exist, Problem 14 is equivalent to:

Problem 15

Find $\mathring{u}_i \in \mathcal{U}$ such that $\forall u_j^\star \in \mathcal{U}^\star$:

$$\begin{cases} & \overbrace{\qquad\qquad}^{f_{\mathcal{D}}^s(u_i, u_j^\star, w)} \\ a_{\mathcal{D}}(\mathring{u}_i, u_j^\star) &= \overbrace{\mathring{f}_{\mathcal{D}}(u_j^\star, w) - \mathring{a}_{\mathcal{D}}(u_i, u_j^\star, w)} \\ c_{\mathcal{D}^c}(\mathring{u}_i, u_j^\star) &= \underbrace{\mathring{l}_{\mathcal{D}^c}(u_j^\star, w) - \mathring{c}_{\mathcal{D}^c}(u_i, u_j^\star, w)} \\ & \underbrace{\qquad\qquad}_{l_{\mathcal{D}^c}^s(u_i, u_j^\star, w)} \end{cases} \tag{II.54}$$

or in a matricial form using the same discretization as before:

$$[\mathbf{K}]\{\mathring{\mathbf{u}}\} = \{\mathbf{f}^s\} \tag{II.55}$$

It is important to notice that the left hand-side operator is the same as in Problem 12. This is numerically convenient as one needs to prepare the left-hand side only once to do multiple solving with different right-hand sides.

Solving Problem 15 gives access to $\mathring{u}_i$ and therefore to $\mathring{\varrho}$. As an example, $\mathring{g}$ (with g defined in the previous chapter) will be expressed in function of $\mathring{u}$. It was defined that $g = D^m/w$ with w the norm of the normal speed at which the front evolves. However this w does not have to be the same as the one used for the normal directional derivative. In order to make this difference it will be set that $g = D^m/w'$. The reader shall be reassured knowing that this particular criteria derivative is the more complex one handled in this thesis.

$$\mathring{g} = \frac{\mathring{D}^m w' - \mathring{w}' D^m}{w'^2} \tag{II.56}$$

Thus, in order to compute $\mathring{g}$, $\mathring{D}^m$ and $\mathring{w'}$ need to be expressed. In the static or quasi static case $\mathring{w'} = \nabla w' \cdot \underline{w}$. For $\mathring{D}$:

$$\mathring{D}^m = -\int_{\mathcal{B}} \mathring{\underline{\underline{C}}} : \nabla \underline{w}' \, \mathrm{d}\Omega - \int_{\mathcal{B}} \underline{\underline{C}} : \overline{\mathring{\nabla \underline{w}'}} \, \mathrm{d}\Omega - \int_{\mathcal{B}} \underline{\underline{C}} : \nabla \underline{w}' \, \mathrm{div}(\underline{w}) \, \mathrm{d}\Omega \tag{II.57}$$

Recalling that:

$$\underline{\underline{C}} = \frac{1}{2}(\underline{\underline{\sigma}} : \underline{\underline{\epsilon}})\underline{\underline{I}} - \nabla \underline{u}^\top \underline{\underline{\sigma}} \tag{II.58}$$

$$\mathring{\underline{\underline{C}}} = (\underline{\underline{\epsilon}}(\mathring{\underline{u}}) - (\nabla \underline{u} \nabla \underline{w})_S) : \underline{\underline{\sigma}} \, \underline{\underline{I}} - \nabla \underline{u}^\top (\underline{\underline{\sigma}}(\mathring{\underline{u}}) - K(\nabla \underline{u} \nabla \underline{w})_S) - (\nabla \mathring{\underline{u}} - \nabla \underline{u} \nabla \underline{w})^\top \underline{\underline{\sigma}} \tag{II.59}$$

and

$$\overline{\mathring{\nabla \underline{w}'}} = \nabla \mathring{\underline{w}} - \nabla \underline{w}' \nabla \underline{w} = \nabla(\nabla \underline{w}' \cdot \underline{w}) - \nabla \underline{w}' \nabla \underline{w} = \nabla \nabla \underline{w}' \cdot \underline{w} \tag{II.60}$$

all the elements are accounted for in order to compute Equation II.57 and thus Equation II.56. From an analytic point of view, the set up is done to apply the Newton's method.

II.3.5 The numerical framework

A general method was designed previously to apply a shape optimization to the contact zone. Nevertheless, the formulation was given for a general displacement $\underline{w}$. In the same way that a discretization was needed to solve the unconstrained problem, a discretization of $\underline{w}$ is needed to compute numerically the directional derivatives.

Several options are available to approximate $\underline{w}$. A difference can be made depending on the problem we are dealing with. Indeed, if the contact zone is 1D its boundary is a set of points. One mode is needed per point to represent its displacement. In the case of a surface as a contact zone, more complicated modes are needed. For instance Fourier modes (see Figure II.20) will be used in this thesis. The advantage of these modes is the span of there influence on the front. With only few modes, a coarse approximation of the contact zone can be made during the first iterations of the method. Then, one can increase the number of modes to capture local details. However, the number of Fourier modes is to be linked to the size of the mesh. Indeed, increasing the frequency (thus the number of nodes) is pointless if the characteristic length of the mesh is to big compare to the wavelength. That is why it seems more interesting to choose more local modes after reaching a coarse approximation of the contact zone.

In any case, the decomposition of the boundary displacement can be formalized as:

$$\underline{w} \approx \sum_{m}^{n_{\mathrm{mode}}} \tau_m w_m \nabla \phi \tag{II.61}$$

with w_m the above-mentioned modes, n_{mode} their number and τ_m their contribution. First taking the weak form of Equation (II.27):

Problem 16

Find $\underline{w} \in L^2(\Gamma)$ such that $\forall q \in L^2(\Gamma)$:

$$\int_\Gamma \varrho q + D_{[\underline{w}]}(\varrho) q \, \mathrm{d}\ell = 0 \tag{II.62}$$

the discretization can be introduced in this formulation for both $\underline{w}$ and q:

Problem 17

Find $\{\tau_m\} \in \mathbb{R}^{n_{\text{mode}}}$ such that $\forall l$:

$$\int_\Gamma \varrho w_l \, \mathrm{d}\ell + \sum_{m=1}^{n_{\text{mode}}} \tau_m \int_\Gamma D_{[w_m \nabla \phi]}(\varrho) w_l \, \mathrm{d}\ell = 0 \tag{II.63}$$

or in its matricial form: Find $\{\tau_m\} \in \mathbb{R}^{n_{\text{mode}}}$ such that:

$$[\mathbf{S}]\{\boldsymbol{\tau}\} = -\{\boldsymbol{\varrho}^\pi\} \tag{II.64}$$

with:

$$\left| \begin{array}{rcl} S_{ml} & = & \displaystyle\int_\Gamma D_{[w_m \nabla \phi]}(\varrho) w_l \, \mathrm{d}\ell \\ \varrho_l^\pi & = & \displaystyle\int_\Gamma \varrho w_l \, \mathrm{d}\ell \end{array} \right. \tag{II.65}$$

Therefore, for every mode w_m the associated directional derivative of the fields needs to be computed. The Problem 15 is thus solved for every w_m. However, in practice, all the directional derivative are computed altogether. This leads to the linear problem:

$$[\mathbf{K}][\{\mathring{\mathbf{u}}_1\}; \cdots ; \{\mathring{\mathbf{u}}_{n_{\text{mode}}}\}] = [\{\mathbf{f}_1^s\}; \cdots ; \{\mathbf{f}_{n_{\text{mode}}}^s\}] \tag{II.66}$$

With the solution to this system every derivative of ϱ can be computed and therefore Equation (II.64) can be solved.

Every aspects of an iteration to update the contact zone was explained above. Finally, lets us discuss the numerical procedures between each iterations. First let us list the evolving parameters in the ILS method:

- number of modes,
- size d_b of the computing band $\mathcal{B}$.

Then lets us also account for the tolerance and limiting parameters:

- maximum number of modes $n_{\text{modes}}^{\max}$ (linked to the computational cost and the characteristic size of the mesh h),

- tolerance on the constraints ε_c, the advance of the front ε_w.

What are the desired adaptations:

- Use the minimal amount of modes. The number of modes is increased each time the norm of the advance of the front is less than ε_w.

- Limit the size of d_b. At one iteration d_b is set to be twice the norm of the advance of the front if no modes are added.

Finally, what should be avoided:

- The advance of the front should not exceed the computational band. If the norm of the front displacement is greater than d_b the advance is reduced proportionally such that the norm is reduced to d_b.

- The size of the band d_b should not inhibit the advance of the front. If modes are added d_b is reinitialized. Furthermore d_b can't be smaller than $2h$.

- Optionally, the advance of the front should not be perturbed by small mode contributions. Every mode contribution τ_m such that $\tau_m < 0.1 \times |\{\boldsymbol{\tau}\}|$ is thus canceled

All this numerical procedure is summarized in the Algorithm 3.

Algorithm 3: ILS algorithm

Initialize: level-set $\phi \longleftarrow \phi_0$; number of modes $n_{\text{modes}} \longleftarrow n_0$; size band $d_b \longleftarrow d_0$;
while $n_{modes} < n_{modes}^{max}$ **do**
  Solve the direct problem $[\mathbf{K}]\{\mathbf{u}\} = \{\mathbf{f}\}$ (I.56);
  if *criterium not small enough* $:|\varrho| > \varrho_{min}$ **then**
    for $m = 1$ **to** n_{modes} **do**
      Compute modes w_m on Γ;
      Extend w_m on $\mathcal{B}$;
      Solve the sensibility problem $[\mathbf{K}][\{\mathring{\mathbf{u}}_m\}] = [\{\mathbf{f}_m^s\}]$(II.66);
    Solve the shape optimization problem $[\mathbf{S}]\{\boldsymbol{\tau}\} = -\{\boldsymbol{\varrho}^\pi\}$(II.64);
    (**if** $\tau_m < 0.1 \times |\{\boldsymbol{\tau}\}|$ **then** $\tau_m = 0$);
    if $|\{\boldsymbol{\tau}\}| < \varepsilon_w$ **then**
      $n_{\text{modes}} \longleftarrow n_{\text{modes}} + 1$;
      $d_b \longleftarrow d_0$;
    if $|\{\boldsymbol{\tau}\}| > d_b$ **then**
      $\{\boldsymbol{\tau}\} \longleftarrow \{\boldsymbol{\tau}\} \times \dfrac{d_b}{|\{\boldsymbol{\tau}\}|}$;
      $d_b \longleftarrow 2d_b$;
    else
      $d_b \longleftarrow \max(2|\{\boldsymbol{\tau}\}|, 2h)$;
    update ϕ ;
  else *criterium small enough* $:|\varrho| < \varrho_{\min}$
    if *check for penetration and traction* $< \varepsilon_c$ **then**
      return *1* ;
    else
      compute ϕ_c and ϕ_p ;
      update ϕ with ϕ_c and ϕ_p;
      $n_{\text{modes}} \longleftarrow n_0$; size band $d_b \longleftarrow d_0$;

Conclusion

This chapter did present the main idea of the Inequality Level Set method. The two key points have been highlighted. The enrichment of the fields coupled with level-sets allow an efficient representation of the constraints zone and the local phenomena. Then, a shape optimization is set up to find the right zone. This optimization is based on the choice of a position criterion ϱ. If found by mean of configurational mechanics, the criterion can be used to model physical phenomenon such as adhesion. The next chapters apply this method to contact problems and try to show its potential.

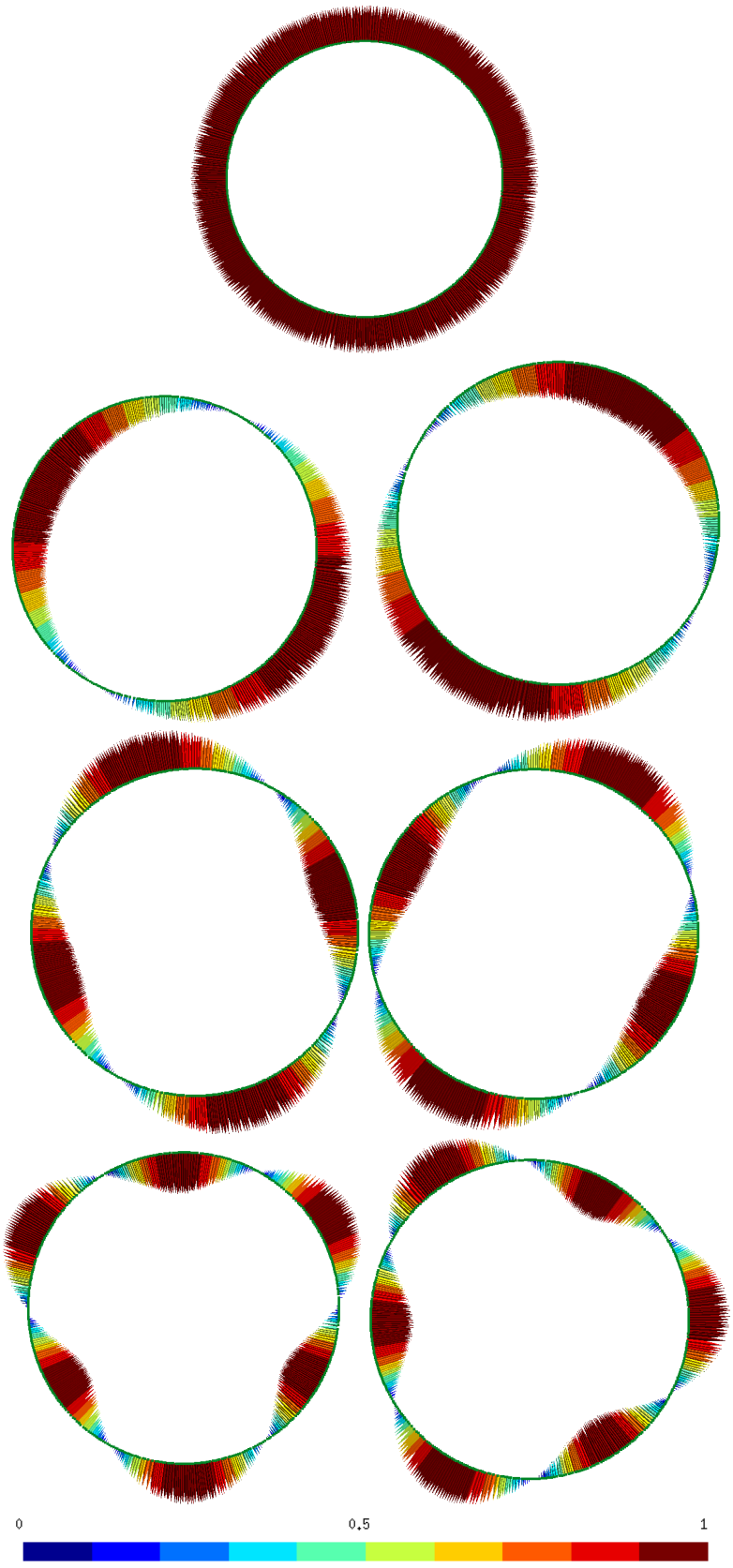

Figure II.20: Fourier modes for the first four frequencies on a circular boundary

III

Contact of a membrane

Contents

Summary

A first problem is studied here with the ILS. The membrane problem was chosen for the simplicity of its equations but also because it is a challenging problem when it comes to comparing the ILS with other methods. Indeed, the contact zone is of the same dimension as the full body and this is the worst case scenario for the ILS. The formulation of the problem is first set. Then some numerical computations are carried in order to show several aspects of the method. The adhesion is studied along with high order interpolation on simple cases. Finally, a more challenging problem is tackled. Through this chapter, comparisons with a classical active-set method are given.

Résumé

Dans ce chapitre, une première application de l'ILS est faite. Elle concerne le cas d'une membrane (sous l'hypothèse des petites déformations) rentrant en contact avec un solide indéformable. Un effort de modélisation à été fait afin d'obtenir une formulation stable. En effet, l'utilisation des quantités duales que sont les multiplicateurs de Lagrange implique des contraintes sur la formulation et la discrétisation du problème. Ces contraintes sont généralement exprimées sous forme de la condition de Babuška-Brezzi (BB). Elle permet de garantir la stabilité et la convergence du problème. Afin de vérifier cette condition, deux approches peuvent être utilisées. La première est de trouver la discrétisation des champs adaptée. La seconde consiste à trouver une formulation adéquate pour minimiser au maximum l'influence de la discrétisation. C'est cette dernière solution qui est choisie ici.

La représentation physique du problème pour une zone de contact erronée (ou dans le cas de l'adhésion) est assurée par un enrichissement Heaviside sur la frontière de la zone de contact, couplé à une force linéique sur cette même frontière. Cette force linéique est en fait des multiplicateurs de Lagrange visant à annuler le saut en déplacement introduit par l'enrichissement, ne laissant ainsi qu'un saut de pente possible.

Dans un premier temps, un problème axi-symétrique, pour lequel une solution analytique est disponible, est traité. Cette étude permet de valider la cohérence de la méthode ainsi que de la comparer à une méthode active-set classique. Sur ce problème simple, des approximations d'ordre deux et trois ont également été éprouvées. Par la suite, la capacité de la méthode à gérer l'apparition, la création et la séparation de zones de contact a été testée. Un problème récapitulant ces phénomènes est présenté ici. Il s'agit d'une membrane rentrant progressivement en contact avec un sol en forme de "boîte à œuf" avec l'augmentation du chargement. Une fois de plus la cohérence de la méthode est mise à l'épreuve en vérifiant que la solution en charge est proche de celle en décharge.

Cette étude nous a permis de valider l'efficacité de la méthode et son intérêt afin de trouver à moindre coup la position précise de la zone de contact. Cependant une amélioration des modes pour prendre en compte des évolutions plus locale reste à prévoir.

III.1 Description of the problem

We will assume the contact to be friction-less and we will focus only on the static problem with small deformation hypothesis. The deformable body occupies the volume Ω, its frontier is $\partial\Omega$ and $\underline{x} = (x, y, z)$ is the coordinate of a point. We will denote $u(\underline{x})$ the displacement of the point $\underline{x}$ and T the tension of the membrane. The distance between the solid and deformable body without any load applied is represented by a function $d(\underline{x}) > 0$. The non penetration of the two bodies can be written $u + d \geq 0$. Without loss of generality zero displacements are imposed on $\partial\Omega$ and only continuous body forces f_d will be applied. Finally, the part of the boundary in contact with the rigid surface will be called Ω^- and its boundary Γ. Figure III.1 illustrates this description.

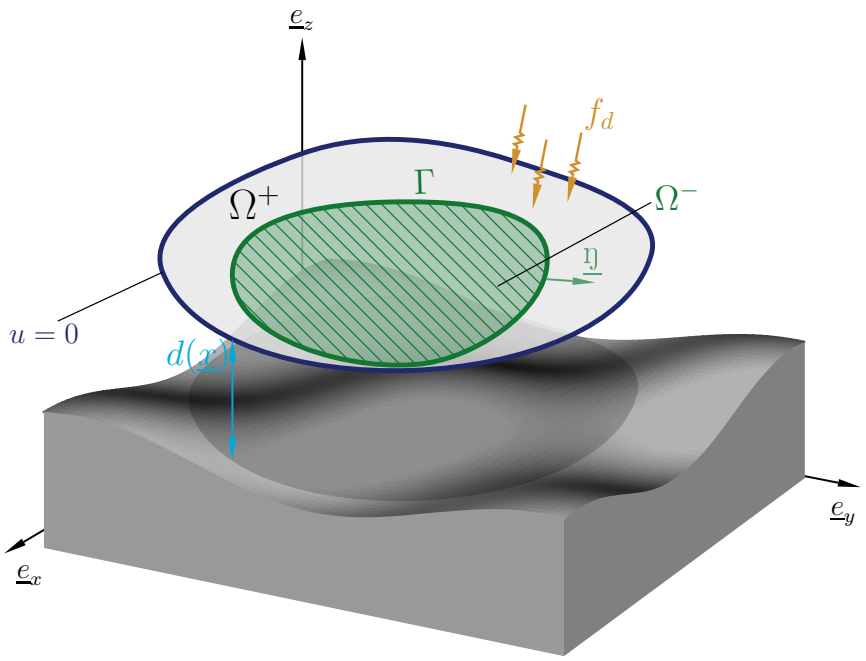

Figure III.1: Membrane into contact with a rigid surface

We recall the well known governing equations of the equilibrium of a membrane given in I.16. Without contact but with the imposed displacement, every point of the membrane has to fulfill the strong equations :

$$\begin{cases} T\Delta u + f_d = 0 & \text{on } \Omega\,, \\ u = 0 & \text{on } \partial\Omega\,. \end{cases} \tag{III.1}$$

With contact, the set of equations is more complex and involves inequalities. If there is contact the classical equivalent of (III.1) can be written with an addition of the Signorini equations (III.3):

Problem 18

Find u and p_n such as:

$$\begin{cases} T\Delta u + f_d + p_n = 0 \quad \text{on } \Omega\,, \\ u = 0 \quad \text{on } \partial\Omega\,. \end{cases} \tag{III.2}$$

$$\begin{cases} u + d \;\geq\; 0 \text{ on } \Omega\,, \\ p_n \;\geq\; 0 \text{ on } \Omega\,, \\ p_n(u+d) \;=\; 0 \text{ on } \Omega\,. \end{cases} \tag{III.3}$$

where p_n is the normal reaction exerted by the rigid surface to the membrane.

In Problem 18, all the equations have been generalized to the whole domain. However, if we split the domain into Ω^+ and Ω^- (being the actual contact zone), as described previously, Problem 18 is equivalent to:

Problem 19

Find u, p_n and Ω^- such that:

	in Ω^+	in Ω^-	on Γ
equality	$T\Delta u + f_d = 0$ $u = 0$ on $\partial\Omega$	$T\Delta u + f_d + p_n = 0$ $-u = d$	$u^+ = u^-$
inequality	$-u \leq d$	$p_n \geq 0$	

Another problem, which is closer to what is solved in practice, is to find the equilibrium solution assuming a contact zone.

Problem 20

Find u, p_n and λ_n for a given Ω^- such that:

	in Ω^+	in Ω^-	on Γ
equality	$T\Delta u + f_d = 0$ $u = 0$ on $\partial\Omega$	$T\Delta u + f_d + p_n = 0$ $-u = d$	$T[\![\nabla u]\!] \cdot \underline{\mathfrak{n}} = \lambda_n$ $u^+ = u^-$

with $[\![\nabla u(s)]\!] = \nabla u(s)^+ - \nabla u(s)^-$ the jump of ∇u at a point of Γ located by its curvilinear abscissa s and λ_n the reaction on the boundary of the rigid solid ($= 0$ if Ω^- is exact). To be equivalent to Problem 19, Problem 20 needs to be solved for the right Ω^-.

Let us show that if the contact conditions are fulfilled, i.e. the contact zone is the right one, we must satisfy $[\![\nabla u]\!] \cdot \underline{\mathfrak{n}} = 0$. First, let us look at the case $[\![\nabla u]\!] \cdot \underline{\mathfrak{n}} > 0$, thus $\lambda_n > 0$. This means that the membrane is attracted by the rigid body. Without adhesion this is not a physical solution. Now, if $[\![\nabla u]\!] \cdot \underline{\mathfrak{n}} < 0$ and therefore $\nabla u^+(s) \cdot \underline{\mathfrak{n}} < \nabla u^-(s) \cdot \underline{\mathfrak{n}}$. As by definition $\nabla d(s)$ is continuous and $\nabla u^-(s) = \nabla d(s)$ we must have $\nabla u^+(s) \cdot \underline{\mathfrak{n}} < \nabla d(s) \cdot \underline{\mathfrak{n}}$ and therefore there is penetration of the rigid surface.

Hence,

$$[\![\nabla u]\!] \cdot \underline{\mathfrak{n}} = 0 \quad \forall s \in \Gamma \tag{III.4}$$

is a necessary condition to have the right contact zone. This property will reveal itself quite useful in the next section.

In any case, as mentioned in Section I.1.1.3, a strong formulation is often not suited for computational purpose. The classical approach is to derive the weak form of this formulation. Let us first define the admissible displacements space that will be used in this chapter:

$$\mathcal{V}_d = \left\{ u \in H^1(\Omega^+ \cup \Omega^-) | u = 0 \text{ on } \partial\Omega \right\} \tag{III.5}$$

Therefore if $u \in \mathcal{V}_d$ it can admit a strong discontinuity on Γ. Problem 20 can be written as the weak formulation:

Problem 21

Find $u \in \mathcal{V}_d$, $p \in P$ and $\lambda \in H^{-1/2}(\Gamma)$ such that:

$$\begin{cases} a(u, u^\star) + \langle p, u^\star \rangle_P + \langle \lambda, [\![u^\star]\!] \rangle_{H^{-1/2}} = f(u^\star) \quad \forall u^\star \in \mathcal{V}_d, \\ \langle p^\star, u + d \rangle_P = 0 \quad \forall p^\star \in P, \\ \langle \lambda^\star, [\![u]\!] \rangle_{H^{-1/2}} = 0 \quad \forall \lambda^\star \in H^{-1/2}(\Gamma). \end{cases} \tag{III.6}$$

with:

$$\left| \begin{array}{ll} a(u, u^\star) = \displaystyle\int_\Omega T \nabla u \cdot \nabla u^\star \, \mathrm{d}S & f(u^\star) = \displaystyle\int_\Omega f_d u^\star \, \mathrm{d}S \\ \langle \lambda^\star, [\![u]\!] \rangle_{H^{-1/2}} = c(\lambda^\star, u) = \displaystyle\int_\Gamma \lambda^\star [\![u]\!] \, \mathrm{d}\Gamma & \end{array} \right. \tag{III.7}$$

Two options for P are available. The most obvious one is $L^2(\Omega^-)$ meaning that the duality pairing reads therefore $\langle p, u \rangle_{L^2} = \displaystyle\int_{\Omega^-} pu \, \mathrm{d}S$. Even if this formulation appears as the straightforward way to impose a Dirichlet condition it is not well suited to satisfy the Babuška-Brezzi (BB) condition. The other choice is $H^1(\Omega^-)$ and the duality pairing becomes $\langle p, u \rangle_{H^1} = \displaystyle\int_{\Omega^-} l_\mathrm{m} \nabla p \cdot \nabla u \, \mathrm{d}S + \int_{\Omega^-} pu \, \mathrm{d}S$. The addition of l_m is only there for dimensional homogenization and will be set to $l_\mathrm{m} = 1\mathrm{m}^2$. This last formulation fulfills naturally the BB condition as the operator is the natural scalar product associated to the space where both u and p live.

Proof: Let us prove that:

$$\sup_{u\in H^1(\Omega^-)} \frac{\langle p,u\rangle_{H^1}}{\|u\|_{H^1}} = \|p\|_{H^1} \tag{III.8}$$

First we have (given $\|u\|_{H^1} \neq 0$)

$$\frac{\langle p,u\rangle_{H^1}}{\|u\|_{H^1}} \leq \frac{\|u\|_{H^1}\|p\|_{H^1}}{\|u\|_{H^1}} = \|p\|_{H^1} \tag{III.9}$$

Furthermore if $u = p$ in the above formula we have:

$$\frac{\langle p,p\rangle_{H^1}}{\|u\|_{H^1}} = \frac{\|p\|^2_{H^1}}{\|p\|_{H^1}} = \|p\|_{H^1} \qquad \text{by Cauchy–Schwarz inequality} \tag{III.10}$$

Thus $\|p\|_{H^1}$ is a supremum of $\frac{\langle p,u\rangle_{H^1}}{\|u\|_{H^1}}$ and is reached by it when $u = p$. Therefore III.8 is verified. Injecting this property into Equation (I.57) allows us to write:

$$\inf_{p\in\mathcal{P}} \sup_{\underline{u}\in\mathcal{U}} \frac{|c(p,\underline{u})|}{\|p\|_{\mathcal{P}}\|\underline{u}\|_{\mathcal{U}}} = \inf_{p\in\mathcal{P}} \frac{\|p\|_{\mathcal{P}}}{\|p\|_{\mathcal{P}}} = 1 \tag{III.11}$$

Thus the BB condition is fulfilled. ■

Consequently, it is chosen for this chapter and Problem 21 writes:

Problem 22

Find $u \in \mathcal{V}_d$, $p \in H^1(\Omega^-)$ and $\lambda \in H^{-1/2}(\Gamma)$ such that:

$$\begin{cases} a(u,u^\star) + c_p(p,u^\star) + c_\lambda(\lambda,u^\star) = f(u^\star) \quad \forall u^\star \in \mathcal{V}_d, \\ c_p(p^\star,u) = l_p(p^\star) \quad \forall p^\star \in H^1(\Omega^-), \\ c_\lambda(\lambda^\star,u) = 0 \quad \forall \lambda^\star \in H^{-1/2}(\Gamma). \end{cases} \tag{III.12}$$

with:

$$\left| \quad b(p,u^\star) = \int_{\Omega^-} l_{\mathrm{m}} \nabla p\cdot\nabla u^\star + p u^\star \,\mathrm{d}S \quad l_p(p^\star) = -\int_{\Omega^-} l_{\mathrm{m}} \nabla p\cdot\nabla d + p d \,\mathrm{d}S \right. \tag{III.13}$$

A drawback of this formulation is the loss of equivalence between both p_n and p just as λ_n and λ. Therefore, post-processing will be needed to compute the reaction of the ground.

Check point

In this section, several ways of expressing the membrane contact problem have been shown. To summarize, it is convenient to break down the full problem given by Problem 18 into two problems: solve Problem 22 for a given Ω^- on one hand and find an admissible Ω^- on the other hand. Let us see how to discretize this formulation and then how the ILS framework is built for this problem.

III.2 ILS formulation for the membrane

III.2.1 Discretization of the problem

It was already explained in Section II.2 that a signed distance function was used to separate contact zones from the rest of the domain. Let us see how an appropriate numerical discretization can be set. We will start with classical shape functions called N_i. For instance it could be the well known hat functions. With such functions we can approximate the value of the level-set at at each point of the domain by:

$$\phi(\underline{x}) = \sum_{i \in I} \phi_i N_i(\underline{x}) \tag{III.14}$$

where I represents the number of shape functions. However in order to represent the displacement field, this classical approximation is not enough. Indeed, the solution might present weak discontinuities on the boundary. Hence, we are using the X-FEM method [Belytschko et al., 2003] to enrich the displacement. If we choose to use an enrichment function F suited to our problem an approximation of the field u is :

$$u_h(\underline{x}) = \sum_{i \in I} u_i N_i(\underline{x}) + \sum_{j \in J} u_j^e N_j(\underline{x}) F(\underline{x}) \tag{III.15}$$

with J the subset of I which is enriched.

A straightforward choice for F would be a ridge function allowing a weak discontinuity of the displacement field. Then Lagrange multiplier have to be defined on Γ in order to represent the linear force needed to physically allow a slope discontinuity in the membrane. Nonetheless, an equivalent strategy is to set F to be an Heaviside function and to use the above mentioned Lagrange multiplier to cancel the jump of the displacement $[\![u]\!]$. A better numerical behavior of the Heaviside function, especially for high order finite element, motivates this choice.

Lagrange multiplier also need to be discretized. In order to have good convergence properties we need to use the right approximation for p and λ such as the BB condition is satisfied. This problem was handled in [Moës et al., 2006] for Lagrange multiplier on a boundary (i.e. for λ) coupled with X-FEM. Rather than degree of freedoms linked directly to the front, a combination of degree of freedoms attached to the elements cut by the level-set is used. Hence this discretization is used here.Furthermore, the choice of the formulation guarantees a good behavior of p. We can then approximate p and λ:

$$p_h(\underline{x}) = \sum_{i \in I^p} p_i N_i^p(\underline{x}) \tag{III.16}$$

$$\lambda_h(\underline{x}) = \sum_{i \in I^\lambda} \lambda_i N_i^\lambda(\underline{x}) \tag{III.17}$$

with I^p and I^λ the set of degrees of freedom for each field. Finally, with such a discretization we can apply a Galerkin method to approximate Problem 22 and write it in a matricial form:

Problem 23

Find $\mathbf{u}$, $\mathbf{u}^e$, $\boldsymbol{p}$ and $\boldsymbol{\lambda}$ such that:

$$[\mathbf{K}]\begin{Bmatrix}\mathbf{u}\\ \mathbf{u}^e\\ \boldsymbol{p}\\ \boldsymbol{\lambda}\end{Bmatrix}=\begin{Bmatrix}\mathbf{f}\\ \mathbf{f}^e\\ \mathbf{l}_p\\ \mathbf{0}\end{Bmatrix}\quad\text{where}\quad[\mathbf{K}]=\begin{bmatrix}\mathbf{A}^{cc} & \mathbf{A}^{ce} & \mathbf{B} & \mathbf{C}\\ \mathbf{A}^{ce\top} & \mathbf{A}^{ee} & \mathbf{B}^e & \mathbf{C}^e\\ \mathbf{B}^\top & \mathbf{B}^{e\top} & \mathbf{0} & \mathbf{0}\\ \mathbf{C}^\top & \mathbf{C}^{e\top} & \mathbf{0} & \mathbf{0}\end{bmatrix}\tag{III.18}$$

with:

$$\begin{array}{llll}
\mathbf{u}=\{u_i\} & A^{cc}_{ij}=\displaystyle\int_\Omega \nabla N_i T\nabla N_j\,\mathrm{d}S & & \mathbf{f}=\left\{\displaystyle\int_\Omega N_i f_d\,\mathrm{d}S\right\}\\
\mathbf{u}^e=\{u^e_i\} & A^{ee}_{ij}=\displaystyle\int_\Omega \nabla N^e_i T\nabla N^e_j\,\mathrm{d}S & A^{ce}_{ij}=\displaystyle\int_\Omega \nabla N_i T\nabla N^e_j\,\mathrm{d}S & \mathbf{f}^e=\left\{\displaystyle\int_\Omega N^e_i f_d\,\mathrm{d}S\right\}\\
\mathbf{p}=\{p_i\} & B_{ij}=\displaystyle\int_{\Omega^-} N_i N^p_j\,\mathrm{d}S & B^e_{ij}=\displaystyle\int_{\Omega^-} N^e_i N^p_j\,\mathrm{d}S & \mathbf{l}_p=\left\{-\displaystyle\int_{\Omega^-} N^p_i d\,\mathrm{d}S\right.\\
 & \quad+\displaystyle\int_\Omega l_{\mathrm{m}}\nabla N_i\nabla N^p_j\,\mathrm{d}S & \quad+\displaystyle\int_\Omega l_{\mathrm{m}}\nabla N^e_i\nabla N^p_j\,\mathrm{d}S & \left.-\displaystyle\int_{\Omega^-} l_{\mathrm{m}}\nabla N^p_i\nabla d\,\mathrm{d}S\right\}\\
\boldsymbol{\lambda}=\{\lambda_i\} & C_{ij}=\displaystyle\int_\Gamma N_i N^\lambda_j\,\mathrm{d}\Gamma & C^e_{ij}=\displaystyle\int_\Gamma N^e_i N^\lambda_j\,\mathrm{d}\Gamma &
\end{array}\tag{III.19}$$

The size of the matrix $\mathbf{A}^{ee}$ is usually very small compare to the size of $\mathbf{A}^{cc}$. This last matrix is not changing through the iteration, which is numerically convenient. Therefore a great deal of computational effort can be spared by working on $\mathbf{A}^{cc}$ only once.

III.2.2 Shape optimization

At this point, we can solve Problem 19 for a given contact zone. However the solution might not fulfill the contact conditions (i.e. the contact zone is not the right one). We are going to search for the exact contact zone with an iterative process. As with an active-set method, we are using the fields computed at the current iteration to determine the evolution of the contact zone. The main difference is that we are not using the same criterion as in active-set method to make the contact zone evolve. An active-set method uses directly the value of the fields. For instance a criterion would be if the Lagrange multiplier are positive then remove the constraint at the node. The ILS is mainly using another criterion ϱ which depend on the problem it is dealing with. This criterion is chosen strictly related to the boundary of the contact zone rather than whole of the solid boundary. Let us denote Γ^k the boundary of the contact zone at the k^{th} iteration. To lighten the notations we will usually only write Γ. The abovementioned criterion must satisfy:

$$\Gamma=\Gamma^{\text{ex}}\Rightarrow\varrho=0\text{ on }\Gamma\tag{III.20}$$

where Γ^{ex} is the exact boundary of the contact zone. Thus if $\varrho \neq 0$, the position of Γ is not the right one . This leads to try to find at each iteration the evolution of the contact zone which cancel ϱ. Nevertheless, having $\varrho = 0$ is not always sufficient to insure that $\Gamma = \Gamma^{\text{ex}}$. Indeed the KKT conditions might not be fulfilled everywhere. Therefore, time to time, these conditions are checked on the full domain in order to take into account contact zone nucleation and disappearance (see Section II.3 for q more detailed explanation).

Here, the obvious choice for ϱ is $[\![\nabla u]\!] \cdot \underline{\mathfrak{n}}$, see equation (III.4). This choice is recovered if the more general configuration mechanics method is used as explained in Section II.3.3. Indeed, the configurational force g defined in this above mentioned section has the following expression if f_d is constant:

$$g = -p[\![\nabla u]\!] \cdot \underline{\mathfrak{n}} \tag{III.21}$$

An efficient way to find the zero of a functional is to use a Newton method. Therefore, if we can compute the derivative of ϱ with respect to a variation of the contact zone shape we can apply a Newton algorithm to update Γ. This correspond to the definition, given in Section II.3.2, of the normal directional derivative. With this definition, normal directional derivative of ϱ is:

$$D\varrho[\underline{w}_\Gamma] = \lim_{\zeta \to 0} \frac{\varrho(\Gamma(\zeta \underline{w}_\Gamma)) - \varrho(\Gamma(0))}{\zeta} \tag{III.22}$$

Then the zero of ϱ can be found by solving:

Problem 24

Find $\underline{w}_\Gamma \in L^2(\Gamma)$ such that:

$$\varrho + D\varrho[\underline{w}_\Gamma] = 0 \text{ on } \Gamma \tag{III.23}$$

$$\Leftrightarrow \int_\Gamma \varrho \underline{w}_\Gamma^\star \, \mathrm{d}\ell + \int_\Gamma D\varrho[\underline{w}_\Gamma] \underline{w}_\Gamma^\star \, \mathrm{d}\ell = 0 \quad \forall \underline{w}_\Gamma^\star \in L^2(\Gamma) \tag{III.24}$$

We recall that we use the notation $D\varrho[\underline{w}_\Gamma] = \mathring{\varrho}$. We can expand this expression in this particular case to $\mathring{\varrho} = \overline{[\![\nabla u]\!] \cdot \underline{\mathfrak{n}}} = [\![\nabla \mathring{u}]\!] \cdot \underline{\mathfrak{n}} - [\![\nabla u]\!] \cdot \nabla \underline{w}_\Gamma \cdot \underline{\mathfrak{n}} + [\![\nabla u]\!] \cdot \nabla \underline{\mathfrak{n}} \cdot \underline{w}_\Gamma$.

With these new tools we are going to take the directional derivative of Problem 22 to have a system with $(\mathring{u}, \mathring{p}, \mathring{\lambda})$ as unknowns. In order to compute $\mathring{u}$, $\mathring{p}$ and $\mathring{\lambda}$ we need to extend the definition of $D[\,]$ to the whole domain. The boundary displacement $\underline{w}_\Gamma$ is then extended onto this domain. This extended displacement is noted $\underline{w}$. But, as we are only, in practice, interested by the evolution of ϱ on the contact boundary, we are going to introduce a function $r(\phi)$. This means that this function depends on the distance from Γ in the normal direction. This function allows us to set the displacement value to zero after a certain distance δ and thus to reduce the computational cost (cf. Figure III.2). This defined the band $\mathcal{B}$ already mentioned in Section II.3.3. Finally, in order to keep the extended displacement normal to the boundary of the contact area we are going to use the gradient of the level-set $\nabla\phi(\underline{x})$ as its norm is one and it is normal to the iso-level-set.

$$\underline{w}(\underline{x}) = w_\Gamma(s_c) \nabla\phi(\underline{x}) r(\varsigma) \tag{III.25}$$

where s_c represent the curvilinear abscissa of the closest point of $\underline{x}$ on Γ.

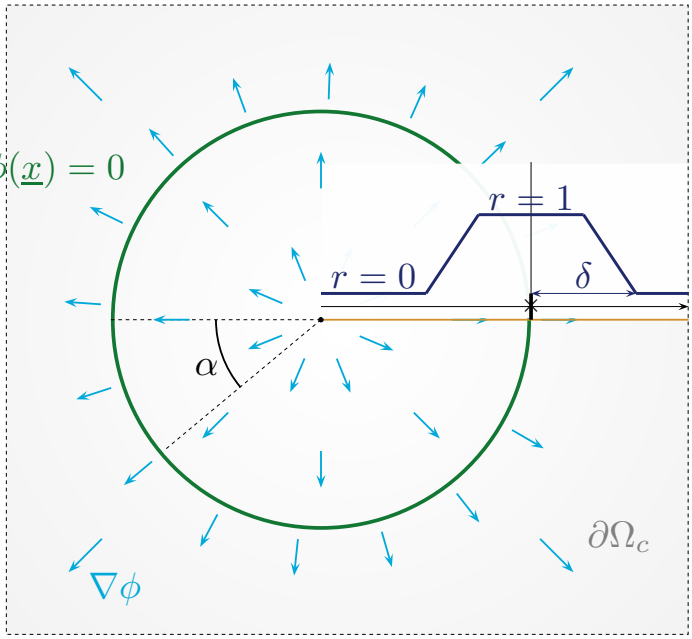

Figure III.2: function r in the case of a circular level-set

Now with this extended displacement, the normal directional derivative can be defined for any quantity f in the same fashion as explained in Section II.3.2.3.

Let us take a moment to give a step by step calculus of every derivatives of Problem 22 members.

$$D(a(u,u^\star))[\underline{w}] = \int_\Omega T\left(\overline{\nabla \mathring{u}}\cdot\nabla u^\star + \nabla u\cdot\overline{\nabla \mathring{u^\star}} + \nabla u\cdot\nabla u^\star \operatorname{div}\underline{w}\right)\mathrm{d}S \tag{III.26}$$
$$= \int_\Omega T\left((\nabla \mathring{u} - \nabla u\cdot\nabla\underline{w})\cdot\nabla u^\star + \nabla u\cdot(\nabla \mathring{u^\star} - \nabla\underline{w}\nabla u^\star) + \nabla u\cdot\nabla u^\star\operatorname{div}\underline{w}\right)\mathrm{d}S$$

$$D(b(p,u^\star))[\underline{w}] = \int_{\Omega^-} l_{\mathrm{m}}(\nabla\mathring{p}\nabla u^\star + \nabla p\nabla\mathring{u^\star} - \nabla p(\nabla\underline{w}^\top + \nabla\underline{w})\nabla u^\star + \nabla p\nabla u^\star\operatorname{div}\underline{w})\,\mathrm{d}S \tag{III.27}$$
$$+ \int_{\Omega^-}\mathring{p}u^\star + p\mathring{u^\star} + pu^\star\operatorname{div}\underline{w}\,\mathrm{d}S$$

$$D(c(\lambda,u^\star))[\underline{w}] = \int_\Gamma \mathring{\lambda}[\![u^\star]\!] + \lambda[\![\mathring{u^\star}]\!] + \lambda[\![u^\star]\!](\operatorname{div}\underline{w} - \underline{\mathfrak{n}}\cdot\nabla\underline{w}\cdot\underline{\mathfrak{n}})\,\mathrm{d}\ell \tag{III.28}$$

$$D(f(u^\star))[\underline{w}] = \int_\Omega \mathring{f}u^\star + f\mathring{u^\star} + fu^\star\operatorname{div}\underline{w}\,\mathrm{d}S \tag{III.29}$$

$$D(l_p(p^\star))[\underline{w}] = -\int_{\Omega^-} l_{\mathrm{m}}(\nabla\mathring{p^\star}\nabla d + \nabla p^\star\nabla\mathring{d} - \nabla p^\star(\nabla\underline{w}^\top + \nabla\underline{w})\nabla d + \nabla p^\star\nabla d\operatorname{div}\underline{w})\,\mathrm{d}S \tag{III.30}$$
$$- \int_{\Omega^-}\mathring{p^\star}d + p^\star\mathring{d} + p^\star d\operatorname{div}\underline{w}\,\mathrm{d}S$$

The test fields $u^\star$, $p^\star$ and $\lambda^\star$ are chosen such that for all $\underline{x}$ where the fields are defined, $\mathring{u^\star}(\underline{x}) = 0$, $\mathring{p^\star}(\underline{x}) = 0$ and $\mathring{\lambda^\star}(\underline{x}) = 0$. This means that the test fields follow the movement of the interface. Therefore if the imposed force field f_d also follow the movement of the interface (i.e. $\mathring{f}_d$=0) we find the formulation of Problem 25.

Hence, gathering all the terms, Problem 22 derivative is:

Problem 25

Find $\mathring{u} \in \mathcal{V}_d$, $\mathring{p} \in H^1(\Omega^-)$ and $\mathring{\lambda} \in H^{-1/2}(\Gamma)$ such that:

$$\left\{\begin{array}{ll} a(\mathring{u}, u^\star) + b(\mathring{p}, u^\star) + c(\mathring{\lambda}, u^\star) = f^s(u^\star, w) & \forall u^\star \in \mathcal{V}_d, \\ b(p^\star, \mathring{u}) = l_p^s(p^\star, w) & \forall p^\star \in L^2(\Omega^-), \\ c(\lambda^\star, \mathring{u}) = l_\lambda^s(\lambda^\star, w) & \forall \lambda^\star \in H^{-1/2}(\Gamma). \end{array}\right. \tag{III.31}$$

where:

$$\left|\begin{array}{rcl} f^s(u^\star, w) & = & -\displaystyle\int_\Omega T\left(\nabla u^\top \nabla u^\star \,\mathrm{div}\underline{w} - (\nabla u^\top(\nabla \underline{w}^\top + \nabla \underline{w})\nabla u^\star)\right) \mathrm{d}S \\ & & -\displaystyle\int_{\Omega^-} l_\mathrm{m}\left(\nabla p^\top \nabla u^\star \,\mathrm{div}\underline{w} - (\nabla p^\top(\nabla \underline{w}^\top + \nabla \underline{w})\nabla u^\star)\right) \mathrm{d}S \\ & & -\displaystyle\int_{\Omega^-} p u^\star \,\mathrm{div}\underline{w}\,\mathrm{d}S - \int_\Gamma \lambda[\![u^\star]\!](\mathrm{div}\underline{w} - \underline{\mathfrak{n}}\cdot\nabla\underline{w}\cdot\underline{\mathfrak{n}})\,\mathrm{d}\ell + \int_\Omega f_d u^\star \mathrm{div}\underline{w}\,\mathrm{d}S \\ l_p^s(p^\star, w) & = & -\displaystyle\int_{\Omega^-} p^\star \mathring{d}\,\mathrm{d}S - \int_{\Omega^-} l_\mathrm{m}\nabla p^\star \nabla \mathring{d}\,\mathrm{d}S \\ l_\lambda^s(\lambda^\star, w) & = & -\displaystyle\int_\Gamma \lambda^\star[\![u]\!](\mathrm{div}\underline{w} - \underline{\mathfrak{n}}\cdot\nabla\underline{w}\cdot\underline{\mathfrak{n}})\,\mathrm{d}\ell \end{array}\right. \tag{III.32}$$

It is important to note that Problem 25 has the same left-hand side as Problem 22. Using the discretization given in (III.15,III.16,III.17) Problem 25 allows the following discrete form:

Problem 26

Find $\mathring{\mathbf{u}}$, $\mathring{\boldsymbol{p}}$ and $\mathring{\boldsymbol{\lambda}}$ such that:

$$[\mathbf{K}]\left\{\begin{array}{c}\mathring{\mathbf{u}} \\ \mathring{\boldsymbol{p}} \\ \mathring{\boldsymbol{\lambda}}\end{array}\right\} = \left\{\begin{array}{c}\mathbf{f}^s \\ \mathbf{l}_p^s \\ \mathbf{l}_\lambda^s\end{array}\right\} \tag{III.33}$$

and thus the left-side matrice is the same as the one of Problem 25. Thereby we can use the matrix decomposition already computed to speed up the process.

However, as u_Γ is unknown, we cannot directly compute Problem 26. Therefore, u_Γ is going to be approximated by n_{mode} given modes w_m. For each mode, a τ_m is associated and represent the m^{th} mode contribution to u_Γ.

$$u_\Gamma = \sum_m \tau_m w_m. \tag{III.34}$$

There is plenty of possibilities to construct the modes. Here we are going to use the Fourier modes $w_m = \mathcal{F}_m(\alpha)$ (α being a parametrization angle for the contact area boundary as in Figure III.2). The Fourier modes are defined fore every $m' \in \mathbb{N}$ such that:

$$\begin{cases} \mathcal{F}_{2m'}(\alpha) = \cos(m'\alpha) \\ \mathcal{F}_{2m'+1}(\alpha) = \sin((m'+1)\alpha) \end{cases} \tag{III.35}$$

At the end of this chapter, a discussion is opened on the advantage and the drawbacks of such modes. In order to get all the $\mathring{\rho}_m$, Problem 26 has to be solved n_{mode} times. In practice, all these problems are solved in one go. This approximation can be passed on to Problem 24, it can thereby be approximated using a Galerkin approximation:

Problem 27

Find $\boldsymbol{\tau} = \{\tau_m\} \in \mathbb{R}^M$ such that:

$$\sum_n \int_\Gamma \varrho w_n \,\mathrm{d}\ell + \sum_m \sum_n \int_\Gamma \tau_m D\varrho[w_m \underline{\mathfrak{n}}] w_n \,\mathrm{d}\ell = 0 \tag{III.36}$$

$$\Leftrightarrow \sum_n \int_\Gamma \varrho w_n \,\mathrm{d}\ell + \sum_m \sum_n \int_\Gamma \tau_m \mathring{\varrho}_m w_n \,\mathrm{d}\ell = 0 \tag{III.37}$$

Again, Problem 27 can be written as:

Problem 28

Find $\boldsymbol{\tau} \in \mathbb{R}^m$ such that:

$$[\mathbf{S}]\,\boldsymbol{\tau} = -\boldsymbol{\varrho}^\pi \tag{III.38}$$

where:

$$S_{nm} = \sum_i \int_\Gamma \varrho_i D N_i^\lambda[w_m] w_n \,\mathrm{d}\ell \tag{III.39}$$

$$\varrho_n^\pi = \sum_i \int_\Gamma \varrho_i N_i^\lambda w_n \,\mathrm{d}\ell \tag{III.40}$$

These steps (Problem 23, n_{mode}-times Problem 26 and Problem 28) are iterated up to convergence. To be able to compute the new Γ we need to update the level-set using the

displacement $\underline{w}$. In order to do so, one of the technique mentioned in Section II.2.1.4 is used. In the case where a fixed number of modes is used, the algorithm is stopped when the norm of projection of ϱ noted $\pi(\varrho_m)$ onto the mode space is small enough (i.e. inferior to a scalar $\pi_{\min}$), which means that we could do no better with the modes used. It is more interesting to have an increasing number of modes through the iterations. Indeed, at the beginning, having only a few modes allow a fast computation to get closer to the solution. Then a greater number of mode allows a better precision.

However, it was already pointed out that, by itself, the algorithm might not converge to a solution as ϱ could be zero for another configuration. That is why, at the end of the convergence of the algorithm (or if there is no convergence at all) extra steps are added. First, as in classical active set methods, we check if there is penetration and also that the reaction of the support is not attracting the membrane. This defines areas where the contact conditions are violated and they should be added in case there is penetration or removed for attraction as it was explained in Section II.2.1.4. The full method was already summed up in the Algorithm 3.

Remark

Let us now consider the influence of adhesion in the contact zone and how it affects the Inequality Level Set approach. For instance, consider that the floor in Figure III.1 is covered with a fluid with surface tension γ_t. At equilibrium, the configurational force on the boundary of the contact zone is no longer zero but needs to match the value of surface tension. Indeed, with adhesion, it takes energy to create new surfaces as the contact zone is reduced in size. As a consequence, at equilibrium the pressure on the boundary of the contact zone is no longer zero but we have

$$\frac{T}{2}\varrho^2 = \gamma_t \rightarrow \varrho = \varrho_a = \sqrt{\frac{2\gamma_t}{T}} \tag{III.41}$$

The ILS algorithm described in section III.2 is still the same except that the pressure is driven to ϱ_a and not zero. An example of this application can be found in the next section (see Figure III.6).

III.3 Results

In this section we are going to study the case of a membrane with a homogeneous loading. Then, the full 2D problem will be dealt with.

III.3.1 The axi-symmetric problem

We recall that the problem we are looking at is a circular membrane (Figure III.3) with radius R (set to 1 m for numerical purpose) and homogeneous tension T (set to 1 Nm^{-1}). This membrane is loaded with an homogeneous loading f_d. The quantity of interest is the vertical displacement u which is prescribed to be zero along the border. This displacement is limited by an undeformable horizontal plane of altitude d.

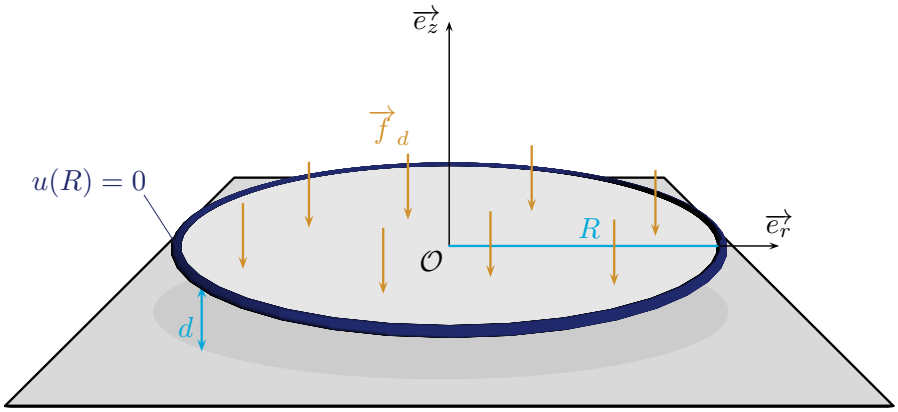

Figure III.3: Axi-symmetric membrane with an homogeneous load

The problem can be summarized into the equations:

$$\begin{cases} T\Delta u + f_d &= 0 & \text{in } \Omega \\ -u &\leq d & \text{in } \Omega \\ u &= 0 & \text{for } r = R \end{cases} \tag{III.42}$$

The analytical solution (see Appendix B) of the equilibrium for a given r_c is :

$$u = -\frac{f_d r^2}{4T} + A \ln\left(\frac{r}{R}\right) + B \tag{III.43}$$

where:

$$\begin{aligned} A &= \frac{f_d(R^2 - r_c^2) + 4dT}{4T\ln(R/r_c)} \\ B &= \frac{f_d R^2}{4T} \\ r_c &\text{ is the radius of the contact zone} \end{aligned} \tag{III.44}$$

However, the only solution which fulfills the contact condition (see Appendix B) imposes that the exact value of r_c is:

$$r_c^{\text{ex}} = R \exp\left(\frac{1}{2}\left(1 + \mathrm{W}_{-1}\left(-\frac{4dT + f_d}{e f_d}\right)\right)\right) \tag{III.45}$$

With $\mathrm{W}_{-1}(x)$ the branch of the Lambert function defined for $-1/e \leq x < 0$ and $e = \exp(1)$. In this section, for every numerical simulation $|f_d| = 1$ N and $d = 0.1$ m.

III.3.1.1 With axi-symmetric hypothesis

As said before, if we take into account the axi-symmetry the problem is simplified in a 1D problem. At a given contact area, we need to find u such that:

$$\begin{cases} T\frac{1}{r}\frac{\partial}{\partial r}\left(r\frac{\partial u}{\partial r}\right) + f_d &= 0 & \text{on } [0, r_c[\\ -u &= d & \text{on } [rc, R] \\ u &= 0 & \text{for } r = R \end{cases} \tag{III.46}$$

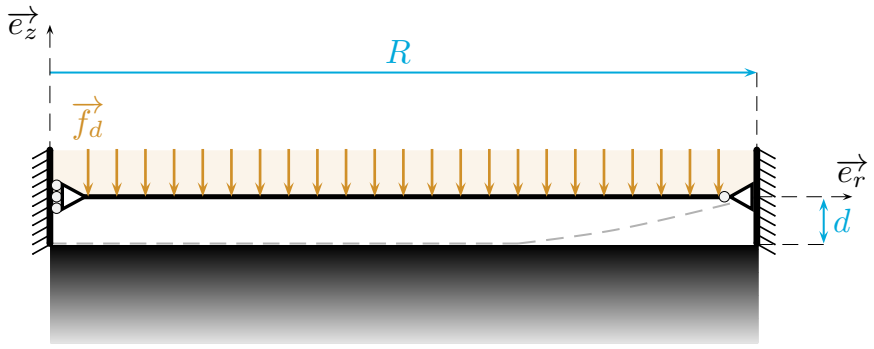

Figure III.4: Axi-symmetric simplification of the membrane (right side) and illustration of the solution

Let us illustrate what was described in Section III.2 with this simplified problem. In order to impose $u = d$ on $[0, rc]$ we use Lagrange multiplier p. Even if p is going to be defined on $[0, R]$ we will be able to take into account their influence only on the contact zone. Indeed, taking advantage of the level-set framework we integrate only on the contact zone.

Problem 29

Find $u \in \mathcal{V}_d$, $p \in H^1(\Omega^-)$ and $\lambda \in \mathbb{R}$ such that:

$$\begin{cases} a(u, u^\star) + b(p, u^\star) + c(\lambda, u^\star) = f(u^\star) \quad \forall u^\star \in \mathcal{V}_d, \\ b(p^\star, u) = l_p(p^\star) \quad \forall p^\star \in H^1(\Omega^-), \\ c(\lambda^\star, u) = 0 \quad \forall \lambda^\star \in \mathbb{R}. \end{cases} \tag{III.47}$$

with:

$$\begin{aligned} a(u, u^\star) &= \int_0^R Tr \frac{\partial u}{\partial r} \frac{\partial u^\star}{\partial r} \, \mathrm{d}\ell & f(u^\star) &= \int_0^R f_d r u^\star \, \mathrm{d}\ell \\ b(u, p) &= \int_0^{r_c} \left(l_\mathrm{m} \frac{\partial p}{\partial r} \frac{\partial u}{\partial r} + pu \right) r \, \mathrm{d}\ell & l_p(p^\star) &= -\int_0^{r_c} \left(l_\mathrm{m} \frac{\partial p}{\partial r} \frac{\partial d}{\partial r} + pd \right) r \, \mathrm{d}\ell \\ c(u, \lambda) &= \lambda r_c [\![u]\!] \end{aligned} \tag{III.48}$$

As we are dealing with a 1D problem we will use only one mode for w which correspond to a unit displacement of r_c in $\underline{e}_r$ direction If we take the normal directional derivative of these equations we obtain the following sensitivity problem.

Problem 30

Find $\mathring{u} \in \mathcal{V}_d$, $\mathring{p} \in H^1(\Omega^-)$ and $\mathring{\lambda} \in \mathbb{R}$ such that:

$$\begin{cases} a(\mathring{u}, u^\star) + b(\mathring{p}, u^\star) + c(\mathring{\lambda}, u^\star) = f^s(u^\star) \quad \forall u^\star \in \mathcal{V}_d, \\ b(p^\star, \mathring{u}) = l_p^s(p^\star) \quad \forall p^\star \in H^1(\Omega^-), \\ c(\lambda^\star, \mathring{u}) = l_\lambda^s(\lambda^\star) \quad \forall \lambda^\star \in \mathbb{R}. \end{cases} \tag{III.49}$$

with:

$$\left| \begin{array}{l} f^s(u^\star) = -(r_c f_d + \lambda) u^{\star +}(r_c) \\ l_p^s(p^\star) = 0 \\ l_\lambda^s(\lambda^\star) = -\lambda^\star r_c \dfrac{\lambda}{T} \end{array} \right. \tag{III.50}$$

First we will use a linear approximation. The $\{N_i\}$ family is therefore the family of the hat functions. The displacement field is enriched at r_c with an Heaviside function. Thus the enriched nodes are the ones surrounding r_c or the node itself if r_c is on a node. One shall keep in mind that the integration of p only on the contact zone is enabled by the knowledge of the position of r_c between two nodes.

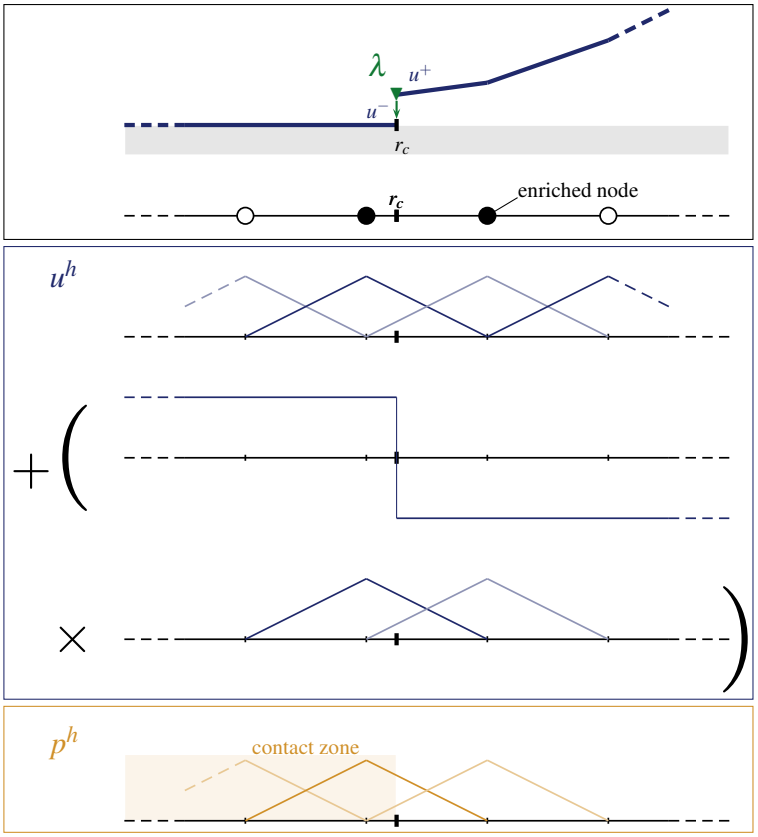

Figure III.5: Approximation of the fields

Once these two problems are solved we have access to ϱ and $\mathring{\varrho}$ and we can solve the Problem 27 associated to our case.

$$\varrho + \mathring{\varrho}\tau = 0 \quad \Leftrightarrow \quad \tau = -\frac{\varrho}{\mathring{\varrho}} \tag{III.51}$$

Thus if we were at the k^{th} iteration the next r_c^{k+1} would be:

$$r_c^{k+1} = r_c^k + \tau = r_c^k - \frac{\varrho}{\mathring{\varrho}} \tag{III.52}$$

An illustration of the results of the ILS method can be seen in Figure III.6. This same problem was also treated adding adhesion as described in Section III.2.2. We need to apply the Newton algorithm on the function $\varrho - \varrho_a$. The weak discontinuity of the displacement is well represented by the X-FEM Heaviside enrichment combined with Lagrange multiplier.

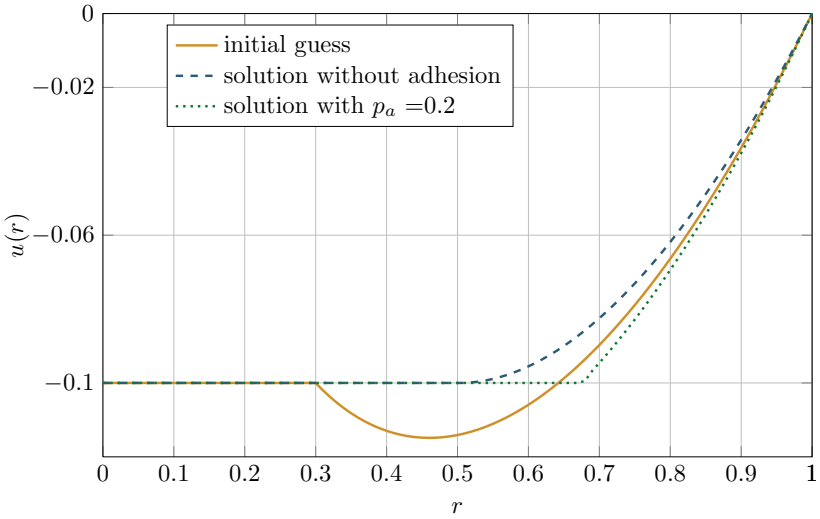

Figure III.6: Solution given by the algorithm with an without adhesion

We compared this method to an active set method with nodal Lagrange multiplier (which will be referred as "classical") in the case without adhesion. The set where the constraint is active (namely where the contact is imposed) is a set of N_c nodes. The coordinates of the k^{th} node in this set is noted $\underline{x}_c^k$. In order to make this contact zone evolve, the penetration and the reaction of the support are checked as explained in the last section. Then, every node which violates the penetration is added in the active set whereas the ones violating the support reaction are removed. The same discretization of u is used without the enrichment. The problem for a given Ω^- is then:

Problem 31

Find $u \in \mathcal{V}_d$, $p \in \mathbb{R}^{N_c}$ such that:

$$\begin{cases} a(u, u^\star) + \sum_{k=1}^{N_c} p_k u^\star(\underline{x}_c^k) = f(u^\star) \quad \forall u^\star \in \mathcal{V}_d, \\ \sum_{k=1}^{N_c} p_k^\star u(\underline{x}_c^k) = -\sum_{k=1}^{N_c} p_k^\star d(\underline{x}_c^k) \quad \forall p^\star \in \mathbb{R}^{N_c}. \end{cases} \tag{III.53}$$

The initial r_c is chosen as $r_{c_0} = 0.3$m. In Figure III.7(a) we are interested in the evolution of the relative error on the position of r_c with the size of the elements h. With ILS method we observe a better convergence rate than with the other one. The stages of the other method are also avoided. They arise because as long as the refinement of the mesh does not add a node closer to r_c^{ex} there is no better approximation available. This problem is avoided by the enrichment of the ILS method. Figure III.7(b) on the other hand shows the power of having an evolution driven by the sensitivity. Indeed, by adding more degree of freedom we increase the number of iterations needed with the classical active set as there is more sets possibilities. Whereas it is not increasing in our case as it is sensitivity driven.

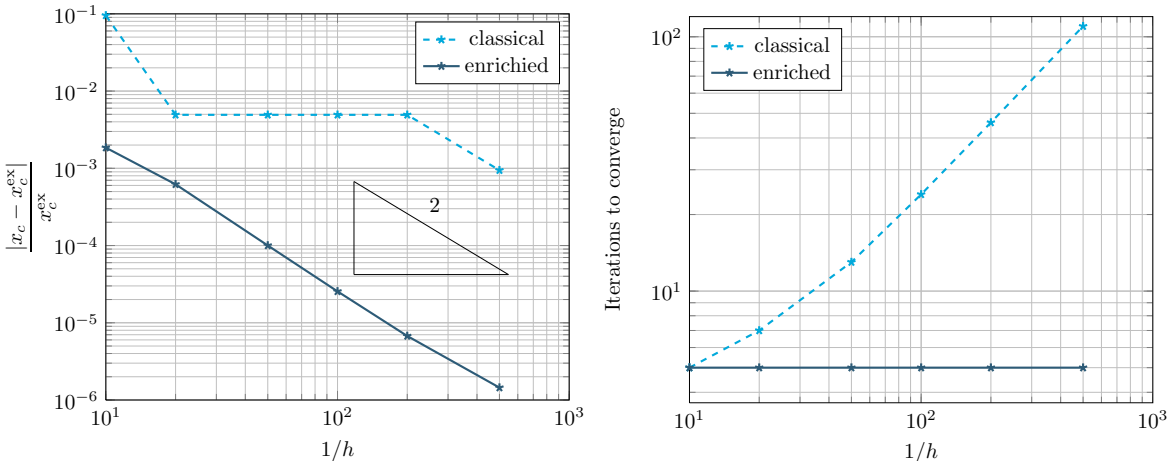

(a) (b)

Figure III.7: Evolution of (a) the error on r_c (b) the number of iterations, with the size of the mesh

III.3.1.2 Higher order interpolation

Using the above set up, higher order interpolations are tried out. Increasing the interpolation degree is often an efficient way of improving the quality of the solution. Compare to mesh refinement (often called h-convergence), the use of higher degree shape functions (p-convergence) is known to be more efficient in most situation. Nevertheless it is harder to implement and may have convergence issues (such as spurious oscillations) in problems like contact. Here, the

Bernstein polynomials are used. For a degree p, there is $p+1$ polynomials defined on $s \in [0,1]$ such that:

$$B_{i,p}(x) = \binom{p}{i} s^i (1-s)^{p-i}, \quad i = 0, \dots, p \tag{III.54}$$

The polynomial up to degree three are made explicit below:

$$\begin{aligned}
&B_{0,0}(s) = 1, \\
&B_{0,1}(s) = 1 - s, && B_{1,1}(s) = s \\
&B_{0,2}(s) = (1-s)^2, && B_{1,2}(s) = 2s(1-s), && B_{2,2}(s) = s^2 \\
&B_{0,3}(s) = (1-s)^3, && B_{1,3}(s) = 3s(1-s)^2, && B_{2,3}(s) = 3s^2(1-s), && B_{3,3}(s) = s^3
\end{aligned}$$

The solution of the problem on a coarse mesh is given in Figure III.8 for different degrees of interpolation:

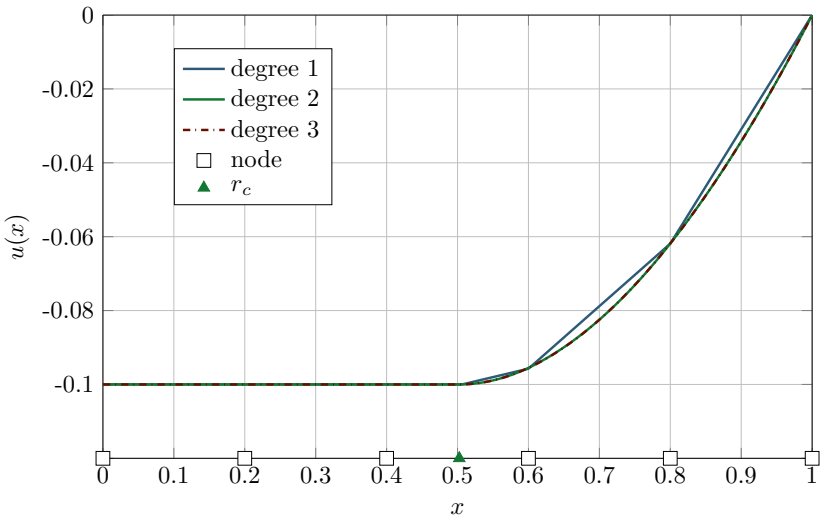

Figure III.8: Solution on a coarse mesh for several degrees of interpolation

The stability of the number of iterations is conserved with h or p-refinement. Furthermore, no oscillation of the fields were to be found.

In Figure III.9 errors are studied. The position of the boundary r_c is better represented using a high order interpolation up to the point where a step is reached at 10^{-12} (see Figure III.9(a)). As expected, Figure III.9(b) shows an increase of the rate of convergence by one when using the next order of interpolation.

III.3.1.3 Without axi-symmetric hypothesis

Without this hypothesis, we recall that the direct problem is Problem 22. Then, if we use the modal base $\{w_m\}$ to approximate the displacement field and note $\underline{w}_m = w_m \underline{\mathrm{n}}$, the sensitivity problem becomes similar to Problem 30 with the above notation and:

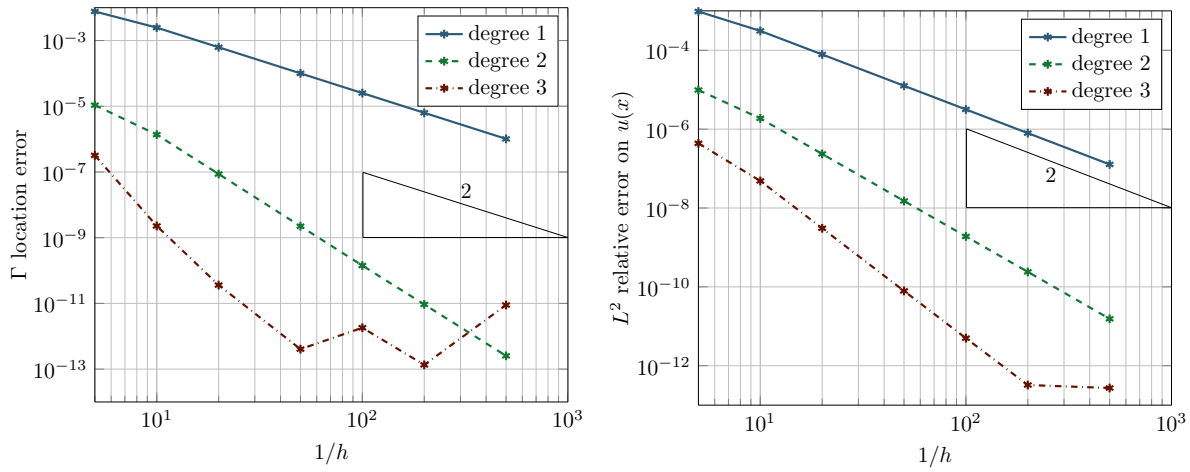

(a) (b)

Figure III.9: Study of the convergence of the method for different interpolation orders

$$
\left|\begin{array}{rcl}
f^s(u^\star, w) &=& -\displaystyle\int_\Omega T\left(\nabla u^\top \nabla u^\star \,\mathrm{div}\underline{w} - (\nabla u^\top(\nabla \underline{w}^\top + \nabla \underline{w})\nabla u^\star)\right)\,\mathrm{d}S \\
&& -\displaystyle\int_{\Omega^-} l_\mathrm{m}\left(\nabla p^\top \nabla u^\star \,\mathrm{div}\underline{w} - (\nabla p^\top(\nabla \underline{w}^\top + \nabla \underline{w})\nabla u^\star)\right)\,\mathrm{d}S \\
&& -\displaystyle\int_{\Omega^-} p u^\star \,\mathrm{div}\underline{w}\,\mathrm{d}S - \int_\Gamma \lambda[\![u^\star]\!](\mathrm{div}\underline{w} - \underline{\mathfrak{n}}\cdot\nabla\underline{w}\cdot\underline{\mathfrak{n}})\,\mathrm{d}\ell + \int_\Omega f_d u^\star \mathrm{div}\underline{w}\,\mathrm{d}S \\
l_p^s(p^\star, w) &=& 0 \\
l_\lambda^s(\lambda^\star, w) &=& -\displaystyle\int_\Gamma \lambda^\star[\![u]\!](\mathrm{div}\underline{w} - \underline{\mathfrak{n}}\cdot\nabla\underline{w}\cdot\underline{\mathfrak{n}})\,\mathrm{d}\ell
\end{array}\right. \tag{III.55}
$$

The primary task is to set the initial contact area boundary to be the solution of the problem without any contact conditions. Therefore, the first guessed contact area is a centered circle of radius 0.77m. Only the first mode should be activated and we should observe a proportional growth of the contact zone. Indeed, the first mode represent an homogeneous growth of the front. The combination of the second and the third allows a translation of the contact zone. Latter modes become more and more localized. A first simulation is done with a non-axi-symmetric mesh. The result can be seen Figure III.10. The jump in the membrane slope, clearly visible in the initial solution, is canceled at the end of the iterations. Here, a small δ was taken on purpose. This explained the constant advance of the front for the first iterations.

In Figure III.11(a) it can be seen that other modes than the first one are activated. This is due to the numerical error during the level-set evolution which breaks the axi-symmetry. Therefore the algorithm needs extra modes to compensate these errors. To ensure that this is due to these numerical aspects an axi-symmetric mesh was used in another simulation. Figure III.11(b) confirmed that no other modes but the first one are activated at first. The activation of the other modes at the 8^{th} iteration is just due to the fact that the convergence stage as

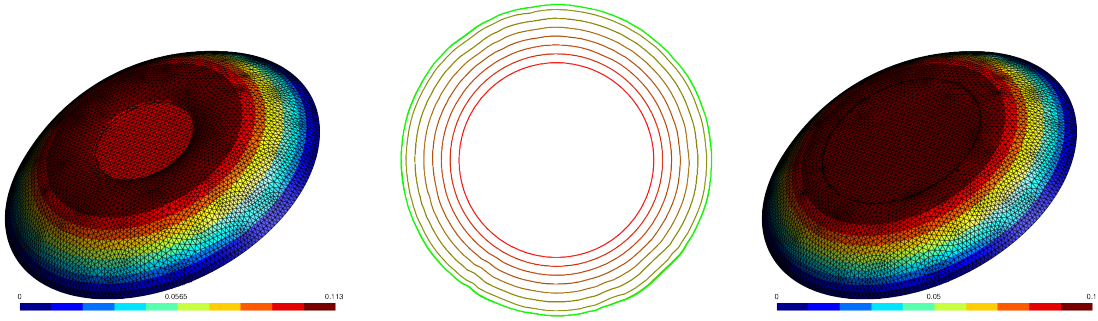

(a) Initial (b) Evolution (c) Final

Figure III.10: Evolution of the contact interface from initial to final configuration (b) with the displacement associated to these to extreme position ((a) and (c)).

been reached as Figure III.12 shows.

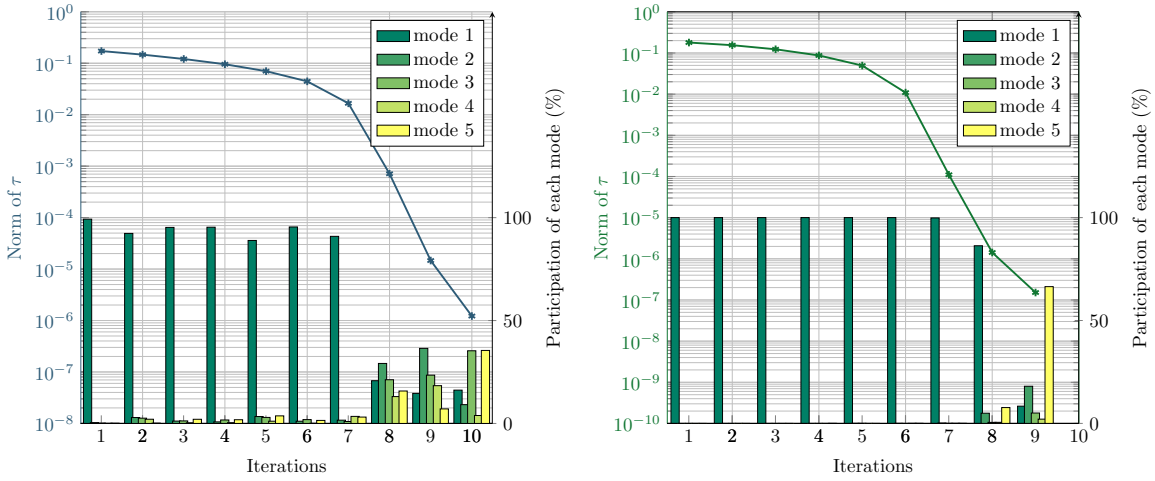

(a) non-axi-symmetric mesh (b) axi-symmetric mesh

Figure III.11: Evolution of the norm of τ and percentage of the contribution of each mode

A stage in the convergence can be observed after some iterations (cf. Figure III.12). It is due to the geometrical approximation of the level set on the mesh. Therefore, it is decreasing with the size of the mesh as we get a better representation of the level-set.

Let us compare again the ILS method to the active set method. The behavior of these methods is quite similar to the axi-symmetric hypothesis case, retrieving the same properties of convergence for the location of Γ (cf. Figure III.13(a)).

In relevance to the efficiency of the algorithm, Table III.1 gives the total computational cost for each method up to convergence as well as the average time per iteration. First the comparison is made for several fixed meshes and then for a targeted error on the location of Γ. First, let us discuss the computational times on fixed meshes. The ILS uses more time on coarse mesh than the classical method. Nonetheless for regular sized or fine meshes this trend is reversed. This is due to both the increase of iterations needed by the classical method and the reduction of the difference of time needed by each method for one iteration. This last point

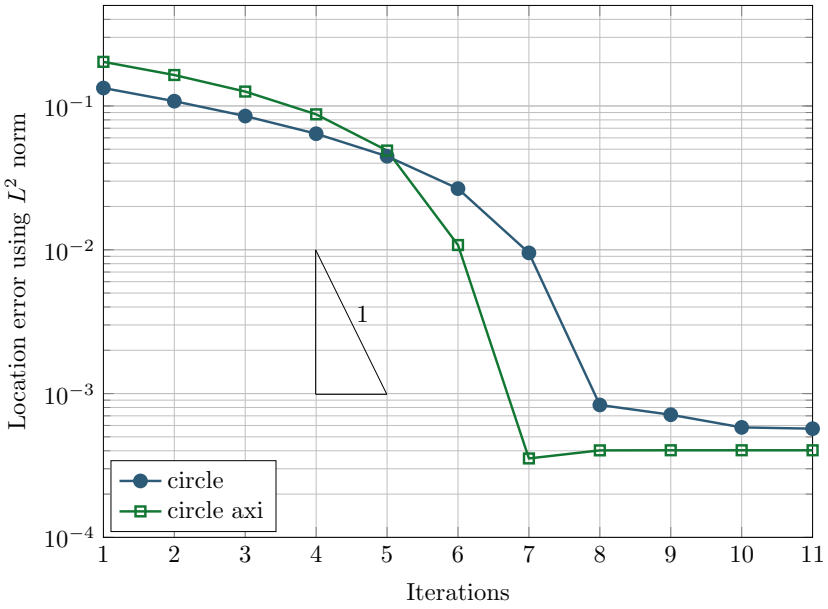

Figure III.12: Error on the position of the contact interface compare to a reference solution for each problem.

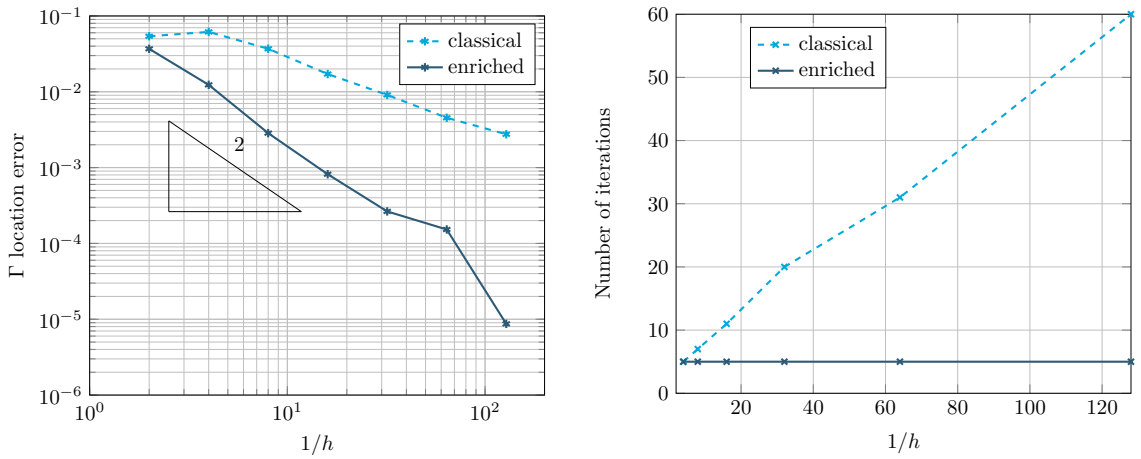

Figure III.13: Evolution of (a) the error on Γ (b) the number of iterations, with the size of the mesh

is explained by the change in the dominant time consuming function. For a coarse mesh, the assembling takes the greatest computational effort. Whereas, for a fine mesh, the solving is the main expense. Also, the ILS algorithm is more elaborate. Thus, it takes more efforts to be optimized and we think there is still room for improvement. But the comparison should also be made with a precision criterion on Γ. Indeed, we have already emphasized the importance of the contact boundary. For this particular purpose, the ILS is far more efficient and does not require an overkill mesh to obtain sufficient accuracy for the contact boundary position.

Mesh	ILS		Classical	
$1/h$	$t_{\text{tot}}^{\text{ILS}}$ (s)	$\overline{t_{\text{iter}}^{\text{ILS}}}$ (s)	$t_{\text{tot}}^{\text{class}}$ (s)	$\overline{t_{\text{iter}}^{\text{class}}}$ (s)
2	0.4	0.08	0.06	0.02
4	1.06	0.212	0.39	0.08
8	2.53	0.506	1.06	0.151
16	7.59	1.52	5.24	0.476
32	36.4	7.28	48.7	2.43
64	243.9	48.78	617.8	19.92
128	2062	412.4	20971	349.5

Error on Γ	ILS	Classical
	$t_{\text{tot}}^{\text{ILS}}$ (s)	$t_{\text{tot}}^{\text{class}}$ (s)
5.10^{-2}	0.4	1.06
5.10^{-3}	2.53	617.8
5.10^{-4}	36.4	$\times$
10^{-5}	2062	$\times$

Table III.1: Time comparison between ILS and active-set method. First on fixed meshes then for a targeted error. All computations have been done on an AMD Opteron 6328 3,2 GHz octocore with 4Go of RAM.

III.3.2 Non-axi-symmetric problems: an end to flatness

In the previous section, we have dealt with axi-symmetric problems. The ILS has been shown to be consistent when keeping the axi-symmetric features. However in these cases, only the first mode was needed to converge. We will now seek examples which need extra modes. In this part, we are going to see to the resolution of a membrane coming into contact with a non-constant floor following the mathematical expression $d(x, y) = -1/1000(15 + 5\cos(2\pi x)\cos(2\pi y))$. A representation of the floor and the used mesh can be found in Figure III.14. The loading

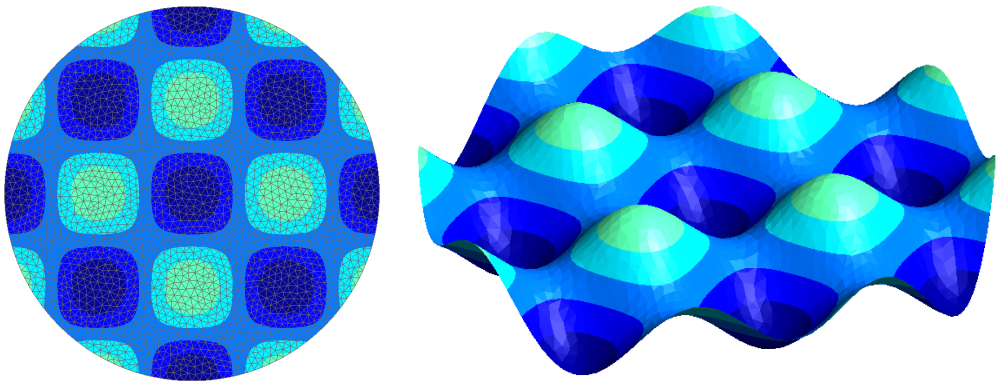

Figure III.14: Floor shape (2D and 3D representation) and associated mesh

will be increased and then decreased such that contact zones appear, then merge and split ($|f_d| = 0.1 \to 0.2 \to 0.3 \to 0.4 \to 0.3 \to 0.2 \to 0.1$). Results of this process can be found in Figure III.15.

The method seems to be consistent as the results are similar for the loading and the unloading of the membrane. The differences come from the different initial level-set between the loading and the unloading. Indeed, using Fourier modes, their number is limited by the number of elements cut by Γ and therefore local errors (mainly arising when penetration or release checks are done) are difficult to overcome. In a future work localized modes will be developed to deal with this issue. Nevertheless, it is notable that few iterations are needed between each steps.

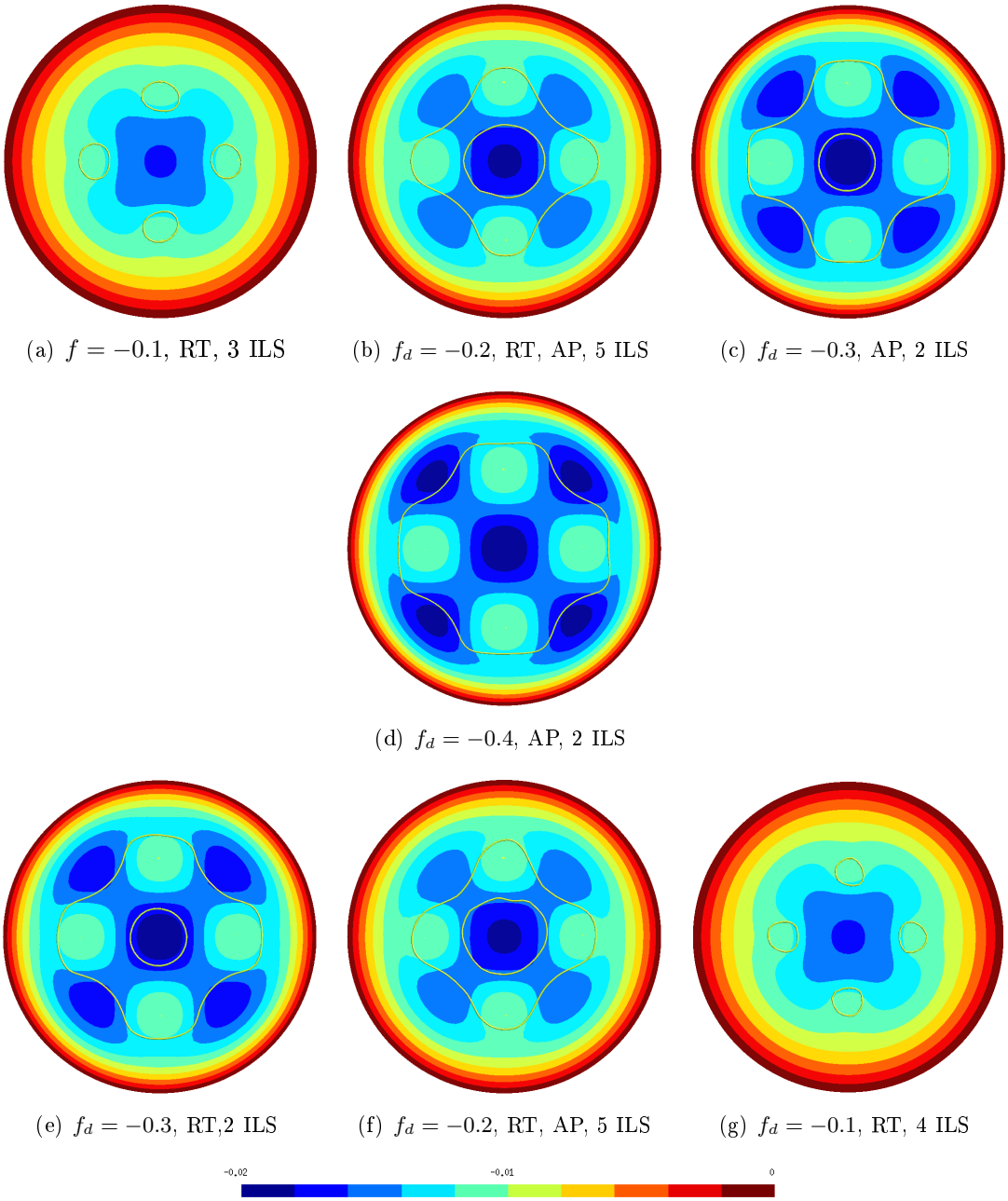

(a) $f = -0.1$, RT, 3 ILS (b) $f_d = -0.2$, RT, AP, 5 ILS (c) $f_d = -0.3$, AP, 2 ILS

(d) $f_d = -0.4$, AP, 2 ILS

(e) $f_d = -0.3$, RT,2 ILS (f) $f_d = -0.2$, RT, AP, 5 ILS (g) $f_d = -0.1$, RT, 4 ILS

Figure III.15: Evolution of the solution and the contact boundary (green line) with the loading (AP meaning addition of the area with penetration to the contact zone, RT meaning removal of the area where there is traction on the membrane and ILS is short for ILS iteration)

Conclusion

The ILS coupled with a particular formulation of the problem seems to be an efficient numerical method to handle the membrane case. It was shown to be particularly effective on a coarse mesh and led to an accurate representation of the contact zone. Few iterations were needed to converge, even with an initial guess far from the solution. The punctual active-set iteration handled quite efficiently the appearance and disappearance of contact zones. Furthermore, adhesion an high order interpolations were easily included in the method.

IV

Contact for plain solids

Contents

Summary

After dealing with membrane problems, plain solids are studied. The general framework is settled. As a modelization choice, a parallel with fracture mechanics is drawn. This allows an access to several shape optimization criteria but also to take into account adhesion phenomenon. An extensive study of the method is made with a comparison with a classical active-set method. Another formulation is proposed in order to fulfill the BB condition when Lagrange multipliers field is enriched. Finally a first step toward high order formulation is made.

Résumé

Pour finir cette étude, des problèmes de contact unilatéraux sont étudiés. Afin d'établir une méthode d'optimisation de forme efficace, une analogie avec la mécanique élastique linéaire de la rupture est faite. Tout d'abord, cela permet d'obtenir des critères d'évolution. En plus de cela, cette formulation permet de gérer les problèmes d'adhésion de manière naturelle. Une fois de plus, une attention particulière est portée au choix de la formulation variationelle afin de vérifier la condition BB. Une étude poussée de l'ILS pour ces problèmes est conduites. Une fois de plus, la comparaison avec une méthode active-set classique est faite. Les performances de l'ILS sont attrayantes autant pour sa rapidité que pour sa qualité. Enfin, un premier pas vers l'utilisation d'interpolations de haut ordre est fait.

IV.1 Summary for the plain solids problem

In the first chapter, we derived several contact formulations. We are going to focus on unilateral contact with small deformations hypothesis. The notations are summarized in Figure IV.1. As usual, Ω denotes the whole domain and Ω^- the contact zone. Before, in the membrane case, the contact zone was of the same dimension as the whole domain whereas here it is one dimension smaller. This is numerically convenient for the ILS as the computation for the shape optimization will involve a lot less dofs than the total number.

We recall briefly some of the notations. The displacement of a material point located at the position $\underline{x}$ is $\underline{u}(\underline{x})$. The distance between the rigid body and the deformable solid is denoted $d(\underline{x})$, the imposed body force $\underline{f}_d$ and the external loading $\underline{t}_d$.

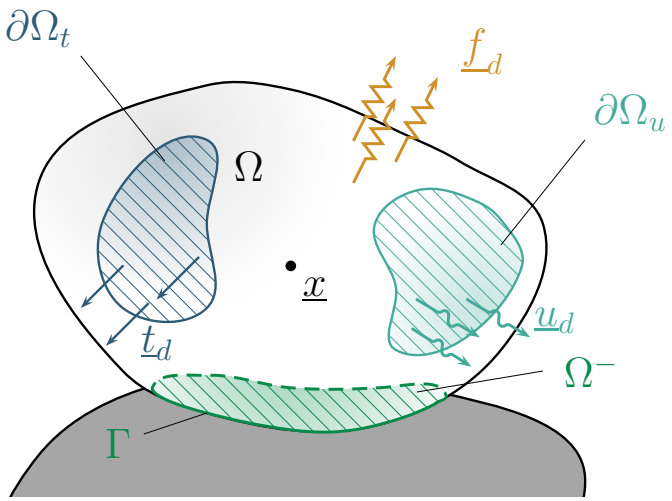

Figure IV.1: Unilateral contact notations

Given that the boundary conditions are respected, the set of equations and inequality to be solved are:

$$\mathrm{div}(\underline{\underline{\sigma}}) + \underline{f}_d = \underline{0} \quad \text{in } \Omega \tag{IV.1}$$

with the boundary conditions:

$$\begin{cases} \underline{u} & = & \underline{u}_d & \text{on } \partial\Omega_u \\ \underline{\underline{\sigma}} \cdot \underline{n} & = & \underline{t}_d & \text{on } \Omega_t \\ \underline{\underline{\sigma}} \cdot \underline{n} & = & p_n \underline{n} & \text{on } \Omega^- \end{cases} \tag{IV.2}$$

and everywhere on $\partial\Omega/\partial\Omega_t \cup \partial\Omega_u$

$$\begin{cases} g_n & \geq & 0 & \text{no penetration} \\ p_n & \leq & 0 & \text{no attraction} \\ p_n g_n & = & 0 & \text{normal condition} \end{cases} \tag{IV.3}$$

with p_n the contact pressure, and g_n the gap function defined as in Section I.1.2 Before being able to apply the ILS method, the formulation associated to the direct problem needs to be picked. As for the membrane case, the Lagrange multiplier formulation is chosen:

Problem 32

Find $\underline{u} \in \mathcal{U}$ and $p \in H^{-1/2}$ such that for all $\underline{u}^\star \in \mathcal{U}_0$ and $p^\star \in H^{-1/2}$

$$\left\{ \begin{array}{lcll} a(\underline{u},\underline{u}^\star) & + & c^l(p,\underline{u}^\star) & = & f(\underline{u}^\star) \\ c^l(p^\star,\underline{u}) & & & = & l^l(p^\star) \end{array} \right. \tag{IV.4}$$

with:

$$\left| \begin{array}{ll} a(\underline{u},\underline{u}^\star) = \displaystyle\int_\Omega \epsilon(\underline{u}) : \underline{\underline{\underline{\underline{\mathrm{K}}}}} : \epsilon(\underline{u}^\star)\,\mathrm{d}V & f(\underline{u}^\star) = \displaystyle\int_\Omega \underline{u}^\star \cdot \underline{f}_d\,\mathrm{d}V + \int_{\partial\Omega_t} \underline{u}^\star \cdot \underline{t}_d\,\mathrm{d}S \\ c^l(p,\underline{u}) = \displaystyle\int_{\Omega^-} p(\underline{u}\cdot\underline{n})\,\mathrm{d}S & l^l(p^\star) = \displaystyle\int_{\Omega^-} dp^\star\,\mathrm{d}S \end{array} \right. \tag{IV.5}$$

In this formulation the Lagrange multipliers p are physically equivalent to the contact pressure p_n.

The choice of the enrichment is discussed in the next section. However, assuming some enrichment F we can use the approximation:

$$\underline{u}(\underline{x}) \approx \left\{ \begin{array}{l} \sum_{i\in I_x} u_{x_i} N_i(\underline{x}) + \sum_{j\in J_x} u^e_{x_j} N_j(\underline{x}) F_x(\underline{x}) \\ \sum_{i\in I_y} u_{y_i} N_i(\underline{y}) + \sum_{j\in J_y} u^e_{y_j} N_j(\underline{y}) F_y(\underline{x}) \\ \sum_{i\in I_z} u_{z_i} N_i(\underline{z}) + \sum_{j\in J_z} u^e_{z_j} N_j(\underline{z}) F_z(\underline{x}) \end{array} \right\} \tag{IV.6}$$

it is to note that different enrichments can be applied to the component of the displacement. For the sake of simplicity, another notation will be used, indexing the degrees of freedom:

$$\underline{u}(\underline{x}) \approx \sum_{i\in I} u_i N_i(\underline{x}) \underline{e}_i + \sum_{j\in J} u^e_j N_j(\underline{x}) F_x(\underline{x}) \underline{e}_j \tag{IV.7}$$

The functions $N_j(\underline{x})$ are kept linear through the whole chapter.

The other unknowns are the Lagrange multiplier on the boundary of the domain, for a first approximation they can be written as:

$$p(\underline{x}) \approx \sum_{i\in I^p} p_i N^p_i(\underline{x}) \tag{IV.8}$$

Injecting this approximation into the variational formulation of Problem 32 leads to the matricial system:

Problem 33

Find $\mathbf{u}$, $\mathbf{u}^e$ and $\boldsymbol{p}$ such that:

$$[\mathbf{K}]\begin{Bmatrix}\mathbf{u}\\ \mathbf{u}^e\\ \boldsymbol{p}\end{Bmatrix}=\begin{Bmatrix}\mathbf{f}\\ \mathbf{f}^e\\ \mathbf{l}_p\end{Bmatrix}\quad\text{where}\quad[\mathbf{K}]=\begin{bmatrix}\mathbf{A}^{cc} & \mathbf{A}^{ce} & \mathbf{C}\\ \mathbf{A}^{ce\top} & \mathbf{A}^{ee} & \mathbf{C}^e\\ \mathbf{C}^\top & \mathbf{C}^{e\top} & \mathbf{0}\end{bmatrix}\tag{IV.9}$$

with:

$$\begin{aligned}
&\mathbf{u}=\{u_i\} \qquad A^{cc}_{ij}=\int_\Omega \nabla(N_i\underline{e_i}):\underline{\underline{\mathrm{K}}}:\nabla(N_j\underline{e_j})\,\mathrm{d}V\\
&\qquad\qquad \mathbf{f}=\left\{\int_\Omega N_i\underline{f_d}\cdot\underline{e_i}\,\mathrm{d}V \quad+\int_{\partial\Omega^t} N_i\underline{t_d}\cdot\underline{e_i}\,\mathrm{d}S\right\}\\
&\mathbf{u}^e=\{u^e_i\} \qquad A^{ee}_{ij}=\int_\Omega \nabla(N^e_i\underline{e_i}):\underline{\underline{\mathrm{K}}}:\nabla(N^e_j\underline{e_j})\,\mathrm{d}V \qquad A^{ce}_{ij}=\int_\Omega \nabla(N_i\underline{e_i}):\underline{\underline{\mathrm{K}}}:\nabla(N^e_j\underline{e_j})\,\mathrm{d}V\\
&\qquad\qquad \mathbf{f}^e=\left\{\int_\Omega N^e_i\underline{f_d}\cdot\underline{e_i}\,\mathrm{d}V \quad+\int_{\partial\Omega^t} N^e_i\underline{t_d}\cdot\underline{e_i}\,\mathrm{d}S\right\}\\
&\mathbf{p}=\{p_i\} \qquad C_{ij}=\int_{\Omega^-} N_iN^p_j\underline{n}\cdot\underline{e_i}\,\mathrm{d}S \qquad\qquad C^e_{ij}=\int_{\Omega^-} N^e_iN^p_j\underline{n}\cdot\underline{e_i}\,\mathrm{d}S\\
&\qquad\qquad \mathbf{l}_p=\left\{-\int_{\Omega^-} N^p_i d\,\mathrm{d}S\right\}
\end{aligned}\tag{IV.10}$$

Even more so than for the membrane problem, the size of the matrix $\mathbf{A}^{cc}$ is preponderant compared to the other ones (see Figure IV.2). Furthermore this matrix is unchanged through the iteration. Therefore a great deal of computational effort can be saved by saving the matrix and its decomposition during the first iteration. Also, the rest of the matrix is really sparse and can be rearranged efficiently.

The reader should by now be familiar with the next steps. Indeed, as well as with the general method given in Chapter II and the application to the membrane case of Chapter III, the problem is decomposed into two parts. First the Problem 32 is solved for a given contact zone. Then this contact zone is updated by mean of a shape optimization problem. This process is detailed in the next section with an emphasis on the particularity linked to plain solids contact.

IV.2 ILS formulation for plain solids

In this section, the specificities of the ILS applied to a plain solid are given. For the sake of simplicity, we will focus the study on 2D problems even if a generalization of the method can be made. Let us first summarize what is needed to be able to use the ILS. The formulation required to solve the equilibrium problem for a given contact zone was already settled by Problem 32.

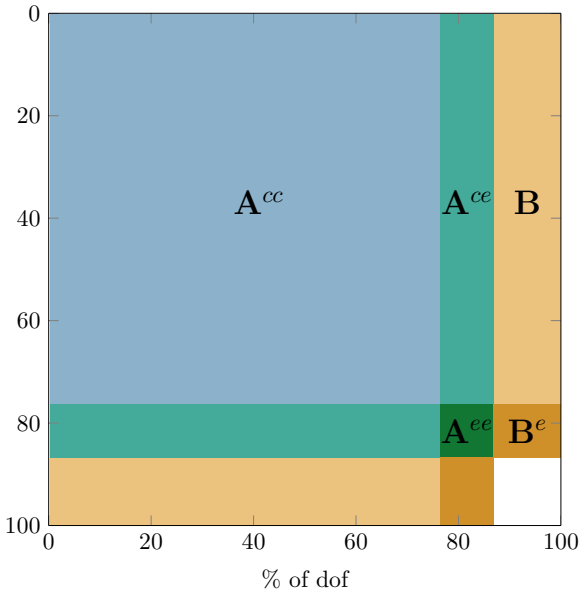

Figure IV.2: Graphical representation of an example of the block components in $\mathbf{K}$

An important aspect in order to use efficiently this formulation is to be able to represent accurately the phenomena at the contact boundary. This is especially true if dealing with adhesion problems. Thereby, in Section IV.2.1 the modelization of the contact phenomenon are discussed. Then, when the problem can be solved accurately for a given contact zone, the shape optimization needs to play its part. This shape optimization is driven by a criterion ϱ. Its choice is of course of a tremendous importance and is discussed in Section IV.2.2. Finally, the numerical framework is recalled before giving some examples.

IV.2.1 Modeling the contact as a crack-like phenomenon

Previously, it was highlighted that the ILS was able to deal efficiently with adhesion problems given the right formulation. In order to be able to handle adhesion problem, but also to have a consistent formulation for non-adhesive one, a general formulation is set up. Indeed, if the method can solve the problem for any surface energy γ it can also tackle the non-adhesive one with $\gamma = 0$.

One of the first model for adhesion was given by [Johnson et al., 1971] and is referred as the JKR model. In [Maugis and Barquins, 1983], it was shown to be equivalent to a Griffith's theory of fracture. In this thesis we consider this model. Other models were proposed and shall be the focus of later work. For instance the use of molecular forces to model adhesion was also developed such as in the DMT model [Derjaguin et al., 1975]. These interactions were also taken into account by mean of an enrichment method like in [Sauer, 2011]. Such models could be integrated into the ILS formulation. To come back to the JKR model, one could see a parallel between two solids coming into contact with one another and a crack propagation in mode I, also call the opening mode. For instance, in Figure IV.3, close to Γ and if both material of Ω^1 and Ω^2 are the same the problem can be seen as a classical crack propagation. In this case Γ would be the crack tip and the opening of the crack goes into the $\underline{e}_\theta$ direction. As for the crack propagation, a local system of coordinate is set at what will be referred as the "crack

tip" (the limit of the contact zone for contact). The coordinate r represents the distance of a point P to the crack tip and θ the angle between the vector $\underline{e}_\theta$ and the vector with direction the line passing through P and it's closest point to the crack tip. Such coordinates are computed in the fashion described in Section II.2.2.2.

With these coordinates it is possible to define an enrichment. An enrichment is necessary if one wants to capture the singularity arising from an erroneous contact zone. Indeed, imposing an erroneous contact zone is equivalent to imposing Dirichlet boundary conditions which create weak discontinuities of the displacement. It is important in our case to capture this singularity in order to compute accurately the sensitivity of the problem regards to the contact zone position. The enrichment mentioned in Section II.2.2.2 as the function $F_{c_1}(r,\theta) = \sqrt{r}\sin(\theta/2)$ is used. It is localized near the crack tip. A limitation parameter r_{lim} is defined such that only the nodes which fulfill the condition $r < r_{\text{lim}}$ are enriched. Such enrichment method is refered as geometrical enrichment (see [Béchet et al., 2005]).

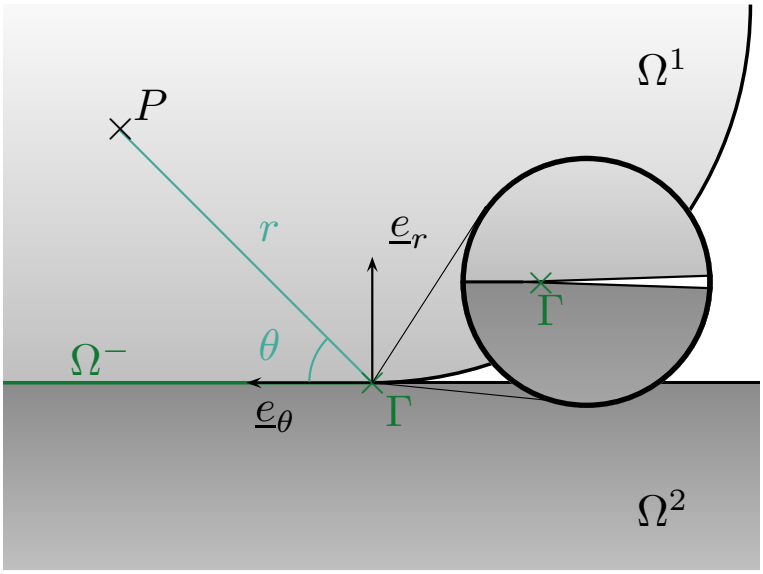

Figure IV.3: Illustration of the parallel between crack and contact problems.

With this model, a stress concentration appears at the boundary of the contact zone if the enrichment is activated. This activation appears if the contact zone is erroneous or if dealing with adhesion. This singularity is the major drawback of the JKR model and this modelization and might motivate the later use of other ones. Nevertheless, except for that point, the JKR model seems to be able to represent efficiently the observed phenomena if one is interested in the global behavior.

IV.2.2 Choice of a criterion

The parallel drawn between fracture mechanics and adhesion motivates the choice of possible criteria. It was shown in Section II.3.3 that a general criterion could be used computing the energy of dissipation associated with the displacement of the contact zone. This approach is really common in fracture mechanics although a different notation is used. The variation of energy associated with an advance of the crack front is called the strain energy release rate G. When $G = 0$ there is no singularity present at the crack tip. Going back to the contact problem

modeled like a crack, $G = 0$ is reached for the solution of the problem without adhesion. As explained Section I.1.4, the modelization of adhesion phenomena often use the surface energy γ. This quantity is equivalent to G in the Griffith's theory of fracture if the contact zone is right ($\gamma = G(\Gamma^{\text{ex}})$) as it was shown in [Maugis and Barquins, 1983].

Practically, the energy release rate is computed using a path independent integral developed in [Rice, 1968] called the J-integral. Several studies were made on this integral and on how to compute it. In this thesis we used the work done in [Dolbow and Gosz, 2002] and [Legrain et al., 2008]. For more details on the subject, the reader is referred to the bibliography therein these articles. In order to define the J-integral we consider a 2D crack with a local coordinate system ($\underline{e}_1$,$\underline{e}_2$). The vector $\underline{e}_1$ represent the direction of advancement of the crack. Let us consider also a contour Γ_J that encloses the crack tip and its normal $\underline{n}_{\Gamma_J}$. Then the J-integral is defined as:

$$J = \int_{\Gamma_J \to 0} \left(\Psi \underline{n}_{\Gamma_J} \cdot \underline{e}_1 - (\nabla \underline{u}^\top \cdot \underline{e}_1) \cdot (\underline{\underline{\sigma}} \cdot \underline{n}_{\Gamma_J}) \right) \mathrm{d}\ell \tag{IV.11}$$

The limit of this integral when $\Gamma_J \to 0$ is the strain energy release rate G. The J-integral can be written in a different form using the Eshelby tensor $\underline{\underline{C}}$ defined Section II.3.3.

$$J = \int_{\Gamma_J \to 0} \left((\underline{\underline{C}} \cdot \underline{n}_{\Gamma_J}) \cdot \underline{e}_1 \right) \mathrm{d}\ell \tag{IV.12}$$

It is often prefered to integrate on a domain rather than on a boundary. Therefore, the above integral is transformed such that it fulfills this condition. In order to do so, a domain $\mathcal{B}$ is defined (as in Section II.3.4) such that Γ is included in it. Then, a virtual velocity field classically called $\underline{q}$ is constructed. It has to satisfy:

- $\underline{q} = q\underline{e}_1$,
- q must be smooth enough,
- $q = 1$ inside the domain enclosed by Γ_J,
- $q = 0$ on $\partial\mathcal{B}$.

With this notation , the equivalent of the J-integral in its domain form is:

$$J = -\int_{\mathcal{B}} \left(\nabla \underline{q} : \underline{\underline{C}} \right) \mathrm{d}S \tag{IV.13}$$

It is clear, from the constructing method and this final form, that the J-integral is a special case (with $\underline{w} = \underline{q}$) of the integral D_m also defined in Section II.3.3 with the Equation (II.43).

Another formulation, which gives access to G, uses another integral computed with auxiliary fields. These auxiliary fields are based on the analytic solution given in [Michell, 1900]. The integral, depending on the choice of the auxiliary fields is :

$$I^{\text{aux}} = \int_{\mathcal{B}} \left(\underline{\underline{\sigma}}(\nabla \underline{u}^\top_{\text{aux}} \cdot \underline{e}_1) + \underline{\underline{\sigma}}_{\text{aux}}(\nabla \underline{u}^\top \cdot \underline{e}_1) - \underline{\underline{\sigma\epsilon}}_{\text{aux}} \cdot \underline{e}_1 \right) \cdot \underline{n}_{\Gamma_J} \mathrm{d}S \tag{IV.14}$$

In order to explained the link between the G and the above defined one, others classical quantities of interest in fracture mechanics need to be introduced. These are the stress intensity

factors which are used to characterized the stress concentration near the tip of the crack. It is usual to decompose the crack into three modes which are, in order, the opening mode, the in-plane shear mode and the tearing mode. In plane crack, the later is of no use and we will focus on the other two. Therefore two associated stress intensity factors are used for the characterization. They can be defined, using the already mentioned polar coordinate system centered at the crack tip, by:

$$\left| \begin{array}{rcl} K_I & = & \lim\limits_{r\to 0} \sqrt{2\pi r}\sigma_{22}(r,0) \\ K_{II} & = & \lim\limits_{r\to 0} \sqrt{2\pi r}\sigma_{12}(r,0) \end{array} \right. \tag{IV.15}$$

such that near the crack tip the stress field can be approximated as:

$$\sigma_{ij} = \frac{K_I}{\sqrt{2\pi r}}\sigma_{ij}^I(\theta) + \frac{K_{II}}{\sqrt{2\pi r}}\sigma_{ij}^{II}(\theta) \tag{IV.16}$$

with σ_{ij}^I and σ_{ij}^{II} appropriate functions of θ.

Using this notation for the computation of the G it is found that:

$$G = \frac{K_I^2 + K_{II}^2}{E^*} \tag{IV.17}$$

with

$$E^* = \left\{ \begin{array}{ll} E & \text{for plane stress} \\ \dfrac{E}{1-\nu^2} & \text{for plane strain} \end{array} \right. \tag{IV.18}$$

It can be shown, using the same expression for the auxiliary fields as in Equation IV.16 that:

$$I^{\text{aux}} = \frac{2}{E^*}(K_I K_I^{\text{aux}} + K_{II} K_{II}^{\text{aux}}) \tag{IV.19}$$

Thus using the right auxiliary fields K_I (with $K_I^{\text{aux}} = 1$ and $K_{II}^{\text{aux}} = 0$) and K_{II} (with $K_I^{\text{aux}} = 0$ and $K_{II}^{\text{aux}} = 1$) are available through the computation of I^{aux}. Once these stress intensity factors are acquired G can be computed.

In the case of slipping contact, only K_I is of interest as the problem correspond to a mode-I crack. Therefore, another possibility rather than using G as a criterion it to use K_I. The reader might point out that there is only a known coefficient differencing the two values and therefore there is no real interest in using one or the other. Nevertheless this remark justify the use of a last criterion which do not require extra computation.

It was already mentioned above that an enrichment was going to be used. To complete this definition, let us precise that only the $\underline{e}_2$ component of the displacement field is enriched with the function $F_{c_1} = \sqrt{r}\sin(\theta/2)$. This is coherent with the hypothesis that the equivalent crack is of a mode-I type. Therefore, for a first order approximation, at every enriched node an extra degree of freedom is added compared to a non-enriched field. Let us consider triangular elements, $\mathcal{T}_c$ denotes the boundary element containing the contact boundary. Using the indices 1 and 2 to refer to the node on the boundary an 3 the node inside the domain the approximation of $u_{\underline{e}_2}$ can be expressed as:

$$u_{\underline{e}_2} \approx u_{\underline{e}_2}^h = \sum_{i=1}^{3} u_{\underline{e}_2 i} N_i(\underline{x}) + \sum_{i=1}^{3} u_{\underline{e}_2 i}^e N_i(\underline{x}) F_{c_1}(\underline{x}) \tag{IV.20}$$

Near the crack tip, a predominant part of the displacement is of the form:

$$u^{\text{tip}}_{\underline{e}_2} = \frac{\sqrt{2}K_I(2\kappa+1)(1+\nu)}{4E\sqrt{\pi}} F_{c_1}(\underline{x}) \tag{IV.21}$$

with again the value of κ linked to the 2D hypothesis:

$$\kappa = \begin{cases} \dfrac{3-\nu}{1+\nu} & \text{for plane stress} \\ 3-4\nu & \text{for plane strain} \end{cases} \tag{IV.22}$$

Thus, one way of comparing the asymptotic solution and the numerical one is to take the limit of their ratio at the crack tip denoted $\underline{x}_c$.

$$\lim_{\underline{x}\to\underline{x}_c} \frac{u^h_{\underline{e}_2}}{u^{\text{tip}}_{\underline{e}_2}} = \lim_{\underline{x}\to\underline{x}_c} \frac{\sum_{i=1}^3 u_{\underline{e}_2 i} N_i(\underline{x}) + \sum_{i=1}^3 u^e_{\underline{e}_2 i} N_i(\underline{x}) F_{c_1}(\underline{x})}{\frac{\sqrt{2}K_I(2\kappa+1)(1+\nu)}{4E\sqrt{\pi}} F_{c_1}(\underline{x})} \tag{IV.23}$$

$$= \frac{4E\sqrt{\pi}\left(u^e_{\underline{e}_2 1} N_1(\underline{x}_c) + u^e_{\underline{e}_2 2} N_2(\underline{x}_c)\right)}{K_I\sqrt{2}(2\kappa+1)(1+\nu)} \tag{IV.24}$$

This expression is simplified by setting $u_c = u^e_{\underline{e}_2 1} N_1(\underline{x}_c) + u^e_{\underline{e}_2 2} N_2(\underline{x}_c)$. The coefficient u_c is the interpolation of the enrichment degrees of freedom at the crack tip. A relation between u_c and K_I is therefore established if we consider the solution of the problem to be close enough to the analytic solution:

$$u_c = K_I \times \frac{\sqrt{2}(2\kappa+1)(1+\nu)}{4E\sqrt{\pi}} \tag{IV.25}$$

It is more convenient to use u_c rather than K_I as only a linear interpolation is to be made after solving Problem 33. This advantage is particularly striking when the total derivative will have to be computed.

Check point

In this section, we started with the notion of surface energy γ. This value is directly link to adhesion phenomenon and is therefore a good criterion to drive the shape optimization ($\gamma = 0$ if there is no adhesion). Thanks to a parallel with fracture mechanics, an equivalence with the energy release rate G was made. Furthermore, a relation with other quantities were exhibited, i.e. $G \propto K_I \propto u_c$, giving three possible criteria for the position of the boundary.

IV.2.3 The shape optimization

At this point, the solution of the problem for a given contact zone can be found. Furthermore we have at our disposal criteria to characterize the rightness of the contact zone. It was already explained in Section II.3 how a shape optimization can be settled in order to find the right contact zone. The application to the plain solid contact is detailed here.

A Newton's method is applied in order to cancel the criterion. The goal is first to determine the evolution of the chosen criterion with a change of the contact boundary shape. This

evolution is characterized by the normal directional derivative of the criterion. Once that derivative is computed, a step of the Newton's method can be done. This process is iterated up to convergence as illustrated in Figure II.16.

IV.2.3.1 Set-up of the boundary displacement

In the case of 2D problems, the boundary of the contact zone is represented by a set of points $\{\underline{x}_c^m\}$. Therefore the evolution of the shape of a contact zone are directly linked to the displacements of these points on the interface (without considering the apparition or nucleation of contact zones which were said to be handled differently). Therefore, for each point $\underline{x}_c^m$, an independent displacement $\underline{w}_m = w_m \underline{\mathrm{n}}$ is associated. In order to keep the parallel with fracture mechanics, the displacement is chosen to correspond to the advance of the crack and therefore to the diminution of the contact zone. In order to compute the normal directional derivative, it was explained that this displacement needs to be extended to the whole domain. Nevertheless, to keep the computational cost as low as possible the displacement is driven to zero outside of a band $\mathcal{B}_m$ including $\underline{x}_c^m$. The influence of this band is studied later on.

IV.2.3.2 Computation of the derivative

For each displacement w_m, defined in the above section, the normal directional derivatives of each criteria have to be computed. Indeed, for every $\underline{x}_c^m$, a criterion ϱ_m is associated (it could be G_m, K_{Im} or u_{cm}) and therefore the influence of the displacement of any $\underline{x}_c^{m'}$ has to be computed. In this section, the indices are dropped for a better understanding and the derivative of the criteria are computed for any displacement w. In this thesis, the method to compute G through K_I is the one using auxiliary fields. The directional derivatives of the auxiliary fields are taken to be zero. This simply means that these fields follow the interface. The first criteria to be introduced was G and it was said to be computed using $G = K_I^2/E^*$ in mode-I. Therefore its derivative is:

$$\mathring{G} = \frac{2K_I\overline{\mathring{K}_I}}{E^*} \tag{IV.26}$$

The derivative of the second criterion K_I is needed. Strictly speaking, the derivative of K_I, which depends directly on $\nabla\underline{u}$, should be (using the notation introduced in Section II.3.4):

$$\overline{\mathring{K}_I(\nabla\underline{u})} = K_I(\overline{\mathring{\nabla}\underline{u}}) + \mathring{K}_I(\nabla\underline{u}) \tag{IV.27}$$

with $\mathring{K}_I$ the derivative of the operator itself. However it was chosen to approximate the derivative by neglecting the last part. This choice was made to simplify the computation as the strategy to compute $K_I(\overline{\mathring{\nabla}\underline{u}})$ is the same as with $K_I(\nabla\underline{u})$. In a later work a more precise determination of $\overline{\mathring{K}_I}$ shall be done. Nevertheless the use of K_I is only there as a reference for the use of the last criterion u_c.

The main advantage of u_c is that it is easy to compute its value and its derivative. Indeed the total derivative of u_c is:

$$\mathring{u}_c = \overline{\mathring{u}^e_{\underline{e}_2 1} N_1(\underline{x}_c) + u^e_{\underline{e}_2 2} N_2(\underline{x}_c)} = \mathring{u}^e_{\underline{e}_2 1} N_1(\underline{x}_c) + \mathring{u}^e_{\underline{e}_2 2} N_2(\underline{x}_c) \tag{IV.28}$$

and is therefore straightforward to compute as soon as $\mathring{\underline{u}}$ is known.

Then let us come to that point. As it was highlighted and then applied to the membrane problem, the directional derivatives of the unknowns of the problem are computed by taking

the derivatives of the full direct problem (Problem 32). For a given $\underline{w}$ the directional derivatives of each term of Problem 32 are:

$$D(a(\underline{u},\underline{u}^\star))[w] = \int_\Omega \underline{\underline{\epsilon}}(\mathring{\underline{u}}) : \underline{\underline{\underline{\underline{K}}}} : \underline{\underline{\epsilon}}(\underline{u}^\star)\,\mathrm{d}V - \int_\Omega \underline{\underline{\epsilon}}(\underline{u}) : \underline{\underline{\underline{\underline{K}}}} : (\nabla\underline{u}^\star\nabla\underline{w})_S\,\mathrm{d}V$$
$$- \int_\Omega (\nabla\underline{u}\nabla\underline{w})_S : \underline{\underline{\underline{\underline{K}}}} : \underline{\underline{\epsilon}}(\underline{u}^\star)\,\mathrm{d}V + \int_\Omega \underline{\underline{\epsilon}}(\underline{u}) : \underline{\underline{\underline{\underline{K}}}} : \underline{\underline{\epsilon}}(\underline{u}^\star)\mathrm{div}(\underline{w})\,\mathrm{d}V \quad \text{(IV.29)}$$

$$D(c^l(p,\underline{u}))[w] = \int_{\Omega^-} p\mathring{\underline{u}}\cdot\underline{n}\,\mathrm{d}S + \int_{\Omega^-} \mathring{p}\underline{u}\cdot\underline{n}\,\mathrm{d}S + \int_{\Omega^-} p\underline{u}\cdot\underline{n}(\mathrm{div}(\underline{w}) - \underline{n}\cdot\nabla\underline{w}\cdot\underline{n})\,\mathrm{d}S \quad \text{(IV.30)}$$

$$D(l^l(p^\star))[w] = -\int_{\Omega^-} \mathring{d}p^\star\,\mathrm{d}S - \int_{\Omega^-} d\mathring{p}^\star\,\mathrm{d}S - \int_{\Omega^-} dp^\star(\mathrm{div}(\underline{w}) - \underline{n}\cdot\nabla\underline{w}\cdot\underline{n})\,\mathrm{d}S \quad \text{(IV.31)}$$

$$D(f(\underline{u}^\star))[w] = \int_\Omega \underline{u}^\star\cdot\mathring{\underline{f}}_d\,\mathrm{d}V + \int_\Omega \mathring{\underline{u}}^\star\cdot\underline{f}_d\,\mathrm{d}V + \int_\Omega \underline{u}^\star\cdot\underline{f}_d\mathrm{div}(\underline{w})\,\mathrm{d}V$$
$$+ \int_{\partial\Omega_t} \underline{u}^\star\cdot\mathring{\underline{t}}_d\,\mathrm{d}S + \int_{\partial\Omega_t} \mathring{\underline{u}}^\star\cdot\underline{t}_d\,\mathrm{d}S + \int_{\partial\Omega_t} \underline{u}^\star\cdot\underline{t}_d(\mathrm{div}(\underline{w}) - \underline{n}\cdot\nabla\underline{w}\cdot\underline{n})\,\mathrm{d}S \quad \text{(IV.32)}$$

Supposing as previously that $\mathring{\underline{u}}^\star = 0$ and $\mathring{p}^\star = 0$ and using the fact that on Ω^- $\underline{u}\cdot\underline{n} = -d$ the sensitivity problem becomes:

Problem 34

Find $\underline{u}\in\mathcal{U}$ and $p\in H^{-1/2}$ such that for all $\underline{u}^\star\in\mathcal{U}_0$ and $p^\star\in H^{-1/2}$

$$\left\{\begin{array}{lcll} a(\mathring{\underline{u}},\underline{u}^\star) & + & c^l(\mathring{p},\underline{u}^\star) & = f^s(\underline{u}^\star) \\ c^l(p^\star,\mathring{\underline{u}}) & & & = l^{ls}(p^\star) \end{array}\right. \quad \text{(IV.33)}$$

with:

$$\begin{aligned} f^s(\underline{u}^\star) &= \int_\Omega \underline{\underline{\epsilon}}(\underline{u}) : \underline{\underline{\underline{\underline{K}}}} : (\nabla\underline{u}^\star\nabla\underline{w})_S\,\mathrm{d}\Omega + \int_\Omega (\nabla\underline{u}\nabla\underline{w})_S : \underline{\underline{\underline{\underline{K}}}} : \underline{\underline{\epsilon}}(\underline{u}^\star)\,\mathrm{d}\Omega \\ &\quad - \int_\Omega \underline{\underline{\epsilon}}(\underline{u}) : \underline{\underline{\underline{\underline{K}}}} : \underline{\underline{\epsilon}}(\underline{u}^\star)\mathrm{div}(\underline{w})\,\mathrm{d}\Omega - \int_{\Omega^-} p\underline{u}^\star\cdot\underline{y}(\mathrm{div}(\underline{w}) - \underline{n}\cdot\nabla\underline{w}\cdot\underline{n})\,\mathrm{d}S \\ &\quad + \int_{\partial\Omega_t} \underline{u}^\star\cdot\mathring{\underline{t}}_d\,\mathrm{d}S + \int_{\partial\Omega_t} \underline{u}^\star\cdot\underline{t}_d(\mathrm{div}(\underline{w}) - \underline{n}\cdot\nabla\underline{w}\cdot\underline{n})\,\mathrm{d}S \\ &\quad + \int_\Omega \underline{u}^\star\cdot\mathring{\underline{f}}_d\,\mathrm{d}V + \int_\Omega \underline{u}^\star\cdot\underline{f}_d\mathrm{div}(\underline{w})\,\mathrm{d}V \\ l^{ls}(p^\star) &= -\int_{\Omega^-} \mathring{d}p^\star\,\mathrm{d}S \end{aligned} \quad \text{(IV.34)}$$

which again exhibits the same left hand side as in Problem 32 and can be written in its matricial form using the same interpolation:

Problem 35

Find $\mathring{\mathbf{u}}$, $\mathring{\mathbf{u}}^e$ and $\mathring{\boldsymbol{p}}$ such that:

$$[\mathbf{K}] \begin{Bmatrix} \mathring{\mathbf{u}} \\ \mathring{\mathbf{u}}^e \\ \mathring{\boldsymbol{p}} \end{Bmatrix} = \begin{Bmatrix} \mathbf{f}^s \\ \mathbf{f}^{es} \\ \mathbf{l}_p^s \end{Bmatrix} \tag{IV.35}$$

with $\mathbf{f}^s$, $\mathbf{f}^{es}$ and $\mathbf{l}_p^s$ computed from Equation IV.34 in the same fashion as in Problem 33.

IV.2.3.3 Newton's iterations

Problem 35 needs to be solved for every w_m. Then the shape optimization problem can be assembled. It is recalled that in order to find the displacement of the contact boundary that cancel the criteria (generalized with the notation ϱ_m), a linearization of their dependence respect to the positions of the boundaries is made. Thus the problem to be solved is:

Problem 36

Find $\boldsymbol{\tau} = \{\tau_m\}$ such that $\forall n \in \{1, .., \text{Card}(\underline{x}_c^m)\}$:

$$\varrho_n + \sum_m \tau_m D_{[w_m]}(\varrho_n) = 0 \tag{IV.36}$$

which translates matricialy into a small system to solve:

Problem 37

Find $\boldsymbol{\tau} = \{\tau_m\}$ such that:

$$[\mathbf{S}]\boldsymbol{\tau} = -\boldsymbol{\varrho} \tag{IV.37}$$

with

$$\left| \quad S_{mn} = D_{[w_m]}(\varrho_n) \qquad \boldsymbol{\varrho} = \{\varrho_n\} \right. \tag{IV.38}$$

Once this problem is solved the positions of the contact boundaries are updated such that:

$$x_c^m \leftarrow x_c^m + \tau_m w_m \tag{IV.39}$$

This full procedure is iterated up to convergence. This process is more detailed in Algorithm 3.

IV.3 Numerical results

As for the mebrane case, we will try in this section to show the assets and the weaknesses of the ILS method. A comparison with a classical method, namely a Lagragian formulation (Section I.1.3.2) coupled with an active-set strategy (Section I.2.2). Also, a study of the influences of the ILS parameters is made.

IV.3.1 A first test case: uplifting of a body

To start with, let us consider a rectangular body of length $2L = 20$ cm and height $l = 2$ cm for which a plane strain hypothesis is made. Furthermore, the axi-symmetry of the problem (axis $\underline{e}_y$ and position $x = 0$) is taken advantage of by imposing the appropriate boundary conditions. The Young's modulus of the material is set to be $E = 100$ MPa and the Poisson's ratio $\nu = 0.3$. The external loading is a boundary force $\underline{t}_d$ such that:

$$\underline{t}_d = \begin{cases} \left(\left(\dfrac{2x}{L}\right)^2 - 1\right)\underline{e}_y & \text{for } x \leq 5 \text{ cm} \\ \underline{0} & \text{for } x > 5 \text{ cm} \end{cases} \tag{IV.40}$$

A flat horizontal rigid body limits the vertical displacement of the solid. This limit is set to be at a zero altitude such that the initial distance of the solid from the rigid body is $d = 0$ cm. A summary of the notations is given in Figure IV.4.

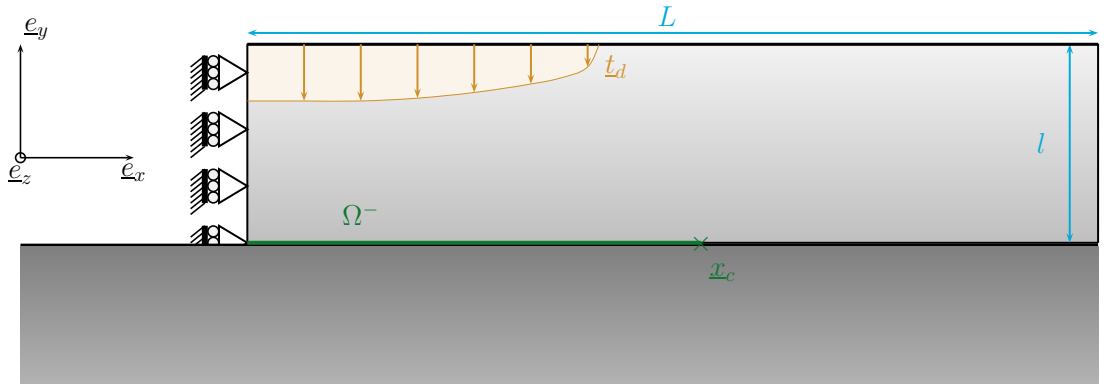

Figure IV.4: Diagram of the uplifting problem

A crucial part for the success of the method is the choice of the criterion. Let us prove in this example the equivalence between K_I and u_c as mentioned in Section IV.2.2. Indeed both values were said to be proportional. In Figure IV.5 this fact is well observed. For different values of $\underline{x}_c = (x_c, 0, 0)$ both K_I and u_c were evaluated. Then their values were normalized by dividing by their maximum and plotted. A pretty fair match is observed with nonetheless some slight variations for u_c.

An example of the result obtained at convergence with a rather coarse mesh is given Figure IV.6. We observe the uplifting of the body out of the contact zone as expected.

Next the results of the method for both criteria are compared along with the active-set strategy.

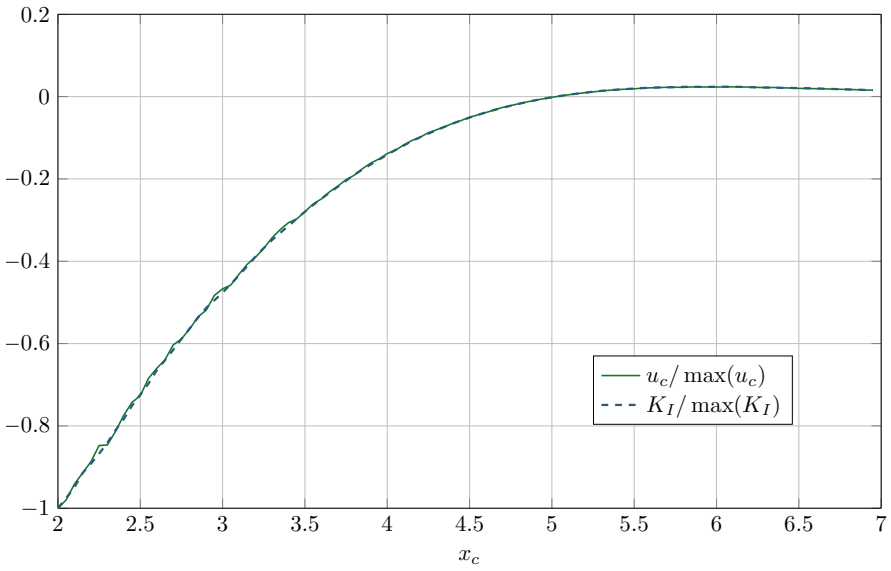

Figure IV.5: Proof of the proportionality of K_I and u_c

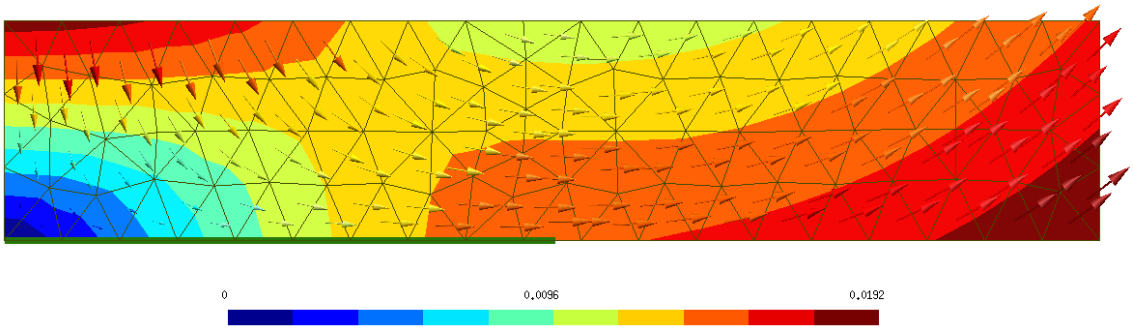

Figure IV.6: Displacement after convergence of the ILS algorithm, the final contact zone is represented by the dark green line

IV.3.1.1 Comparison with the classical active-set

Here, a comparison is drawn between a widely used active-set strategy coupled with a Lagrangian formulation and the ILS method with both criterion K_I and u_c. As a reference solution, the active-set strategy was used coupled with an overkill mesh. The limit of the contact zone coming from this overkill computation is referred as x_c^{ref}. Then, it is possible to compute an error on the position of the contact boundary. A relative error is chosen following the formula error $= |x_c^{\text{ref}} - x_c|/x_c^{\text{ref}}$ as can be seen in Figure IV.7(a). The convergence criteria for the ILS method is linked to the value of ϱ. The Newton's method is considered converged if $|\varrho| < \varrho_{\min}$. The limit here is set to $\varrho_{\min} = 10^{-6}$.

Let us first study the evolution of the error with the size of the mesh described in Figure IV.7(a). As expected, the error is always lower with the ILS method. Nevertheless, the overall behavior of the error is different between the ILS and the active-set method. A noticeable evolution of the active-set error with the mesh is observed. However, as it was observed before in Figure III.7(a) some stage can happened if the refinement of the mesh does not add any node closer to the solution. It is easy to understand that the only guarantee one has on the

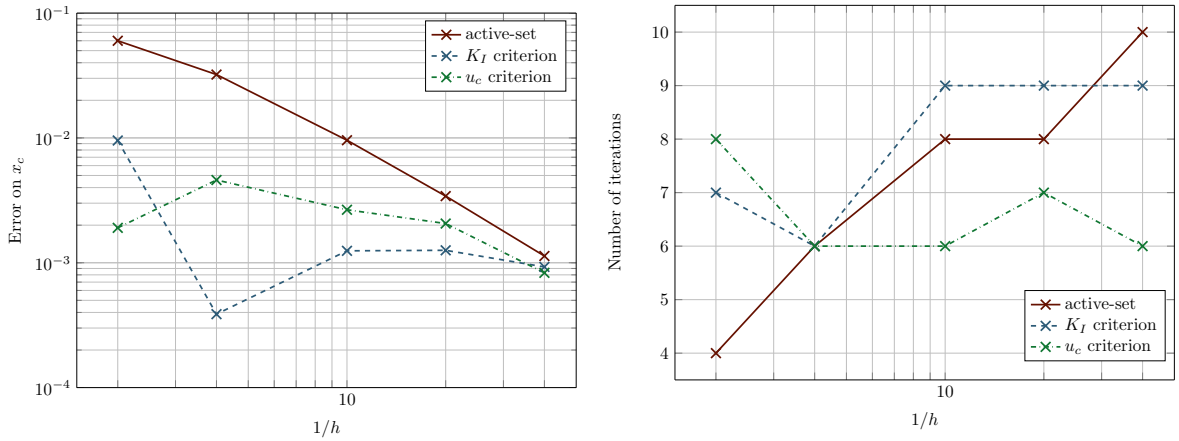

(a) (b)

Figure IV.7: Comparison of the error on the contact boundary position in (a) and the number of iterations needed to converge (b)

error with the active-set strategy is that it is less than $h/2$. Indeed that correspond to the case where the exact solution is in the middle of one element. On the other hand, the error with the ILS does not seem to be directly linked to the size of the mesh which is not consistent with what was observed in the membrane case. This is not due to a lack of convergence of the Newton's method. If the method is not stopped when $|\varrho| < \varrho_{\min}$ one can reached $|\varrho| < 10^{-10}$ without any noticeable improvement on the position x_c. Therefore it can be supposed that the problem is the computation of the criteria. Indeed, if the criteria can't be computed with a good enough precision even on a fine mesh, it is not possible to improve the accuracy of the contact zone. Several explanations are plausible to justify this barrier. First, some work can be done on the enrichment. Indeed there is a conflict close to the solution. The enrichment should not be needed but without enrichment no uplifting is possible. Also the accuracy of the computation of K_I is limited by the quality of the integration. Classical numerical integration is not adapted to handle the singularity at the boundary of the contact zone. Thus, the two options that should be investigated in a later work are: the improvement of the enrichment to allow an uplifting without activating the singular enrichment and the use of a more suited integrations as proposed for instance in [Minnebo, 2012, Chevaugeon et al., 2013].

It is now interesting to look into the computational cost of both methods. In order to do so, two sources of information are available: the evolution of the number of iterations needed to converge in Figure IV.7(b) and the time needed Table IV.3.1.1.

It was chosen to pick the u_c criterion for the ILS as it is the easiest criterion to implement and to use. One ILS iteration is of course more costly than an active-set iteration. However, as expected it is less noticeable than in the membrane case. Except for the coarser mesh, both methods are similarly costly. Again, the ILS seems to be interesting both for coarse and fine mesh. For coarse meshes, the increase in the cost is fully compensated by the gain in accuracy. For fine meshes, the stabilization of the number of iterations needed and the diminution of the difference of time for one ILS and active-set iteration make it computationally efficient.

Mesh	ILS		Classical	
$1/h$	$t_{\text{tot}}^{\text{ILS}}$ (s)	$\overline{t_{\text{iter}}^{\text{ILS}}}$ (s)	$t_{\text{tot}}^{\text{class}}$ (s)	$\overline{t_{\text{iter}}^{\text{class}}}$ (s)
2	0.32	0.04	0.08	0.02
4	0.6	0.10	0.48	0.08
10	5.52	0.92	6.08	0.76
20	17.57	2.51	16.72	2.09
40	60.6	10.1	97.1	9.71

Table IV.1: Time comparison between ILS with u_c criterion and active-set method. All computations have been done on an AMD Opteron 6328 3,2 GHz octocore with 4Go of RAM.

IV.3.1.2 Influence of ILS parameters

In Chapter II and in this chapter several user chosen parameters were introduced. It is interesting to study the influence of these parameters on the solution.

First, let us look into the size of the enriched area. The enriched zone consists of the set of all the elements such that at least one of their node is no further than a certain distance (r_{lim}) from $\underline{x}_c$. This distance is referred as the enrichment zone size. A good touchstone to evaluate the influence of the size of the enriched zone is the value of u_c. In Figure IV.8, the value of u_c is normalized by dividing by an arbitrary value u_c^{far}. This value is taken as a reference for the value of u_c with a big enriched zone but not to much to avoid the possible influence of the boundary of the solid. Here it is taken for an enriched zone of size 1.8. This study was conducted for two meshes in order to know if the influence of the size of elements plays a part in the impact of the size of the enriched zone. The coarse mesh has a mesh size $h = 0.5$ cm and for the fine mesh $h = 0.05$ cm.

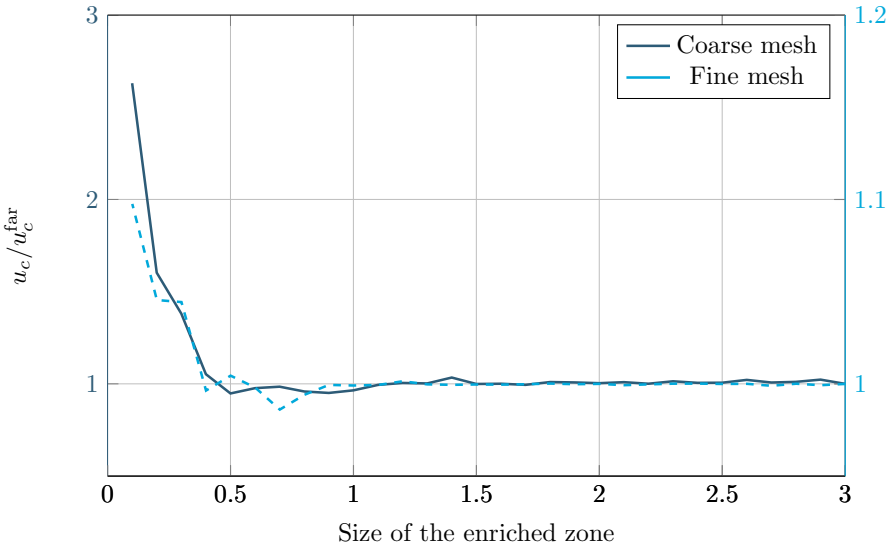

Figure IV.8: Evolution of the normalized value of the criterion u_c with the size of the enriched zone r_{lim} in cm

The solution seems to stay consistent if the size of the enriched zone is greater than 0.5 cm. The size of the mesh does not seems to be linked to this limit. This was expected as it means

that the solution needs, in order to approximate accurately the exact solution, a contribution of the enriched field up to this limit. Further than that, the classical interpolation are enough to represent efficiently the exact solution.

The same study is made for the size of the band $\mathcal{B}$. This band directly influence the value of $\underline{w}$ and therefore the directional derivative of the fields. Therefore, in Figure IV.9 the consistency of $\mathring{u}_c$ is studied in the same fashion as before.

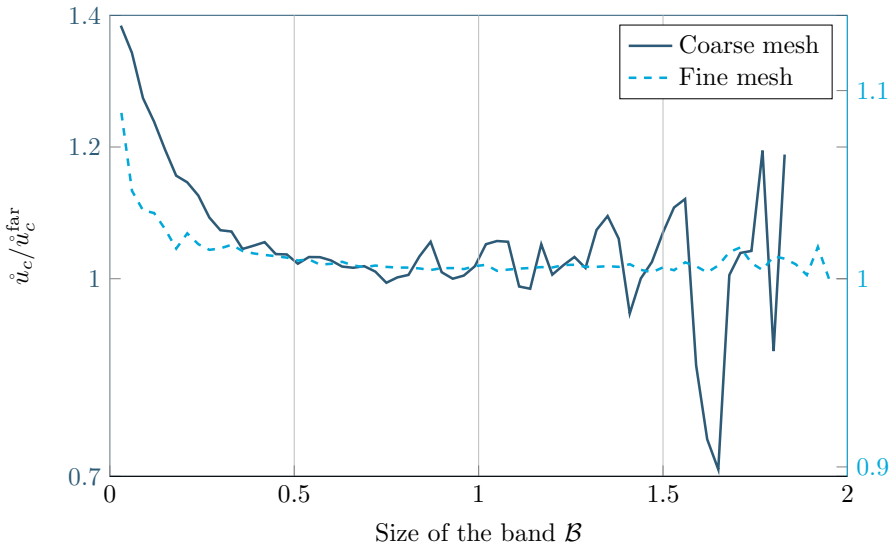

Figure IV.9: Evolution of the normalized value of the derivative of the criterion $\mathring{u}_c$ with the size of the band $\mathcal{B}$ in cm

The same conclusion is drawn for the influence of the band $\mathcal{B}$ size as for the influence of the enriched zone size. It does not depend strongly on the size of the mesh and the consistency limits is linked to where the solution became smooth enough. Nonetheless, it is also to be observed that oscillations appears when the band $\mathcal{B}$ get close to the boundary of the solid (as the thickness of the solid is 2 cm).

Therefore, the parameters need to be picked in order to capture the singularity of the solution and avoid the boundary influence. However, these restrictions leave much liberty in the choice of the parameters.

IV.3.2 Evolution of the loading with a curvy floor

In order to observed multiple contact zones the former problem is modified. The floor is no longer flat but sinusoidal leading to the initial distance $d = 0.15\left(\cos\left(\frac{\pi x}{4}\right) - 1\right)$. Furthermore, the external loading $\underline{t}_d$ is maintained constant other the top boundary. This description is summarized in Figure IV.10. The value of $\underline{t}_d$ (like it was done for the membrane problem) is increased then decreased following the same path in order to check the consistency of the method. The chosen loading path is $t_d = -0.25 \to -0.75 \to -1.5 \to -2.5 \to -3.5 \to -2.5 \to -1.5 \to -0.75 \to -0.25$ such that the contact zones merge for the higher loading. The displacements resulting from these loads are shown Figure IV.11. The criterion chosen here is u_c. Indeed, due to the shape of the floor and the scale at which the computation is carried, the approximation of a straight crack is not computationally valid anymore. Computational

methods of the J-integral were proposed for curved cracks (see [Gosz et al., 1998]) or notch (see [Li et al., 1985]) but they are more complicated. Therefore using u_c save a lot of burden.

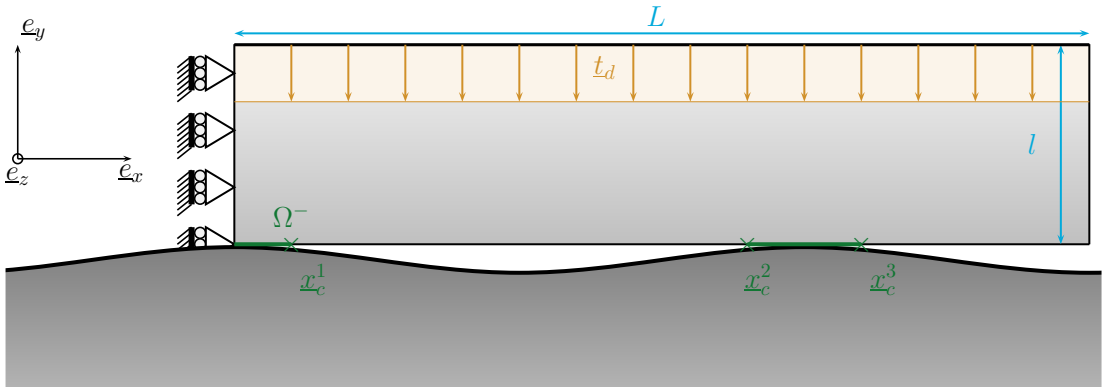

Figure IV.10: Diagram of the problem leading to multiple contact zones

Overall, few iterations are needed for each loading steps. On top of the separation from one to two contact zones during the unloading $-3.5 \rightarrow -2.5$ which is compulsory, an active-set iteration was only needed to go from $-2.5 \rightarrow -1.5$. This confirm a good stability of the method.

In Table IV.3.2, a study of the difference between the solutions for a same load but a different starting point (loading or unloading) is made. Two quantities are defined:

$$\begin{cases} \delta_{\min} &= \min\limits_i \left(\dfrac{x_c^i(\text{loading}) - x_c^i(\text{unloading})}{x_c^i(\text{loading})} \right) \\ \delta_{\max} &= \max\limits_i \left(\dfrac{x_c^i(\text{loading}) - x_c^i(\text{unloading})}{x_c^i(\text{loading})} \right) \end{cases} \tag{IV.41}$$

Obviously $x_c^i(\text{loading})$ refers to the boundary limits obtained while increasing the load and $x_c^i(\text{unloading})$ while decreasing it.

t_d	-0.25	-0.75	-1.5	-2.5
$\delta_{\min}$	$1.2 \cdot 10^{-3}$	$1.7 \cdot 10^{-4}$	$8.9 \cdot 10^{-4}$	$1.9 \cdot 10^{-4}$
$\delta_{\max}$	$2 \cdot 10^{-2}$	$6.1 \cdot 10^{-3}$	$4.7 \cdot 10^{-3}$	$1.7 \cdot 10^{-2}$

Table IV.2: Consistency of the contact zones positions

The results obtained in Table IV.3.2 are really encouraging as the maximum variation of the results is of $2 \cdot 10^{-2}$.

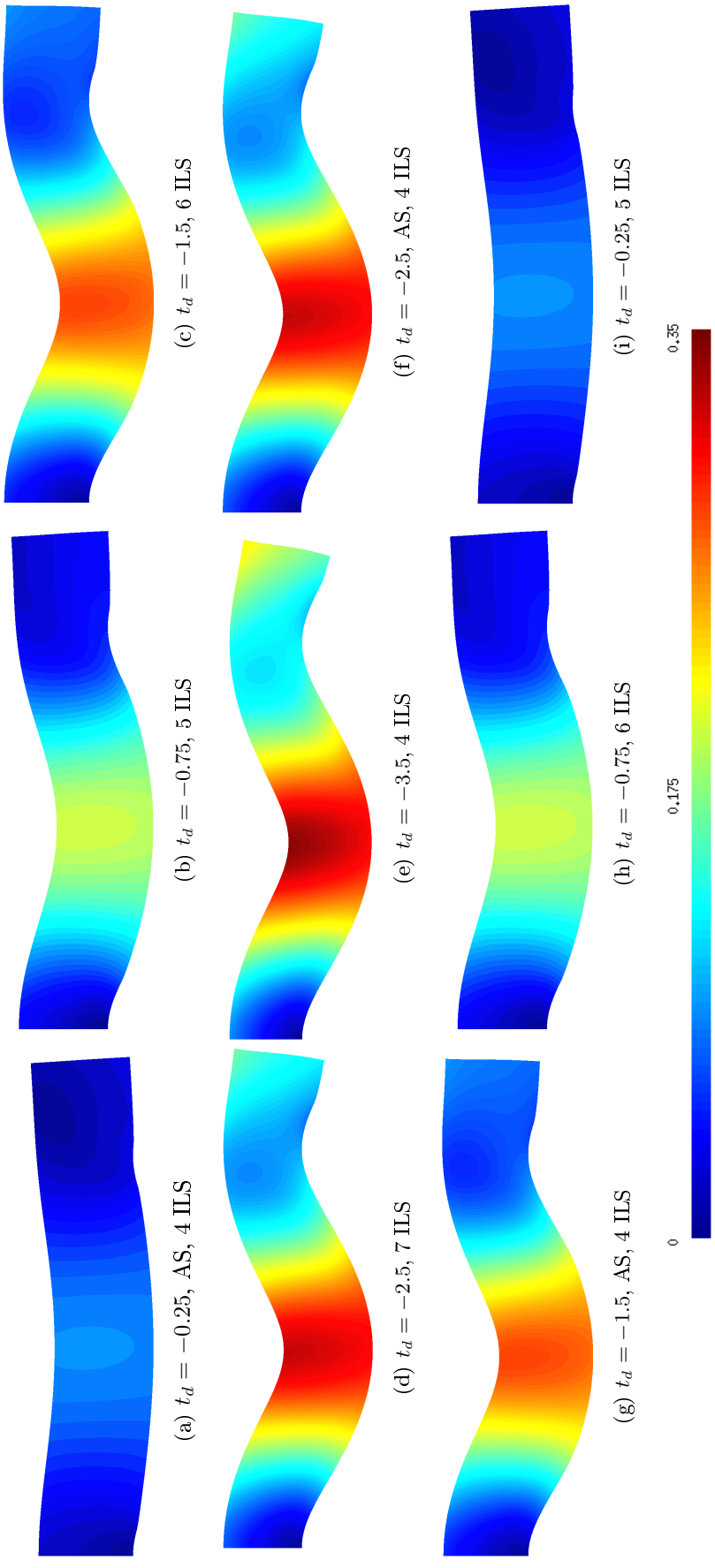

Figure IV.11: Evolution of the solution with the loading (AS meaning an active-set iteration and ILS is short for ILS iteration). The mesh was made of 2624 nodes homogeneously distributed with a characteristic length $h = 0.1$ cm

IV.3.3 The enrichment of the pressure field

In the previous section, we have proven the potential of the method for classical contact problems. However, only the displacement field was enriched. What about the Lagrange multipliers? In order to handle the singularity of the constrain on Γ, it seems logical to enrich the Lagrange multipliers field. The function $1/\sqrt{r}$ is used such that it can handle the contact pressure $\underline{n}\cdot\underline{\underline{\sigma}}\cdot\underline{n} \propto 1/\sqrt{r}$ on Ω^-. This should definitely improve the solution, particularly the pressure field, when the enrichment is needed (i.e. when adhesion need to be modeled or when the contact zone is not yet close to the exact contact one). Furthermore it is hoped that it will also improve the above results.

However, enriching the Lagrange multipliers field is not a straightforward matter. Without any modifications, the enrichment implies that the BB conditions are not fulfilled anymore. Two options are offered. First, the discretization can be modified. This lead was followed without success using the mortar discretization field defined in Section I.2.1. The other option is to adapt the formulation as it was done for the membrane. In [Hansbo, 2005], a stabilization term is proposed. In addition to both the total and contact energy, the following stabilization term is joined:

$$\Pi_{\text{stab}} = \frac{1}{2\delta}(p - \underline{n}\cdot\underline{\underline{\sigma}}\cdot\underline{n})^2 \tag{IV.42}$$

with δ a parameter of dimension N.m^{-1} such that $1/\delta = O(h)$. This lead to the new variational problem replacing Problem 32:

Problem 38

Find $\underline{u} \in \mathcal{U}$ and $p \in H^{-1/2}$ such that for all $\underline{u}^\star \in \mathcal{U}_0$ and $p^\star \in H^{-1/2}$

$$\left\{\begin{array}{rcl} a(\underline{u},\underline{u}^\star) + a^{\text{stab}}(\underline{u},\underline{u}^\star) + c^l(p,\underline{u}^\star) + c^{\text{stab}}(p,\underline{u}^\star) &=& f(\underline{u}^\star) \\ c^l(p^\star,\underline{u}) + c^{\text{stab}}(p^\star,\underline{u}) + c^p(p^\star,p) &=& l^l(p^\star) \end{array}\right. \tag{IV.43}$$

with:

$$\begin{aligned} a^{\text{stab}}(\underline{u},\underline{u}^\star) &= \frac{1}{\delta}\int_{\Omega^-} (\underline{n}\cdot\underline{\underline{\sigma}}(\underline{u})\cdot\underline{n})(\underline{n}\cdot\underline{\underline{\sigma}}(\underline{u}^\star)\cdot\underline{n})\,\mathrm{d}S \\ c^{\text{stab}}(p,\underline{u}) &= -\frac{1}{\delta}\int_{\Omega^-} p(\underline{n}\cdot\underline{\underline{\sigma}}(\underline{u})\cdot\underline{n})\,\mathrm{d}S \qquad\qquad c^p(p,p^\star) = \frac{1}{\delta}\int_{\Omega^-} pp^\star\,\mathrm{d}S \end{aligned} \tag{IV.44}$$

The addition of these terms changes also the sensibility problem given by Problem 34 into the new set of equations:

Problem 39

Find $\underline{u} \in \mathcal{U}$ and $p \in H^{-1/2}$ such that for all $\underline{u}^\star \in \mathcal{U}_0$ and $p^\star \in H^{-1/2}$

$$\left\{ \begin{array}{rcrcl} a(\mathring{\underline{u}}, \underline{u}^\star) + a^{\text{stab}}(\mathring{\underline{u}}, \underline{u}^\star) & + & c^l(\mathring{p}, \underline{u}^\star) + c^{\text{stab}}(\mathring{p}, \underline{u}^\star) & = & f^s(\underline{u}^\star) + f^s_{\text{stab}}(\underline{u}^\star) \\ c^l(p^\star, \mathring{\underline{u}}) + c^{\text{stab}}(p^\star, \mathring{\underline{u}}) & + & c^p(p^\star, \mathring{p}) & = & l^{ls}(p^\star) + l^{ls}_{\text{stab}}(\underline{u}^\star) \end{array} \right. \tag{IV.45}$$

with:

$$\left| \begin{array}{l} f^s_{\text{stab}}(\underline{u}^\star) = \dfrac{1}{\delta} \displaystyle\int_{\Omega^-} \left(\underline{n} \cdot \underline{\underline{\mathrm{K}}}(\nabla \underline{u} \nabla \underline{w})_S \cdot \underline{n} \right) (\underline{n} \cdot \underline{\underline{\sigma}}(\underline{u}^\star) \cdot \underline{n}) \, \mathrm{d}S \\ -l^{ls}_{\text{stab}}(p^\star) = \dfrac{1}{\delta} \displaystyle\int_{\Omega^-} \left(\underline{n} \cdot \underline{\underline{\mathrm{K}}}(\nabla \underline{u} \nabla \underline{w})_S \cdot \underline{n} \right) p^\star \, \mathrm{d}S \end{array} \right. \tag{IV.46}$$

The first step with this new formulation is to compare the results obtained with and without this enrichment for the previous problem. Figure IV.12 shows the error on the position of the contact zone in the two cases. Even if the solution is closer for most of the cases with the enriched formulation, it is not enough to conclude that it improves the accuracy of the contact zone. However Figure IV.13 shows the normalized pressure field on the bottom boundary of the solid. The enriched field allows a better representation at the boundary of the contact zone.

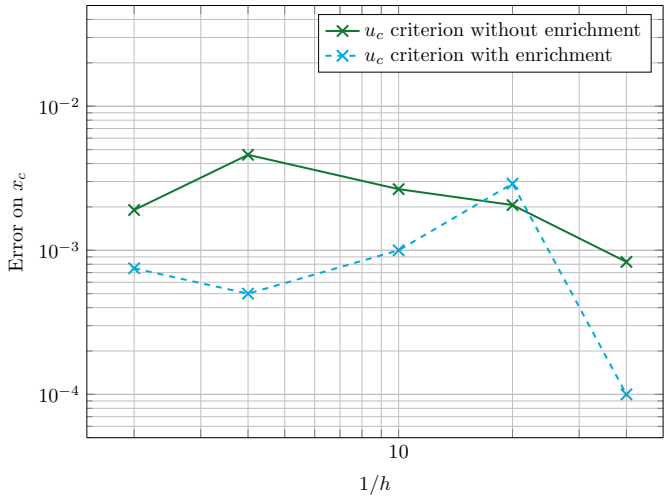

Figure IV.12: Comparison of the relative error on x_c with an without the enrichment of the Lagrange multipliers field for different mesh sizes

Nevertheless, the improvement of the pressure field is striking when we consider adhesion. In order to do the comparison, we solve the same problem as before but with a surface energy $\gamma = 10^{-3}$. Without enrichment an oscillation of the field appears (see Figure IV.14) whereas with the enrichment the singularity is well represented and fit the JKR model.

The influence of the parameter δ is important. If it is not well calibrated spurious oscillations appear. On one hand, if the parameter is too big the stabilization term does not play its part.

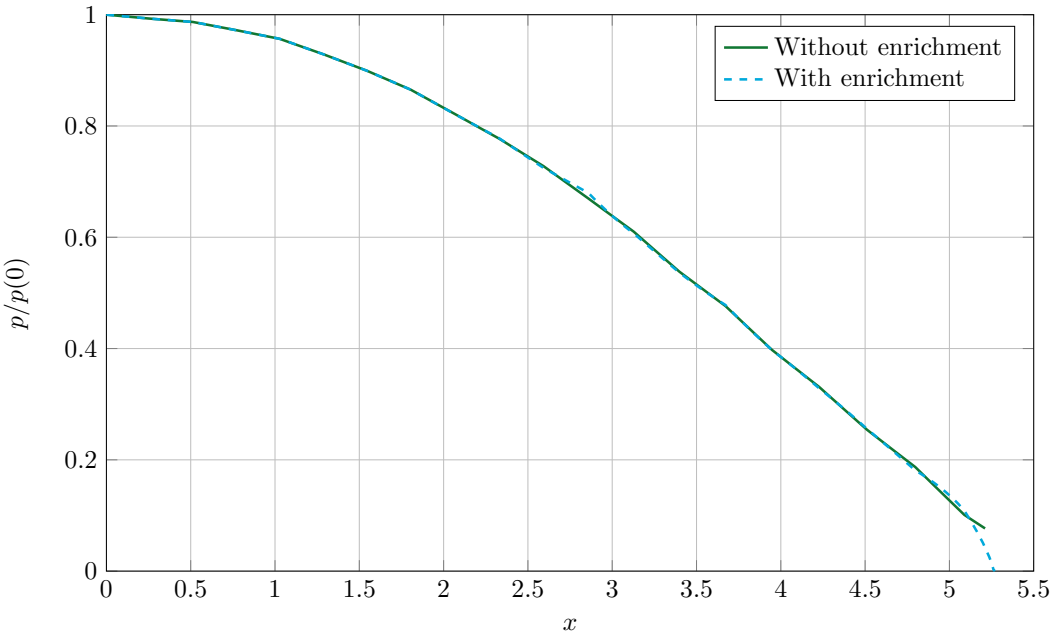

Figure IV.13: Comparison of the pressure field with an without the enrichment without adhesion

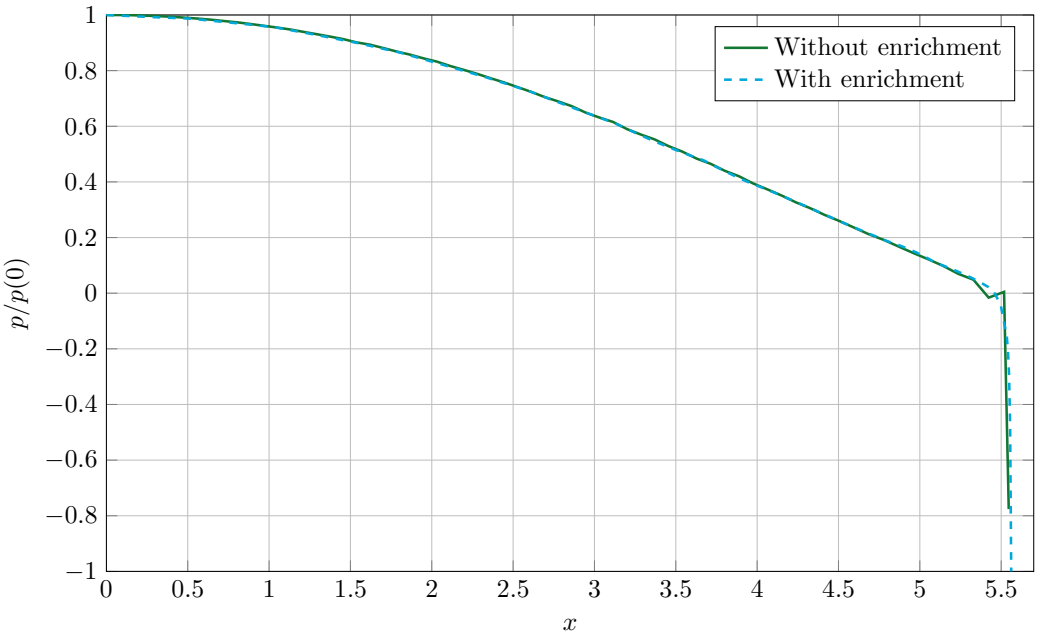

Figure IV.14: Comparison of the pressure field with an without the enrichment with adhesion

On the other hand, if the parameter is too small the constrain on the pressure field is to strong. Even if the evolution of the parameter with the mesh size is known, we haven't developed a framework to find it for a first given mesh. A mathematical study of the problem shall be done in a later work to solve this problem.

IV.3.4 Hertz cylinder, toward higher order approximation

The final example in this report will be an approximation of a classical Hertz problem. The same set-up as in [Franke et al., 2010] is used and the reader is referred to this article in order to compare the obtained results. An unilateral contact of a cylinder of radius R and length l on a rigid flat surface is studied. A point-wise force $F\underline{e}_y$ is applied on its top. The solution of this Hertz's problem gives, among others, two quantities of interest:

- the half-width of the contact zone:

$$b = \sqrt{\frac{4F}{\pi l}\frac{(1-\nu^2)R}{E}} \tag{IV.47}$$

- the contact pressure:

$$p_n\left(\frac{x}{b}\right) = \frac{E}{2R(1-\nu^2)}\sqrt{\frac{4F(1-\nu^2)R}{\pi l E} - \left(\frac{x}{b}\right)^2 b^2} \tag{IV.48}$$

An approximation of this problem is made. Only a quarter of this cylinder is considered (see Figure IV.15). The symmetry is taken into account with appropriate boundary conditions and the loading is modeled by a homogeneous displacement on the top boundary. This approximation was said to be negligible in [Franke et al., 2010] however we will not be surprised if the contact zone obtained numerically is not exactly equivalent to the Hertz's solution. This set-up is illustrated in Figure IV.15.

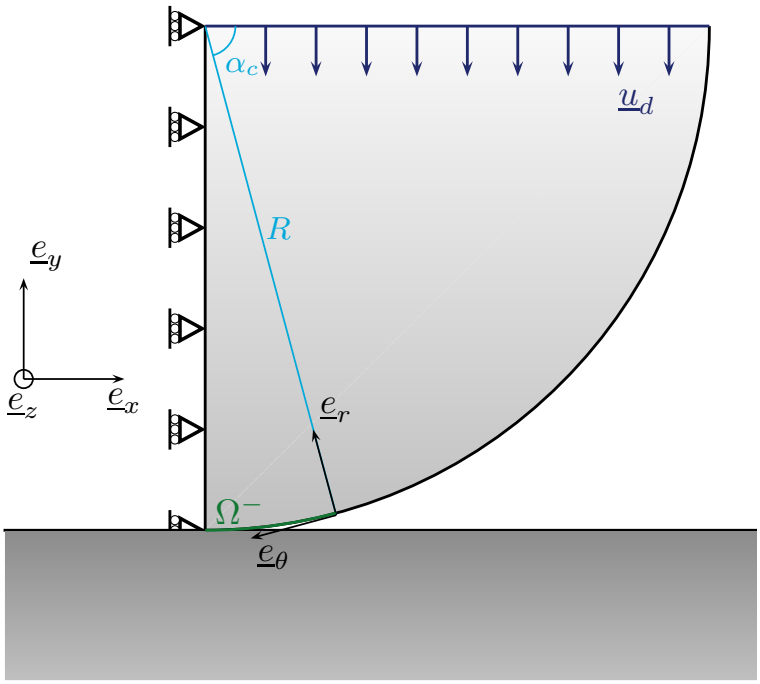

Figure IV.15: Diagram of the Hertz's cylinder problem

The parameters used for the simulations are the same as in the above mentioned article, that is to say:

$$\left|\begin{array}{llll} E = 2.1 \times 10^5 \text{N.mm}^{-2} & \nu = 0.29 & R = 10\text{mm} & l = 1\text{mm} \\ F = 70000\text{N} & \rightarrow & u_d = 0.490559880766923\text{mm} & \end{array}\right. \tag{IV.49}$$

The originality on this example compared to the previous one is that an order two interpolation is also tested. The computation is carried on two different meshes. The first one is composed of 1072 elements with a high concentration of elements on the contact zone ($h = 0.05$mm). The other one is a coarse mesh of 217 elements with a mesh size of $h = 0.5$mm on the contact zone. On these two meshes, computation are made with an active-set method with an order 1 approximation and the ILS method with both an order 1 and an order 2 interpolation. For the ILS order 1 approximation we used $1/\delta = |h| \cdot 10^{-4}\text{m.N}^{-1}$ and for the order 2 we used $1/\delta = |h| \cdot 10^{-5}\text{m.N}^{-1}$. The stress fields obtained with these different configurations can be seen in Figure IV.18.

First, let us study the pressures obtained with the different solutions on the finer mesh, given in Figure IV.16. The advantage of the ILS is clear around the contact zone. As mentioned before the position of the contact zone is better than with the classical formulation. Furthermore, the pressure field is well represented in this area with the ILS whereas big oscillations are observed with the active-set. On the rest of the boundary, some oscillations are still present but less noticeable with the order 2 interpolation.

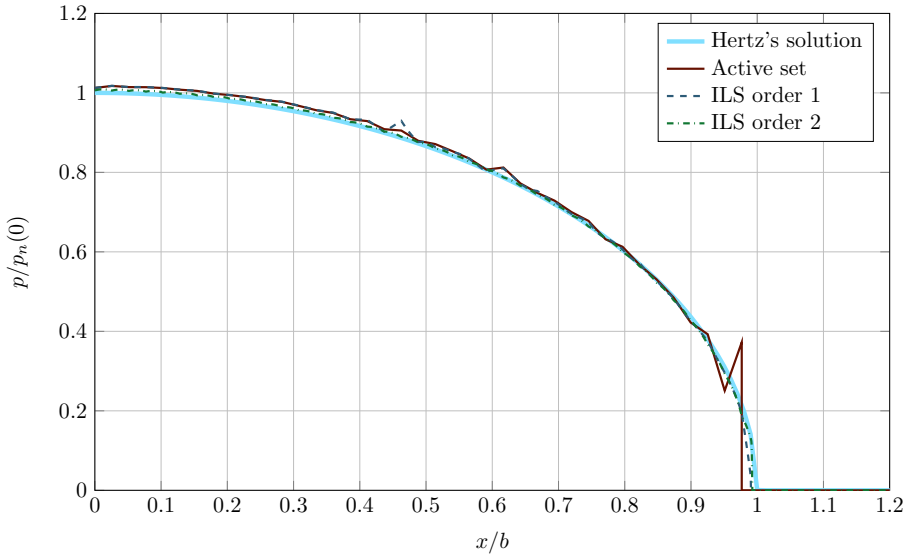

Figure IV.16: Comparison of the pressure field for the different methods on a classical mesh of 1072 elements

The advantage of the order 2 approximation is more noticeable on the coarser mesh (see Figure IV.17). On this coarse mesh, the ILS order 1 interpolation does not give a satisfactory solution. The position of the contact zone is rather good but the pressure field is not well represented. On the other hand, the order 2 interpolation shows its potential with both a good representation of the pressure field and the the contact zone.

The results we obtained are consistent with the work of [Franke et al., 2010] which underlines the assets of high order interpolation as long as the contact zone is well approximated.

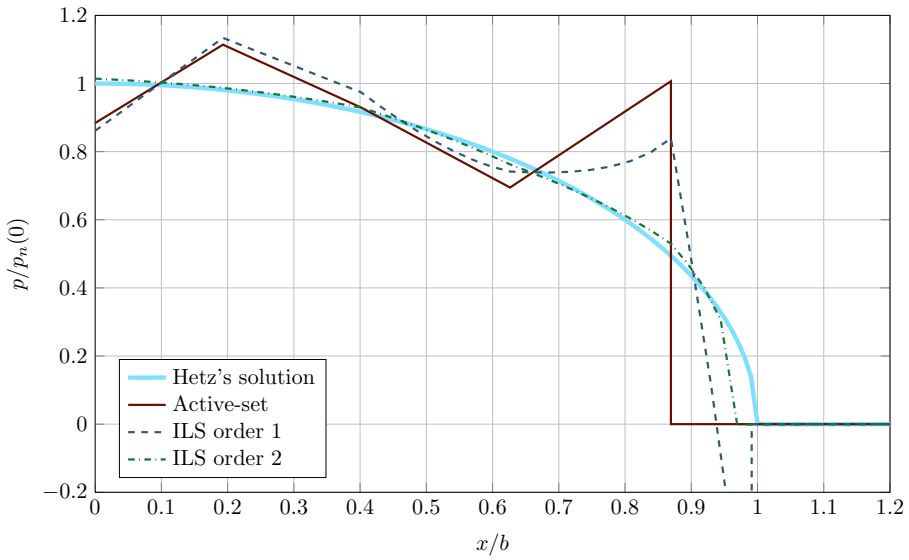

Figure IV.17: Comparison of the pressure field for the different methods on a coarse mesh of 217 elements

Conclusion

The results of this chapter are consistent with the results obtained in the membrane chapter (Chapter III). The ILS gives a good representation of the contact zone with an attractive computational cost. Furthermore, the pressure field is also well approximated, especially using a higher order interpolation. The importance of the formulation choice was also highlighted in order to fulfill the BB condition. These first results do encourage an effort to improve the method. The integration method is to be improved to handle the singularity. Furthermore, the use of high order interpolation was opened with the order 2 interpolation but higher order will be implemented too. Finally a mathematical study need to be carried out in order to give an effective way to chose the parameter δ.

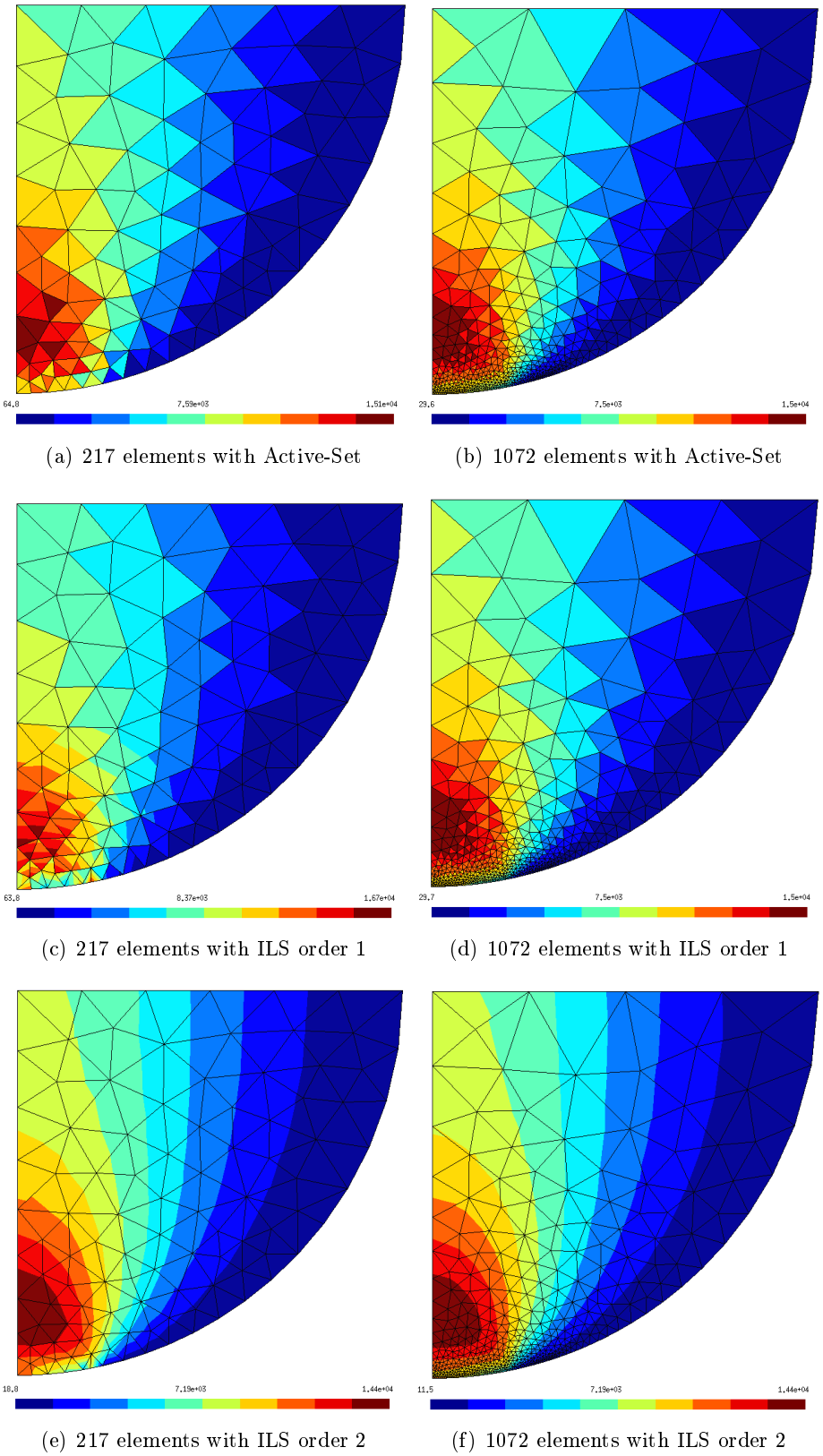

(a) 217 elements with Active-Set

(b) 1072 elements with Active-Set

(c) 217 elements with ILS order 1

(d) 1072 elements with ILS order 1

(e) 217 elements with ILS order 2

(f) 1072 elements with ILS order 2

Figure IV.18: Stress at convergence for different methods on a first mesh composed of 217 elements and a second of 1072 elements

Conclusion

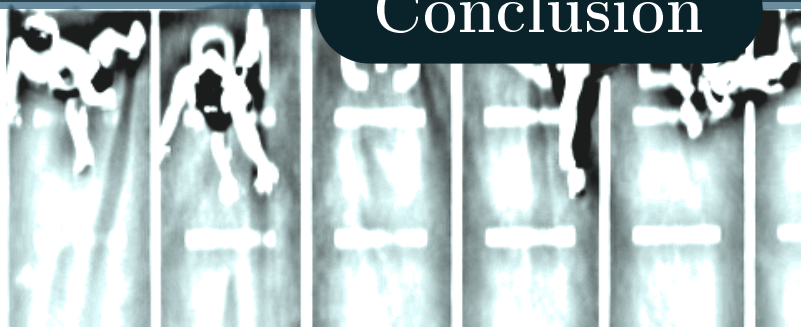

In this report, a first application of the ILS to contact problems was done with success. The use of level-sets is definitely a great asset. First it gives a good representation of the contact zone without a strong dependence on the mesh. Furthermore, it paves the way to more advance techniques. By using the level-set, an enrichment method can be set-up to represent more efficiently several phenomena, including adhesion. Moreover, a shape optimization is possible in order to find the contact zone. The key points of this shape optimization are the choice of a positioning criterion and the computation of its directional derivative. Configurational mechanics gives an answer to both of them, even if a physical knowledge can also motivate the choice of the criterion.

Let us take a moment to summarize what was achieved. First, it is important to emphasize the importance of the Babuška-Brezzi condition for the stability of mixed formulations. In order to fulfill this condition, two schools of thought are present. One works on the compatibility of the discretization spaces between every fields. This method seemed too complicated, especially when enrichment is involved. The other one proposes the modification of the variational formulation such that the discretization spaces constraints are lighten. The usual method is to add a stabilization term which cancel itself if the exact solution is injected into the formulation. This is the method we used in this thesis as it was efficient and worked with the enrichment. Once the variational formulation is settled, a general framework was given in order to make the contact zone evolve. It is based on a Newton's method for which the influence of the contact zone position is modeled thanks to the directional derivative. This framework was intensively tested on several problems. The algorithm handled well the contact zone evolution, even the merging or the nucleation. Furthermore, due to the good approximation of the contact zone, higher order interpolation can be used efficiently.

The comparison with a classical formulation with an active-set strategy has shown the potential of the ILS. The gain on the accuracy of the method truly compensate the slight increase in computational cost.

It is clear that the work of this thesis has opened a door toward new developments of the ILS for contact. Before giving a glance at what is behind this door let us wipe our feet on the front mat. Indeed this first approach has left some untidy part due to a lack of time and it is important to underline them in order to correct it in a later work. More local modes should be implemented in order to handle less smooth contact zones. Finally a mathematical study is to be made in order to calibrate *a priori* the stabilization parameter.

Several possible improvements of the method are considered. First, even if the plain solid

problem was solved with an order two approximation, higher order interpolations can be implemented in order to benefit from the good representation of the contact zone with a coarse mesh. Others model of adhesion could also be considered by changing the type of enrichment used. Also, other phenomena such as friction shall be integrated in the method.

A

Formulae

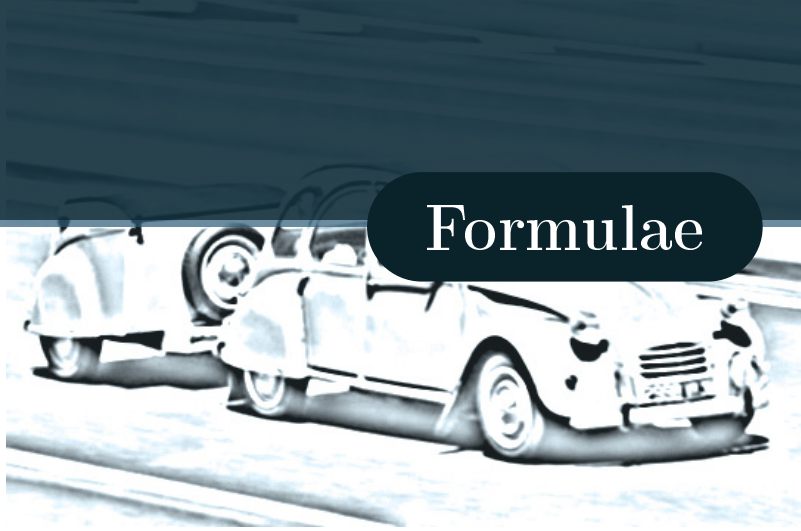

In order to understand from where the formulae associated with the directional derivative come from we will use a classical framework. It was mentioned that the directional derivative was linked to a quantity $\underline{w}$. This quantity could be seen as a displacement or a velocity depending on the framework chosen. The most general one and the closer to what the reader might be familiar with is the one leading to see $\underline{w}$ as a velocity. Therefore we chose this framework here. Let us imagine that a body in an initial configuration Ω_0, with an internal zone Ω_0^- undertakes a transformation in time Φ_t into the current configuration Ω_t (see Figure A.1). Every points $\underline{x}_0$ evolves with a speed $\underline{w}$.

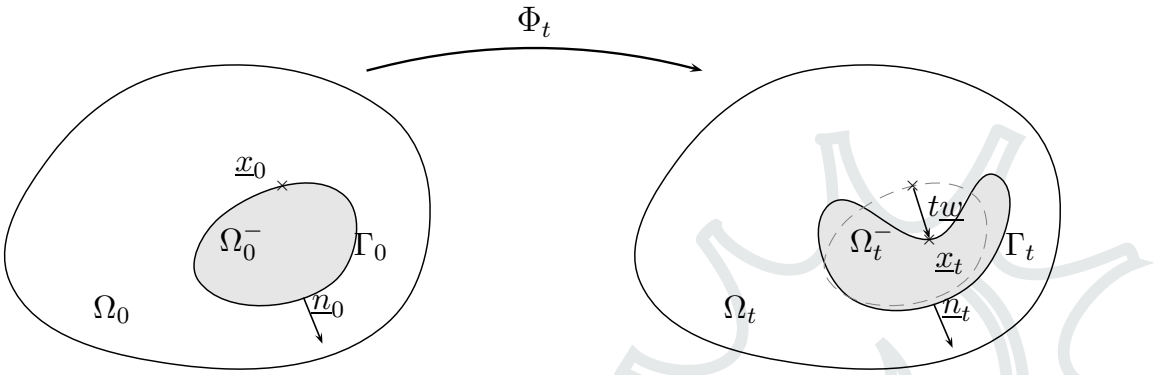

Figure A.1: Body undergoing a transformation defined by $\underline{w}$

From this, the basic notations are recalled, for a function u: $\mathring{u} = D_{[\underline{w}]}(u)$ and $\dot{u} = \dfrac{\partial u}{\partial t}$. The mathematical definition of $\mathring{u}$ is :

$$\mathring{u} = \lim_{t \to 0} \frac{u_t - u_0}{t} \tag{A.1}$$

The link between $\mathring{u}$ and $\dot{u}$ is $\mathring{u} = \dot{u} + \nabla u \cdot \underline{w}$. Thus we can deduce a useful formula:

$$\overline{\mathring{\nabla} u} = \nabla \dot{u} + \nabla \nabla u \cdot \underline{w} = \nabla(\dot{u} + \nabla u \cdot \underline{w}) - \nabla u \cdot \nabla \underline{w} = \nabla \mathring{u} - \nabla u \nabla \underline{w} \tag{A.2}$$

and compute directly:

$$\begin{aligned} D(\underline{\underline{\epsilon}}(\underline{u}))[w] &= \tfrac{1}{2} D(\nabla \underline{u}^T + \nabla \underline{u})[w] \\ &= \tfrac{1}{2}(\mathring{\nabla} \underline{u}^T + \mathring{\nabla} \underline{u}) \\ &= \tfrac{1}{2}\left(\nabla \mathring{\underline{u}}^T - (\nabla \underline{u} \nabla \underline{w})^T + \nabla \mathring{\underline{u}} - (\nabla \underline{u} \nabla \underline{w})\right) \\ &= \underline{\underline{\epsilon}}(\mathring{\underline{u}}) - (\nabla \underline{u} \nabla \underline{w})_S \end{aligned} \tag{A.3}$$

More generally, the total derivative of a functional is done by computing the limit given Equation A.1. In order to do so, the quantity in the current configuration needs to be expressed in the initial configuration. It was explained how to do in Section I.1.1 by mean of the deformation gradient $\underline{\underline{F}}$ (for instance $\nabla_{\underline{x}_t} u = \nabla_{\underline{x}_0} \underline{\underline{F}}^{-1}$ and $\mathrm{d}V_t = \mathrm{d}V_0 \det(\underline{\underline{F}})$).

This leads to the ready to use formulae for any smooth function f (all subscripts are dropped as the configuration are equivalent at the limit):

$$D\left(\int_\Omega f \,\mathrm{d}V\right)[\underline{w}] = \int_\Omega D(f)[\underline{w}] + f\mathrm{div}\underline{w}\,\mathrm{d}V \tag{A.4}$$

$$D\left(\int_\Gamma f \,\mathrm{d}S\right)[\underline{w}] = \int_\Gamma D(f)[\underline{w}] + f(\mathrm{div}\underline{w} - \underline{n}\cdot\nabla\underline{w}\cdot\underline{n})\,\mathrm{d}S \tag{A.5}$$

If the reader is interested in verifying the above formulae some useful limits are given:

$$\left|\begin{array}{lcl} \lim\limits_{t\to 0} \underline{\underline{F}} & = & \underline{\underline{\mathrm{I}}} \\ \lim\limits_{t\to 0} \overset{\circ}{\underline{\underline{F}}} & = & \nabla\underline{w} \\ \lim\limits_{t\to 0} \overset{\circ}{\underline{\underline{F}}}^{-1} & = & -\nabla\underline{w} \\ \lim\limits_{t\to 0} \overset{\circ}{\det(\underline{\underline{F}})} & = & \mathrm{div}\underline{w} \\ \lim\limits_{t\to 0} \overset{\circ}{\left(\frac{\mathrm{d}S_t}{\mathrm{d}S_0}\right)} & = & \mathrm{div}\underline{w} - \underline{n}\cdot\nabla\underline{w}\cdot\underline{n} \end{array}\right. \tag{A.6}$$

B

Analitycal solution: membrane

The setting of the problem of an axy-symmetric membrane was already done partially Section III.1 and completed Section III.3.1. The governing equations are :

$$\begin{cases} T\frac{1}{r}\frac{\partial}{\partial r}\left(r\frac{\partial u}{\partial r}\right)+f_d &= 0 \quad \text{on } [0,r_c[\\ -u &= d \quad \text{on } [rc,R] \\ u &= 0 \quad \text{for } r=R \end{cases} \tag{B.1}$$

From the first equation it can be deduced:

$$\begin{aligned} T\frac{1}{r}\frac{\partial}{\partial r}\left(r\frac{\partial u}{\partial r}\right)+f_d=0 &\xRightarrow{\text{integration}} \frac{\partial u}{\partial r}=\frac{A}{r}-\frac{f_d r}{2T} \\ &\xRightarrow{\text{integration}} u=B+A\ln\left(\frac{r}{R}\right)-\frac{f_d r^2}{4T} \end{aligned} \tag{B.2}$$

First let us use the the boundary condition $u=0$ for $r=R$:

$$\begin{cases} u=B+A\ln\left(\frac{r}{R}\right)-\frac{f_d r^2}{4T} \\ u=0 \text{ for } r=R \end{cases} \Rightarrow 0=B-\frac{f_d R^2}{4T} \Leftrightarrow B=\frac{f_d R^2}{4T} \tag{B.3}$$

Then let us use the other Dirichlet's condition $-u=d$ for $r=r_c$:

$$\begin{cases} u=A\ln\left(\frac{r}{R}\right)+\frac{f_d(R^2-r^2)}{4T} \\ -u=d \text{ for } r=r_c \end{cases} \Rightarrow d=\frac{f_d(r_c^2-R^2)}{4T}-A\ln\left(\frac{r_c}{R}\right) \Leftrightarrow A=\frac{\frac{f_d(r_c^2-R^2)}{4T}-d}{\ln\left(\frac{r_c}{R}\right)} \tag{B.4}$$

At this point, all the Dirichlet's conditions are verified. Nevertheless, the equilibrium is not satisfied for any r_c. Writing the equilibrium of a piece of membrane centered at r_c and having its length shrinking to zero, the equilibrium condition becomes:

$$\frac{\partial u(r_c)}{\partial r}=0 \Leftrightarrow \frac{\frac{f_d(r_c^2-R^2)}{4T}-d}{\ln\left(\frac{r_c}{R}r_c\right)}-\frac{f_d r_c^2}{2T}=0 \tag{B.5}$$

Solving this equation gives the position of the exact contact zone:

$$r_c^{\text{ex}}=R\exp\left(\frac{1}{2}\left(1+\text{W}_{-1}\left(-\frac{4dT+f_d}{\exp(1)f_d}\right)\right)\right) \tag{B.6}$$

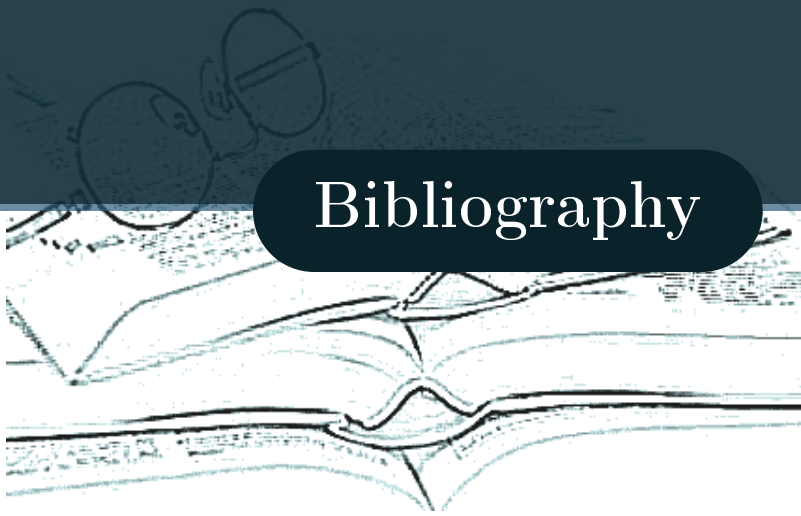

Bibliography

[Alart and Curnier, 1991] Alart, P. and Curnier, A. (1991). A mixed formulation for frictional contact problems prone to Newton like solution methods. *Computer methods in applied mechanics and engineering*, 92(3):353–375. [p. 17]

[Annavarapu et al., 2014] Annavarapu, C., Hautefeuille, M., and Dolbow, J. E. (2014). A Nitsche stabilized finite element method for frictional sliding on embedded interfaces. Part I: single interface. *Computer Methods in Applied Mechanics and Engineering*, 268:417–436. [p. 18]

[Autumn et al., 2002] Autumn, K., Sitti, M., Liang, Y. A., Peattie, A. M., Hansen, W. R., Sponberg, S., Kenny, T. W., Fearing, R., Israelachvili, J. N., and Full, R. J. (2002). Evidence for van der Waals adhesion in gecko setae. *Proceedings of the National Academy of Sciences*, 99(19):12252–12256. [p. 20]

[Babuška, 1973] Babuška, I. (1973). The finite element method with Lagrangian multipliers. *Numerische Mathematik*, 20(3):179–192. [p. 22], [p. 43]

[Banerjee et al., 1981] Banerjee, P. K., Banerjee, P. K., and Butterfield, R. (1981). *Boundary element methods in engineering science*. McGraw-Hill Book Co. (UK). [p. 20]

[Béchet et al., 2005] Béchet, E., Minnebo, H., Moës, N., and Burgardt, B. (2005). Improved implementation and robustness study of the X-FEM for stress analysis around cracks. *International Journal for Numerical Methods in Engineering*, 64(8):1033–1056. [p. 93]

[Béchet et al., 2009] Béchet, É., Moës, N., and Wohlmuth, B. (2009). A stable Lagrange multiplier space for stiff interface conditions within the extended finite element method. *International Journal for Numerical Methods in Engineering*, 78(8):931–954. [p. 43]

[Belgacem et al., 1998] Belgacem, F. B., Hild, P., and Laborde, P. (1998). The mortar finite element method for contact problems. *Mathematical and Computer Modelling*, 28(4):263–271. [p. 22]

[Belytschko et al., 2003] Belytschko, T., Parimi, C., Moës, N., Sukumar, N., and Usui, S. (2003). Structured extended finite element methods for solids defined by implicit surfaces. *International Journal for Numerical Methods in Engineering*, 56(4):609–635. [p. 36], [p. 38], [p. 67]

[Bernardi et al., 1993] Bernardi, C., Maday, Y., and Patera, A. T. (1993). Domain Decomposition by the Mortar Element Method. In Kaper, H. G., Garbey, M., and Pieper, G. W., editors, *Asymptotic and Numerical Methods for Partial Differential Equations with Critical Parameters*, number 384 in NATO ASI Series, pages 269–286. Springer Netherlands. [p. 23]

[Bertsekas, 1982] Bertsekas, D. P. (1982). Constrained optimization and Lagrange Multiplier methods. *Computer Science and Applied Mathematics, Boston: Academic Press, 1982*, 1. [p. 25]

[Björkman et al., 1995] Björkman, G., Klarbring, A., Sjödin, B., Larsson, T., and Rönnqvist, M. (1995). Sequential quadratic programming for non-linear elastic contact problems. *International Journal for Numerical Methods in Engineering*, 38(1):137–165. [p. 25]

[Bonfils, 2011] Bonfils, N. (2011). *Traitement des contraintes d'inégalité volumiques dans un mimlieu continu par la méthode X-FEM et level-set*. PhD thesis, École Centrale Nantes. [p. 27], [p. 31]

[Bonfils et al., 2012] Bonfils, N., Chevaugeon, N., and Moës, N. (2012). Treating volumetric inequality constraint in a continuum media with a coupled X-FEM/level-set strategy. *Computer Methods in Applied Mechanics and Engineering*, 205–208:16–28. [p. 31]

[Brezzi, 1974] Brezzi, F. (1974). On the existence, uniqueness and approximation of saddle-point problems arising from Lagrangian multipliers. *Revue française d'automatique, informatique, recherche opérationnelle. Analyse numérique*, 8(2):129–151. [p. 22]

[Chevaugeon et al., 2013] Chevaugeon, N., Moës, N., and Minnebo, H. (2013). Improved crack tip enrichment functions and integration for crack modeling using the extended finite element method. *International Journal for Multiscale Computational Engineering*, 11(6). [p. 102]

[Chouly et al., 2015] Chouly, F., Hild, P., and Renard, Y. (2015). Symmetric and non-symmetric variants of Nitsche's method for contact problems in elasticity: theory and numerical experiments. *Mathematics of Computation*, 84(293):1089–1112. [p. 18]

[Chu et al., 2005] Chu, Y.-S., Dufour, S., Thiery, J. P., Perez, E., and Pincet, F. (2005). Johnson-Kendall-Roberts Theory Applied to Living Cells. *Physical Review Letters*, 94(2):028102. [p. 20]

[Cottrell et al., 2009] Cottrell, J. A., Hughes, T. J. R., and Bazilevs, Y. (2009). *Isogeometric Analysis: Toward Integration of CAD and FEA*. John Wiley & Sons. [p. 20]

[Crisfield, 2000] Crisfield, M. A. (2000). Re-visiting the contact patch test. *International Journal for Numerical Methods in Engineering*, 48(3):435–449. [p. 22]

[Derjaguin et al., 1975] Derjaguin, B. V., Muller, V. M., and Toporov, Y. P. (1975). Effect of contact deformations on the adhesion of particles. *Journal of Colloid and Interface Science*, 53(2):314–326. [p. 20], [p. 92]

[Dolbow and Gosz, 2002] Dolbow, J. E. and Gosz, M. (2002). On the computation of mixed-mode stress intensity factors in functionally graded materials. *International Journal of Solids and Structures*, 39(9):2557–2574. [p. 94]

[Dréau et al., 2010] Dréau, K., Chevaugeon, N., and Moës, N. (2010). Studied X-FEM enrichment to handle material interfaces with higher order finite element. *Computer Methods in Applied Mechanics and Engineering*, 199(29–32):1922–1936. [p. 36], [p. 38]

[Duvaut and Lions, 1976] Duvaut, G. and Lions, J. L. (1976). *Inequalities in Mechanics and Physics*, volume 219 of *Grundlehren der mathematischen Wissenschaften*. Springer Berlin Heidelberg, Berlin, Heidelberg. [p. 14]

[Fichera, 1973] Fichera, G. (1973). Boundary value problems of elasticity with unilateral constraints. In *Linear Theories of Elasticity and Thermoelasticity*, pages 391–424. Springer. [p. 10]

[Fischer-Cripps, 2011] Fischer-Cripps, A. C. (2011). *Nanoindentation*. Springer Science & Business Media. [p. 20]

[Franke et al., 2010] Franke, D., Düster, A., Nübel, V., and Rank, E. (2010). A comparison of the h-, p-, hp-, and rp-version of the FEM for the solution of the 2d Hertzian contact problem. *Computational Mechanics*, 45(5):513–522. [p. 22], [p. 110], [p. 111]

[Fremond, 1982] Fremond, M. (1982). Adhérence des solides. *Journal de mécanique théorique et appliquée*, 6(3):383–407. [p. 20]

[Goryacheva, 2001] Goryacheva, I. G. (2001). Mechanics of friction interaction. *Mir, Moscow*. [p. 10]

[Gosz et al., 1998] Gosz, M., Dolbow, J., and Moran, B. (1998). Domain integral formulation for stress intensity factor computation along curved three-dimensional interface cracks. *International Journal of Solids and Structures*, 35(15):1763–1783. [p. 105]

[Griffith, 1921] Griffith, A. A. (1921). The Phenomena of Rupture and Flow in Solids. *Philosophical Transactions of the Royal Society of London. Series A, Containing Papers of a Mathematical or Physical Character*, 221:163–198. [p. 20], [p. 41]

[Gurtin, 2000] Gurtin, M. E. (2000). *Configurational forces as basic concepts of continuum physics*, volume 137. Springer Science & Business Media. [p. 50]

[Hansbo, 2005] Hansbo, P. (2005). Nitsche's method for interface problems in computa-tional mechanics. *GAMM-Mitteilungen*, 28(2):183–206. [p. 107]

[Harlow et al., 1965] Harlow, F. H., Welch, J. E., and others (1965). Numerical calculation of time-dependent viscous incompressible flow of fluid with free surface. *Physics of fluids*, 8(12):2182. [p. 32]

[Harten et al., 1987] Harten, A., Engquist, B., Osher, S., and Chakravarthy, S. R. (1987). Uniformly high order accurate essentially non-oscillatory schemes, III. *Journal of Computational Physics*, 71(2):231–303. [p. 37]

[Heegaard and Curnier, 1996] Heegaard, J. H. and Curnier, A. (1996). Geometric properties of 2d and 3d unilateral large slip contact operators. *Computer Methods in Applied Mechanics and Engineering*, 131(3–4):263–286. [p. 13]

[Hertz, 1882] Hertz, H. (1882). Über die Berührung fester elastischer Körper. [p. 10]

[Hestenes, 1969] Hestenes, M. R. (1969). Multiplier and gradient methods. *Journal of Optimization Theory and Applications*, 4(5):303–320. [p. 16]

[Hirt and Nichols, 1981] Hirt, C. W. and Nichols, B. D. (1981). Volume of fluid (VOF) method for the dynamics of free boundaries. *Journal of computational physics*, 39(1):201–225. [p. 32]

[Hughes, 2012] Hughes, T. J. R. (2012). *The Finite Element Method: Linear Static and Dynamic Finite Element Analysis*. Courier Corporation. [p. 20], [p. 23]

[Hughes et al., 1977] Hughes, T. J. R., Taylor, R. L., and Kanoknukulchai, W. (1977). A finite element method for large displacement contact and impact problems. *Formulations and Computational Algorithms in FE Analysis*, pages 468–495. [p. 22]

[Irwin, 1957] Irwin, G. R. (1957). Analysis of stresses and strains near the end of a crack traversing a plate. *Spie Milestone Series MS*, 137:167–170. [p. 20], [p. 41]

[Ji and Dolbow, 2004] Ji, H. and Dolbow, J. E. (2004). On strategies for enforcing interfacial constraints and evaluating jump conditions with the extended finite element method. *International Journal for Numerical Methods in Engineering*, 61(14):2508–2535. [p. 43]

[Johnson, 1987] Johnson, K. L. (1987). *Contact Mechanics*. Cambridge University Press. [p. 10]

[Johnson et al., 1971] Johnson, K. L., Kendall, K., and Roberts, A. D. (1971). Surface energy and the contact of elastic solids. *Proceedings of the royal society of London. A. mathematical and physical sciences*, 324(1558):301–313. [p. 20], [p. 92]

[Khoei and Nikbakht, 2006] Khoei, A. R. and Nikbakht, M. (2006). Contact friction modeling with the extended finite element method (X-FEM). *Journal of Materials Processing Technology*, 177(1–3):58–62. [p. 36]

[Kikuchi and Oden, 1988] Kikuchi, N. and Oden, J. T. (1988). *Contact problems in elasticity: a study of variational inequalities and finite element methods*, volume 8. siam. [p. 10], [p. 23]

[Klarbring, 1990] Klarbring, A. (1990). Examples of non-uniqueness and non-existence of solutions to quasistatic contact problems with friction. *Ingenieur-Archiv*, 60(8):529–541. [p. 10]

[Klarbring, 1999] Klarbring, A. (1999). Contact, Friction, Discrete Mechanical Structures and Mathematical Programming. In Wriggers, P. and Panagiotopoulos, P., editors, *New Developments in Contact Problems*, number 384 in International Centre for Mechanical Sciences, pages 55–100. Springer Vienna. [p. 25]

[Krstulović-Opara et al., 2002] Krstulović-Opara, L., Wriggers, P., and Korelc, J. (2002). A C1-continuous formulation for 3d finite deformation frictional contact. *Computational Mechanics*, 29(1):27–42. [p. 13]

[Laursen, 2002] Laursen, T. A. (2002). *Computational contact and impact mechanics: fundamentals of modeling interfacial phenomena in nonlinear finite element analysis*. Springer. [p. 10]

[Legrain et al., 2012] Legrain, G., Chevaugeon, N., and Dréau, K. (2012). High order X-FEM and levelsets for complex microstructures: Uncoupling geometry and approximation. *Computer Methods in Applied Mechanics and Engineering*, 241–244:172–189. [p. 36], [p. 38]

[Legrain et al., 2008] Legrain, G., Moës, N., and Verron, E. (2008). Robust and direct evaluation of J2 in linear elastic fracture mechanics with the X-FEM. *International journal for numerical methods in engineering*, 76(10):1471–1488. [p. 94]

[LeVeque, 2002] LeVeque, R. J. (2002). *Finite volume methods for hyperbolic problems*, volume 31. Cambridge university press. [p. 20]

[Li et al., 1985] Li, F. Z., Shih, C. F., and Needleman, A. (1985). A comparison of methods for calculating energy release rates. *Engineering Fracture Mechanics*, 21(2):405–421. [p. 105]

[Liu et al., 1994] Liu, X.-D., Osher, S., and Chan, T. (1994). Weighted Essentially Non-oscillatory Schemes. *Journal of Computational Physics*, 115(1):200–212. [p. 37]

[Luenberger, 1984] Luenberger, D. G. (1984). Linear and nonlinear programming. [p. 25]

[Marsden and Hughes, 1994] Marsden, J. E. and Hughes, T. J. (1994). *Mathematical foundations of elasticity*. Courier Corporation. [p. 5]

[Martins et al., 1994] Martins, J. A. C., Monteiro Marques, M. D. P., and Gastaldi, F. (1994). On an example of non-existence of solution to a quasistatic frictional contact problem. *European journal of mechanics. A. Solids*, 13(1):113–133. [p. 10]

[Maugin, 2010] Maugin, G. A. (2010). *Configurational forces: thermomechanics, physics, mathematics, and numerics*. CRC Press. [p. 50]

[Maugis, 1992] Maugis, D. (1992). Adhesion of spheres: the JKR-DMT transition using a Dugdale model. *Journal of Colloid and Interface Science*, 150(1):243–269. [p. 20]

[Maugis and Barquins, 1983] Maugis, D. and Barquins, M. (1983). Adhesive contact of sectionally smooth-ended punches on elastic half-spaces: theory and experiment. *Journal of Physics D: Applied Physics*, 16(10):1843. [p. 20], [p. 92], [p. 94]

[McDevitt and Laursen, 2000] McDevitt, T. W. and Laursen, T. A. (2000). A mortar-finite element formulation for frictional contact problems. *International Journal for Numerical Methods in Engineering*, 48(10):1525–1547. [p. 22]

[Melenk and Babuška, 1996] Melenk, J. M. and Babuška, I. (1996). The partition of unity finite element method: basic theory and applications. *Computer methods in applied mechanics and engineering*, 139(1):289–314. [p. 39]

[Michell, 1900] Michell, J. H. (1900). Some elementary distributions of stress in three dimensions. *Proceedings of the London mathematical society*, 1(1):23–61. [p. 94]

[Minnebo, 2012] Minnebo, H. (2012). Three-dimensional integration strategies of singular functions introduced by the XFEM in the LEFM. *International Journal for Numerical Methods in Engineering*, 92(13):1117–1138. [p. 102]

[Moës et al., 2006] Moës, N., Béchet, E., and Tourbier, M. (2006). Imposing Dirichlet boundary conditions in the extended finite element method. *International Journal for Numerical Methods in Engineering*, 67(12):1641–1669. [p. 67]

[Moës et al., 2003] Moës, N., Cloirec, M., Cartraud, P., and Remacle, J. F. (2003). A computational approach to handle complex microstructure geometries. *Computer Methods in Applied Mechanics and Engineering*, 192(28–30):3163–3177. [p. 40]

[Moës et al., 1999] Moës, N., Dolbow, J., and Belytschko, T. (1999). A finite element method for crack growth without remeshing. *Int. J. Numer. Meth. Engng*, 46(1):131–150. [p. 38], [p. 40], [p. 41]

[Nour-Omid and Wriggers, 1987] Nour-Omid, B. and Wriggers, P. (1987). A note on the optimum choice for penalty parameters. *Communications in Applied Numerical Methods*, 3(6):581–585. [p. 15]

[Nübel et al., 2006] Nübel, V., Düster, A., and Rank, E. (2006). An rp-adaptive finite element method for the deformation theory of plasticity. *Computational Mechanics*, 39(5):557–574. [p. 22]

[Oliver et al., 2009] Oliver, J., Hartmann, S., Cante, J. C., Weyler, R., and Hernández, J. A. (2009). A contact domain method for large deformation frictional contact problems. Part 1: Theoretical basis. *Computer Methods in Applied Mechanics and Engineering*, 198(33–36):2591–2606. [p. 22]

[Osher and Fedkiw, 2003] Osher, S. and Fedkiw, R. (2003). *Level Set Methods and Dynamic Implicit Surfaces*. Springer. [p. 32], [p. 37]

[Osher and Sethian, 1988] Osher, S. and Sethian, J. A. (1988). Fronts propagating with curvature-dependent speed: algorithms based on Hamilton-Jacobi formulations. *Journal of computational physics*, 79(1):12–49. [p. 32]

[Persson, 2000] Persson, B. N. J. (2000). *Sliding Friction: Physical Principles and Applications*. Springer Science & Business Media. [p. 11]

[Peskin, 2002] Peskin, C. S. (2002). The immersed boundary method. *Acta numerica*, 11:479–517. [p. 32]

[Powell, 1969] Powell, M. (1969). A method for nonlinear constraints in minimization problems. In Fletcher, R., editor, *Optimization*, pages 283–298. Academic Press. [p. 16]

[Pradeilles-Duval and Stolz, 1995] Pradeilles-Duval, R.-M. and Stolz, C. (1995). Mechanical transformations and discontinuities along a moving surface. *Journal of the Mechanics and Physics of Solids*, 43(1):91–121. [p. 50]

[Raous et al., 1999] Raous, M., Cangémi, L., and Cocu, M. (1999). A consistent model coupling adhesion, friction, and unilateral contact. *Computer Methods in Applied Mechanics and Engineering*, 177(3–4):383–399. [p. 20]

[Rice, 1968] Rice, J. R. (1968). A Path Independent Integral and the Approximate Analysis of Strain Concentration by Notches and Cracks. *Journal of Applied Mechanics*, 35(2):379–386. [p. 20], [p. 94]

[Sauer, 2011] Sauer, R. A. (2011). Enriched contact finite elements for stable peeling computations. *International Journal for Numerical Methods in Engineering*, 87(6):593–616. [p. 20], [p. 92]

[Sethian, 1999] Sethian, J. A. (1999). *Level set methods and fast marching methods: evolving interfaces in computational geometry, fluid mechanics, computer vision, and materials science*, volume 3. Cambridge university press. [p. 32], [p. 37]

[Shu and Osher, 1988] Shu, C.-W. and Osher, S. (1988). Efficient implementation of essentially non-oscillatory shock-capturing schemes. *Journal of Computational Physics*, 77(2):439–471. [p. 37]

[Signorini, 1933] Signorini, A. (1933). Sopra alcune questioni di elastostatica. *Atti della Societa Italiana per il Progresso delle Scienze*. [p. 10]

[Signorini, 1960] Signorini, A. (1960). *Questioni di elasticità non linearizzata*. Edizioni Cremonese. [p. 10]

[Spellucci, 1998] Spellucci, P. (1998). An SQP method for general nonlinear programs using only equality constrained subproblems. *Mathematical Programming*, 82(3):413–448. [p. 25]

[Taroco, 2000] Taroco, E. (2000). Shape sensitivity analysis in linear elastic fracture mechanics. *Computer Methods in Applied Mechanics and Engineering*, 188(4):697–712. [p. 50]

[Temizer et al., 2011] Temizer, I., Wriggers, P., and Hughes, T. J. R. (2011). Contact treatment in isogeometric analysis with NURBS. *Computer Methods in Applied Mechanics and Engineering*, 200(9–12):1100–1112. [p. 20]

[Tryggvason et al., 2001] Tryggvason, G., Bunner, B., Esmaeeli, A., Juric, D., Al-Rawahi, N., Tauber, W., Han, J., Nas, S., and Jan, Y. J. (2001). A Front-Tracking Method for the Computations of Multiphase Flow. *Journal of Computational Physics*, 169(2):708–759. [p. 32]

[Tsitsiklis, 1995] Tsitsiklis, J. N. (1995). Efficient algorithms for globally optimal trajectories. *Automatic Control, IEEE Transactions on*, 40(9):1528–1538. [p. 38]

[Vorovich and Aleksandrov, 2001] Vorovich, I. I. and Aleksandrov, V. M. (2001). Mechanics of Contact Interactions. *Fizmatlit, Moscow*. [p. 10]

[Wohlmuth, 2001] Wohlmuth, B. I. (2001). *Discretization Methods and Iterative Solvers Based on Domain Decomposition*, volume 17 of *Lecture Notes in Computational Science and Engineering*. Springer Berlin Heidelberg, Berlin, Heidelberg. [p. 22], [p. 23]

[Wriggers, 2006] Wriggers, P. (2006). *Computational contact mechanics*, volume 30167. Springer. [p. 10], [p. 17], [p. 25]

[Wriggers et al., 2001] Wriggers, P., Krstulovic-Opara, L., and Korelc, J. (2001). Smooth C1-interpolations for two-dimensional frictional contact problems. *International Journal for Numerical Methods in Engineering*, 51(12):1469–1495. [p. 13]

[Wriggers et al., 1985] Wriggers, P., Simo, J. C., and Taylor, R. L. (1985). Penalty and augmented Lagrangian formulations for contact problems. In *Proceedings of the NUMETA*, volume 85, pages 97–105. Swansea, British Technique Press. [p. 16]

[Zavarise and De Lorenzis, 2009] Zavarise, G. and De Lorenzis, L. (2009). A modified node-to-segment algorithm passing the contact patch test. *International Journal for Numerical Methods in Engineering*, 79(4):379–416. [p. 22]

[Zhao et al., 2003] Zhao, Y. P., Wang, L. S., and Yu, T. X. (2003). Mechanics of adhesion in MEMS—a review. *Journal of Adhesion Science and Technology*, 17(4):519–546. [p. 20]

[Zienkiewicz and Taylor, 2005] Zienkiewicz, O. C. and Taylor, R. L. (2005). *The finite element method for solid and structural mechanics*. Butterworth-heinemann. [p. 20]

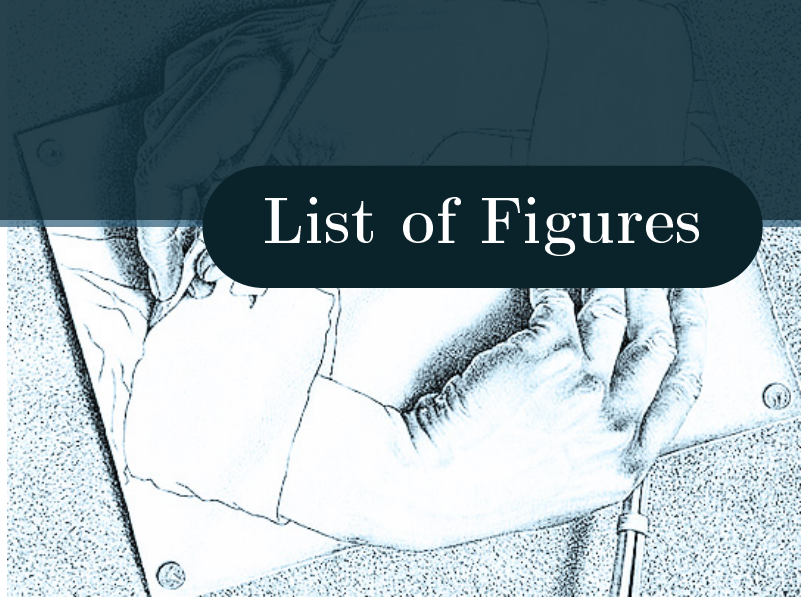

List of Figures

Abstract

This thesis proposed a method which takes advantage of the level-sets to solve contact problems. The importance of the variational formulation and the discretization is highlighted trough the whole manuscript. First enrichments are proposed in order to give an accurate representation of contact phenomena. Then suitable formulations are given such that the Babuška-Brezzi condition is fulfilled. Nevertheless, the most original contribution of this work is the way the contact zone is found. A shape optimization is set-up and coupled with a Newton's method. Criteria are proposed in order to drive this shape optimization problem. Their derivative is computed using the directional derivative of the equilibrium variational problem which allows to use the numerical work already done to solve this first problem.
This method is shown to be efficient and accurate on a wide variety of unilateral contact problems such that a membrane or a Hertz problem. Thus, this work ascertains the possibilities of this method and encourage further development in this direction.

Keywords: Adhesion, Contact, Configurational mechanics, Inequality Level-Set, Shape optimization, X-FEM

Résumé

Cette thèse propose une méthode qui tire avantage des fonctions de niveau pour résoudre des problèmes de contact. L'importance de la formulation variationnelle et de la discrétisation est mise en exergue tout au long de ce manuscrit. Premièrement, des enrichissements sont proposés afin de donner une représentation précise des phénomènes de contact. Par la suite, des formulations adaptées sont suggérées afin que la condition de Babuška-Brezzi soit vérifiée. Quoi qu'il en soit, la plus grande originalité de ce travail réside dans la manière de trouver la zone de contact. Une optimisation de forme couplée à une méthode de Newton sont mises en place. Différents critères sont proposés afin de conduire cette optimisation de forme. Leur dérivées sont déterminées en calculant la dérivée directionnelle de la formulation variationnelle du problème d'équilibre, permettant ainsi de réutiliser le travail fait pour résoudre ce dernier problème.
Cette méthode s'est montrée efficace et précise pour une grande gamme de problèmes dont les membranes ou les problèmes de Hertz. Ce travail permet donc de conclure sur le potentiel de cette méthode et encourage à continuer les développements dans cette direction.

Mots-clés: Adhésion, Contact, Inequality Level-Set, Mécanique configurationnelle, Optimisation de forme, X-FEM